THE UNIVERSITY of HULL

THE PLASTICITY of DIAMOND

being a thesis submitted for the Degree of

DOCTOR of PHILOSOPHY

in the University of Hull

by

Jill Brookes, MSc (Bristol), AIM

June, 1992

PAGE NUMBERING AS ORIGINAL

SUMMARY

Aspects of the crystal structure of diamond, and its associated defects, have been considered with reference to the effect such characteristics might have on its mechanical properties. Also, established resolved shear stress models, which account for anisotropy in conventional Knoop indentation hardness of all single crystals, have been reviewed. Particular attention has been given to the role of microplasticity and the nature of crack formation in the deformed zone formed beneath the indenter. It is then shown that a similar approach can be applied to the case where a cone, made from a softer material, replaces the conventional rigid indenter. By using different materials covering a range of hardness, impressions can be formed beneath which there is a controlled density and depth of dislocations.

In this work, the 'soft' indenter technique has been extended to high temperatures and applied to study the plasticity of various types of natural and synthetic diamond. Consequently, the effect of temperature on the critical resolved shear stress of synthetic type Ib, and natural type Ia and type IIa has been established.

Above a critical threshold temperature for the onset of plasticity, time dependent growth of the impression volume occurs whilst the mean contact pressure is decreasing. It is shown that geometrical similarity, i.e. the ratio of the impression size to dislocated volume, is maintained whilst the critical mean pressure continues to be exceeded during this process of 'impression creep.' Activation energies of about 2.9 eV and 1.2 eV were determined, from rates of volume change, for natural (both type I and II) and synthetic type Ib respectively.

Whilst no significant differences were observed between 98.9% 12C (natural abundance) and 99.9% 12C (isotopically enriched) synthetic diamonds, their behaviour was most like that of a type IIb diamond. Finally, by studying type Ia diamonds with a nitrogen concentration ranging from 14 - 750 ppm, evidence is obtained which supports the suggestion that this element reduces the intrinsic resistance to dislocation movement and encourages the initiation of cracks in the diamond structure.

Preface

I would like to express my gratitude to the Head of Department, Professor Chris Brookes, for extending the facilities of the Department of Engineering Design and Manufacture, at the Universty of Hull, and to DeBeers Industrial Diamond Division for the provision of the diamonds and a maintenance grant. My sincere thanks also go to Dr. Clive Waddington for his advice and encouragment in the preparation of this thesis.

Many collegues in EDM and Applied Physics have contributed in a variety of ways during the completion of this work and I am gratetful to them all. A special mention goes to my support 'team' of Farad Nabhani (general encouragement) Garry Robinson (photography) and especially, Phil Radcliffe (word processing).

However, my greatest debt is due to my family, Toby and Jenny, for their unending patience and support over the past years and to their friends and their friends parents who have kept them occupied, and to my husband, Chris, the inspiration for much of this work, and whose never ending support has made it possible.

Table of Contents.

Chapter 1. The structure and mechanical properties of diamond.

1.1 General description.

Diamond - the hardest material yet known to man, with a refractive index for visible light exceeded by only a few minerals, also has the highest thermal conductivity at room temperature (Berman, 1965), the highest bulk modulus, and the highest critical tensile stress for cleavage (Field, 1979). A low coefficient of friction (Bowden and Hanwell, 1966) and a remarkable inertness, coupled with excellent electrical insulating properties (with the exception of type II diamond which is semi-conducting), provide in diamond a unique set of properties in a single element material. However, diamond exhibits brittle behaviour under most experimental conditions, will cleave easily in air and will begin to graphitise at 600°C in air. Some useful physical constants of diamond are summarised in Table 1.1.

Structure.

Diamond is composed of the covalently bonded single element carbon and, as with silicon and germanium, crystallizes in the diamond cubic (A4) crystal structure. Covalent bonding is essentially quantum mechanical in nature and the simplest covalent bond is between two atoms joined together to form a molecule. Carbon has a valency of four and in diamond the four sp^3 hybrid orbitals, each containing an unpaired electron, form a tetrahedron. When the orbitals overlap, the electrons form two-atom orbits, an energetically favourable state. All the electrons in the solid are tightly bound, but as the interatomic distance decreases, the outer states merge and broaden into bands of states with gaps on the energy ladder.

The four outer electrons per atom fill the valence band making diamond electrically insulating. The valence band states, when occupied by electrons, give a lower overall energy than the corresponding single atoms states. Thus the valence band states are

Table 1.1 Physical constants of diamond.

unit cell		a	0.357 nm
C - C bond length			0.154 nm
density		ρ	3.52 x 10^3 Kg m^{-3}
refractive index		n	2.417
Young's modulus		E	1141 GPa
shear modulus		G	553 GPa
Poisson's ratio		ν	0.07
bulk modulus		K	442 GPa
{111} cleavage energy		γ	5.5 Jm^{-2}
stress intensity factor		K_{Ic}	3.4 MN $m^{-3/2}$
compressive strength (grit)		σ	10 GPa
thermal conductivity at 293K		Ia	600 - 1000 $Wm^{-1}K^{-1}$
		II	2000 - 2100 $Wm^{-1}K^{-1}$
	80K	Ia	2000 - 4000 $Wm^{-1}K^{-1}$
		II	1.5 x 10^5 $Wm^{-1}K^{-1}$
electrical resistivity		I & IIa	> 10^{18} Ω m
		IIb	10^3 - 10^5 Ω m

responsible for the strong bonding and this strong directional bonding imparts rigidity to the structure.

Another key to the exceptional properties of diamond lies in the relatively small size of the carbon atom. Carbon is the smallest atom in the fourth group of the periodic table of elements; the next group IV elements are silicon and then germanium. The silicon atom is larger than the carbon atom and the resultant larger distance between atoms makes silicon a less strongly bonded lattice than diamond. In diamond, each carbon atom lies at the centre of a regular tetrahedron which is formed by equidistant neighbouring carbon atoms positioned at the apices of that tetrahedron. Figure 1.1(a) shows the carbon atoms in the tetrahedral arrangement.

The diamond cubic crystal structure, Figure 1.1(b), is frequently described as two interpenetrating face-centred cubic (f.c.c.) lattices, the displacement of the second lattice being a/4 [111] from the first lattice site. The bonds are at an angle of 109.5° to each other and are 0.154 nm long. The f.c.c. stacking sequence is commonly described as ABCABC and a similar description of the diamond cubic structure gives rise to the stacking sequence AaBbCcAaBb, shown in Figure 1.1(c).

Sources of diamond.

Most diamonds are found in continental areas of geographical stability. Diamond crystallized from carbon, over long periods of time in reservoirs of molten magma in favourable areas of the earth's mantle of peridotite. Temperature and pressure estimates (Meyer, 1987) show that for diamonds from specific African and Siberian mines, the temperature range is 900 to 1300°C with a pressure range spanning 4.5 to 6.5 GPa, indicating that these particular diamonds originated at depths of between 140 to 200 km in the upper mantle. Various other minerals crystallized in the same magma and this was driven upwards by explosive pressures of gases from great depths, to pierce the earth's crust in small fissures or pipes and to solidify there. During this journey the magma became altered, collecting other rocks and minerals, to become kimberlite or lamproite. The diamonds vary in crystal habit, colour, and quality, from pipe to pipe.

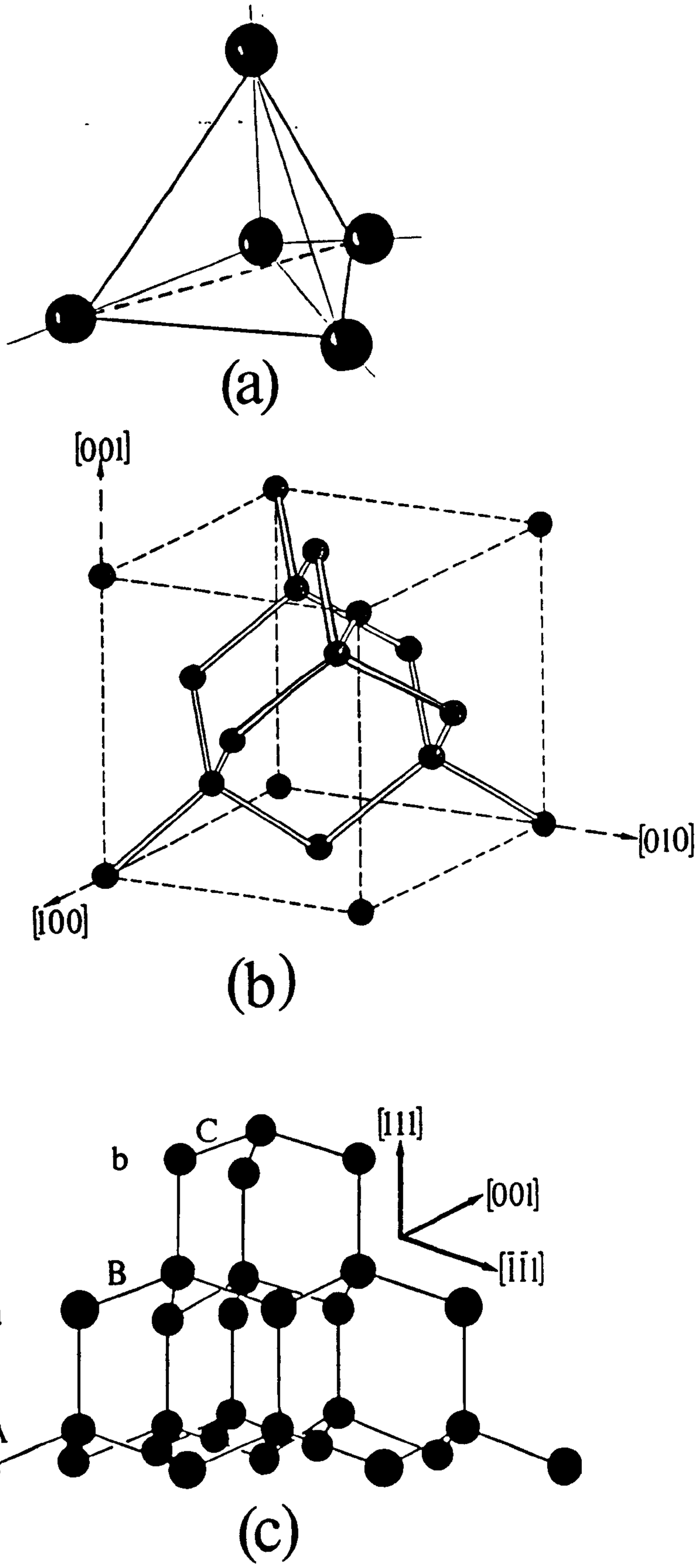

Figure 1.1 (a) the tetrahedral arrangement of the carbon atoms, (b) the diamond cubic crystal structure, (c) the stacking sequence.

Alchemists have for centuries tried to make diamond, however scientific work began in earnest only after the Second World War. Based on the work of Nobel Prize winner P. W. Bridgeman, General Electric were the first to announce success in 1955. In their process, a short cylinder of pyrophyllite is filled with the reaction material, graphite or another form of carbon, and tanatalum or nickel, and placed in a ring of tungsten carbide, known as the belt. Pressure is then applied and a current of electricity passed through the centre to provide the necessary temperature, The pyrophyllite acts as a gasket to seal the gaps. Material flow occurs under very high pressures and permits the pistons to advance, compressing the carbon and the metal. Pressures employed are over 11 GPa with temperatures over 2000°C.

Synthetic diamonds are now grown by many different techniques:

(a) growth from a molten solvent-catalyst

(b) shock wave synthesis

(c) direct transformation in the absence of a solvent

(d) growth from a carbon melt

(e) metastatic synthesis from a carbonaceous gas using a diamond seed crystal.

The process of diamond synthesis from carbon can be regarded as a three stage process:

(i) carbon by catalytic graphitization → graphite, (ii) dissolution → metal carbon solution, (iii) nucleation and growth → diamond.

Classification of diamonds.

In 1934, Robertson *et al* classified diamonds into two broadly defined categories, **type I** and **type II**. Sharp differences in transparency to ultra-violet light and infra-red radiation were observed. These and other differences in the physical properties between the two types of diamond are listed in Table 1.2.

In 1959 Kaiser and Bond determined that type I diamonds can be broadly defined as those containing nitrogen and type II diamonds as those containing virtually no nitrogen. Nitrogen has a valency of five which might suggest that the presence of nitrogen would free electrons and make diamond electrically conducting. However, almost all diamonds

Table 1.2 Differences between the two types of diamond.

	type I	type II
Infra-red absorption	between 8 - 10 μm.	none, 8 - 10 μm
	bands at 4-5μm	bands at 4-5 μm
ultra-violet absorption	complete beyond 340 nm	IIa complete beyond 225 nm
x-ray diffraction	extra spots due to platelets	normal
photoconductivity	poor	good
thermal conductivity	very good	excellent
electrical conductivity	insulating	IIb is semi-conducting
photoluminescence	present	present but diffuse
{111} cleavage	uneven	near perfect

contain some aluminium which, with a valency of three, compensates for the free electrons. The band gap in diamond is large, ≈ 6 eV, and is the reason why most diamonds are good insulators.

Type I diamonds were then categorised type Ia and type Ib according to the position of the nitrogen in the lattice. Type Ib contains dispersed paramagnetic nitrogen, substituting for carbon, leaving one unsaturated bond. This type is rare in nature, but commercially synthesized high pressure:temperature diamond is generally of this type. However, 97% of natural diamonds are type Ia where the nitrogen form is not paramagnetic. Type I diamond may have up to one thousand parts per million (ppm) nitrogen in the structure, in other words there is one nitrogen to every one thousand carbon atoms. This nitrogen may be singly substitutional, which would colour the diamonds (as in type Ib), or form structures ranging from a few atomic diameters, to several micrometers in size (type Ia). A further subdivision of type Ia diamond was made by Sutherland *et al* (1954) and Clark *et al* (1956), who divided the absorption features in the ultraviolet, visible and infrared of this type into two classes, A and B. Most states of nitrogen in diamond have been experimentally induced in the laboratory by a combination of pressure and temperature treatments (Evans and Zengdu, 1982).

Subdivision of type II diamond was proposed in 1952 and 1954, by Custers, on the basis of differences in luminescence and photoconductivity. Type IIa diamonds contain no appreciable amounts of nitrogen and are often brown in colour, although a few are a fine gem colour, like the Cullinan diamond. Type IIb diamonds constitute a very small proportion of the type II group and are electrically semi-conducting, due to the presence of boron, which has a valency of three and therefore introduces holes. They are frequently blue in colour due to an absorption tail in the blue part of the spectrum. Type IIb diamonds include all the natural blue diamonds, eg the Hope diamond. The main features of the different types of diamond are summarised in Table 1.3.

Table 1.3 Summary of the types of diamond.

type Ia	Nitrogen in fairly significant quantities. 97% of natural diamond Electrically insulating All colours.
type Ib	Nitrogen dispersed as a single substitutional element. 0.1% natural diamonds but most synthetic diamonds are of this type. Electrically insulating Yellow to green in colour.
type IIa	Relatively nitrogen free. Rare in nature. Electrically insulating but enhanced thermal properties Frequently brown in colour
type IIb	Boron as substitutional impurity. Extremely rare Semi-conducting Blue in colour.

1.2 Imperfections in diamond.

Perfect order in crystalline solids does not exist and all crystals contain a variety of impurities and defects. These include point defects, line defects, volume defects, interfacial defects and inclusions. Those defects which are of major importance in diamond, and so can influence the mechanical properties, are discussed in the following sections.

Inclusions.

Impurities in diamond can be separated into two categories. One is typified by the nitrogen atom, the other by a particle of olivine. The main difference is that an impurity atom is bonded into the diamond, forming a continuity with the lattice, whereas an inclusion is not bonded to the carbon atoms but sits in a space within the diamond.

Inclusions in diamond are composed of a wide range of materials, the translucent appearance of many diamonds being due to light scattered from the multi-faceted surfaces of these inclusions. The conditions under which natural diamonds are formed may be revealed by a study of the chemistry of these inclusions and evaluations have been made which indicate that the physical growth conditions are very similar to those used in diamond synthesis although the chemical environs are very different.

Point defects.

The simplest point defect is the *neutral vacancy* i.e. a vacancy with four electrons and is often referred to as a *GR1 centre*. This may be formed during solidification or as a result of atomic lattice vibrations causing displacement of an atom from its normal lattice site. The introduction of vacancies into a perfect lattice results in a lowering of the free energy of the crystal until an equilibrium concentration is reached. The equilibrium

number of vacancies depends on and increases exponentially with temperature according to the relationship:

$$N_v = N e^{-Q_v / kT}$$

where N is the total number of atomic sites, Q_V is the energy of activation (the vibrational energy required for the formation of a vacancy), T is the absolute temperature and k, Boltzman's constant, is 8.62 eV / atom K.

Theoretical calculations of the energies of self diffusion in diamond have used semi-empirical methods to determine the formation and migration energies of the vacancy and interstitial defect. Swalin (1961) calculated the activation energy for self diffusion in diamond to be 6.18 eV, where the simple mechanism for self-diffusion must be that of vacancy diffusion. More recent results from *ab initio* calculations differ somewhat. Bernholc *et al* (1988) calculated the energy of formation of a vacancy in diamond as 7.2 eV and the migration energy as 1.7 - 1.9 eV. The migration energy of the vacancy has been measured by Davies and Lawson (1988) and agrees well with the theoretical value. Bernholc *et al*, (1988), assume that the activation energy for self diffusion is the sum of the formation and migration energies, and on this basis suggest a value of 9.1 eV for diamond, derived from the calculated energy of formation and the measured energy of migration.

Bernholc *et al*, (1988), also calculated the formation energies of other point defects, including the saddle point energy for direct exchange mechanisms in diamond. These values are as follows:

GR1 centre	7.2 eV
direct exchange	13.2 eV
tetrahedral interstitial	23.6 eV
bond-centred interstitial	15.8 eV
split interstitial	16.7 eV

The lowest energy elementary defect is the neutral vacancy, with a relaxation of nearest atomic neighbours of about 5% of the bond distance and a total energy gain of

0.3 eV. Therefore, self-diffusion processes in diamond are likely to be dominated by the vacancy mechanism and this dominance is due to (1) rigidity of the C-C bond preventing twisting or large relaxations around defects, (2) a large band gap of $\approx$ 6 eV, and high electron density resulting in a highly repulsive potential energy surface for interstitial configurations.

In comparison with the value of 1.7 - 1.9 eV for the migration energy for carbon in diamond, the activation energy for nitrogen diffusion is high. In radiation damage experiments, (Collins, 1980) the vacancy was found to become mobile above 800°C and was ultimately trapped at one of the forms of nitrogen. The activation energy for nitrogen diffusion in diamond is given as 2.6 eV (Chrenko *et al*, 1977) and 5 eV (Evans and Zengdu, 1982) measured as the rate of transformation of singly substitutional nitrogen in type Ib diamond into aggregated nitrogen, as in type IaA diamond, over the temperature range 1600 - 2100°C.

The *self-interstitial* is an atom from the crystal structure sitting in an interstice i.e. occupying a small void space in the crystal structure which would not normally be occupied. This introduces a relatively large distortion in the surrounding lattice and requires a high activation energy for formation. Consequently this defect exists in very small concentrations, significantly lower than vacancy concentrations.

The *substitutional point defect* involves the replacement of the host atom by a solute or impurity atom and may be accommodated only when the difference in atomic radii is less than about ± 15%. Alternative sites for impurity atoms are voids or interstitial sites or the enlarged sites at dislocations. The atomic diameter of the interstitial impurity is normally smaller than that of the host atom, but even very small impurity atoms will be larger than the interstitial sites available and some lattice distortion plus an overall effect on the density is the result.

Diamond usually contains a significant proportion of atoms of other elements in the lattice. Among these, nitrogen is the most abundant, but aluminium and boron may also be present. These elements have a decisive effect on the physical properties of diamond. Recent research has shown that there are significant amounts of hydrogen and oxygen both in the bulk and at the surface of diamond (Madiba *et al*, 1984).

Twins.

Twins in crystalline materials fall into two categories, growth and deformation twins.

Growth twins, as favoured by covalent bonding, occur in diamond on {111} planes and their orientation is such that a rotation of 60° about the ⟨111⟩ axis common to both the twin axis and the matrix would bring the lattice of the twin into conformity with the matrix. Growth twins can be further sub-divided into two types - contact and penetration twins. Both contact twins, where the single plane interface separates two individual crystals, and penetration twins where the interface follows a number of different planes, are found in diamond (Slawson, 1950).

Deformation twins can be produced in the diamond cubic lattice by lattice shear. Twins have been observed on {111} and {123} planes, although the only coherent boundary between crystal and twin is the {111} plane. The shear involved in the formation of deformation twins has to satisfy two conditions: (i) shear on any plane parallel to the twinning plane is proportional to the distance from the twinning plane, (ii) the shear produces a lattice of the same symmetry as the matrix but is mirrored across the twin boundary. The twinning element for {111} deformation twins is a translational shear of 0.4084 a in the $[11\bar{2}]$ direction with $(\bar{1}10)$ as the shear plane, shown in Figure 1.2, and the twinning element for (123) twins is a translational shear of 0.6552a in the $[41\bar{2}]$ direction with $(1\bar{2}1)$ as the shear plane (Churchman *et al*, 1956). The resultant fault is one of low energy.

Dislocations.

The dislocation is a line defect in the crystal structure and is defined by its relation to the Burgers vector b i.e. the dislocation displacement vector. In the diamond cubic structure dislocations are similar to those in f.c.c. materials, but at low temperatures the high Peierls stress confines them largely to the ⟨110⟩ valleys. Slip is on the {111} planes in the ⟨110⟩ directions with a Burgers vector $b = a/2\ \langle 110\rangle$, i.e. half the diagonal of a cube face, or the shortest distance between two equivalent atoms. There are three simple dislocations observed: (a) the screw dislocation, with the Burgers vector parallel to the

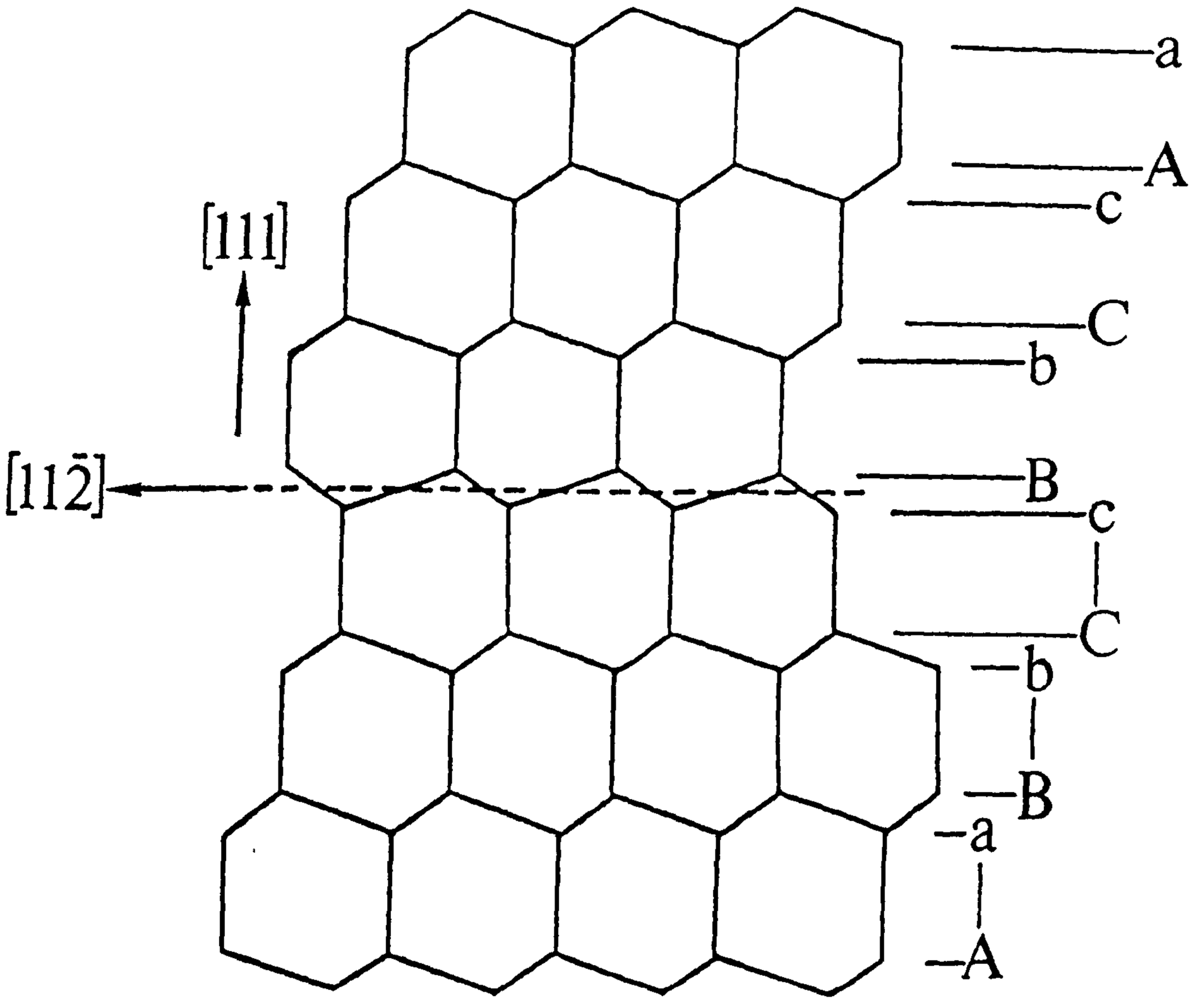

(111) twin plane

Figure 1.2 The twinning element for {111} deformation twins.

dislocation line; (b) the edge dislocation, with the Burgers vector normal to the dislocation line; (c) the 60° dislocation, with the Burgers vector at 60° to the dislocation line, and they are illustrated in Figure 1.3. The edge and the 60° dislocation are characterised by free or "dangling" bonds along the axis of the dislocation, whereas these are absent in the screw dislocation. These so-called "dangling" bonds are of importance in understanding the electrical properties of diamond cubic materials.

The {111} slip plane is the plane on which a 'perfect' dislocation with a/2 ⟨110⟩ Burgers vector may dissociate into two Shockley partial dislocations:

$$a/2\,[\bar{1}10] = a/6\,[\bar{1}2\bar{1}] + a/6\,[\bar{2}11]$$

an energetically favourable reaction. Due to the double occupancy of the Bravais lattice the displacement is spread over two planes with one of the partial dislocations leading and the other trailing producing an extrinsic stacking fault. Stacking faults can also form with no shear between the planes, by the removal of part of a {111} layer of atoms, i.e. when excess vacancies collect together on a {111} plane. A Frank partial dislocation may also form, in which slip occurs on planes normal to the {111} planes. The resultant fault is a high energy stacking fault and is sessile.

The dissociation of dislocations is possible in many ways but in general it occurs by the rotation of a ribbon of atoms in the core of the original dislocation. Motion of a partial dislocation includes successive rotation of neighbouring ribbons. The distance between the leading and the trailing partial dislocation is determined by the stacking fault energy, i.e. the lower the energy, the wider the fault. In diamond, the stacking fault energy is high at 279 mJm^{-2} (Pirouz *et al*, 1983) and the separation is only 2.5 nm to 4.3 nm and is therefore quite difficult to resolve. The screw dislocation dissociates into two 30° partials and the 60° dislocation dissociates into an edge dislocation and a 30° partial dislocation.

Volume defects.

The *A centre* is considered to be two nitrogen atoms on adjacent atomic sites and gives rise to the 'A' absorption features observed in the ultra violet, visible and infra-red

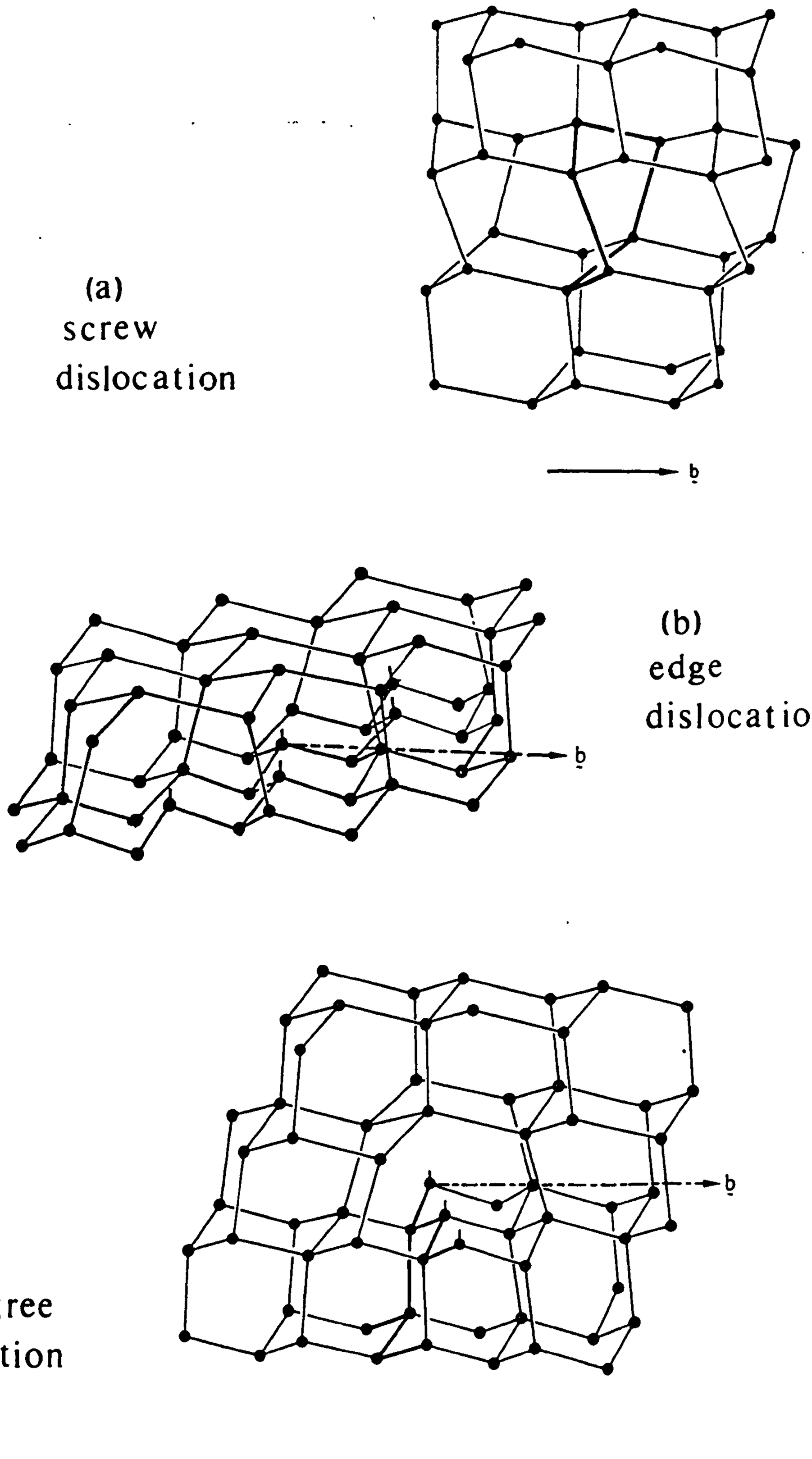

(a)
screw
dislocation

(b)
edge
dislocation

(c)
60° degree
dislocation

Figure 1.3 (a) the screw dislocation, (b) the edge dislocation in the {111} plane, (c) the 60° dislocation.

regions. Moreover, the height of the infra-red peak at 1282 cm^{-1} (7.8 μm) was found to correlate directly with the nitrogen concentration (Kaiser and Bond, 1959).

A second type of aggregate, termed the *N3 centre*, is considered to consist of three nitrogen atoms and a vacancy (Loubser and Wright, 1973; Davies *et al*, 1978) The N3 peak results in an absorption in the visible region at 24,000 cm^{-1} (415 nm).

A third type of aggregate is attributed to the 'B' absorption peak and it has been suggested that it consists of a carbon vacancy with four nearest neighbour carbons atoms on {111} planes replaced by nitrogen atoms in a tetrahedral arrangement. Relaxation outwards gives rise to an almost perfect octahedral void. Details of these and other important small defects are given in Table 1.4.

In type Ia diamonds there are often but not always, *platelets*. Platelets lie in {100} planes, and are visible only by transmission electron microscopy (Evans and Phaal, 1962). They vary in density and size from specimen to specimen and have been observed up to 5 μm in diameter (Woods, 1976). Frank (1956) predicted the existence of platelets to account for anomalous x-ray spikes associated with certain Laue spots for some diamonds (Raman and Nilakantan, 1940). Sobolev *et al* (1967), using infra-red studies, confirmed the presence of platelets giving an absorption peak at about 1370 cm^{-1}. The precise wavenumber depends on the size of the platelets i.e. the larger the platelets, the lower the wavenumber.

Another volume defect, *voidites*, were first reported by Stephenson (1978) and Evans (1978). Barry *et al* (1987) subsequently established that voidites are octahedral, bounded by {111} planes and 1-10 nm in diameter. Hirsch *et al* (1986) have proposed that voidites contain crystalline ammonia, with a unit cell of about 0.5 nm, but this is as yet unsubstantiated.

1.3 The crystallography of deformation.

In general the mechanical behaviour of materials may be described in one of two ways, ductile behaviour or brittle behaviour. If plastic flow precedes the initiation of a crack and the propagation of that crack is relatively slow, the material is considered to be

Table 1.4 Summmary of nomenclature and structure of small defects in diamond.

Defect name	**Description**
GR1 centre	neutral vacancy; four unsaturated bonds
N centre	nitrogen replacing a carbon atom at a normal site: one unsaturated bond
A centre	two nitrogen atoms substituting for carbon on adjacent sites
B centre	four nitrogen atoms substituting for carbon forming a tetrahedron around a vacant lattice site
H3 centre	A centre trapped at a vacant carbon site; two unsaturated bonds
H4 centre	B centre and a vacancy
N3 centre	three nitrogen atoms substituting for carbon around a vacancy or common carbon atom: one unsaturated bond
N-V centre	one nitrogen substituting for carbon adjacent to a vacant site: three unsaturated bonds
split-self-interstitial	two carbon atoms fill one original site; two unsaturated bonds
split-nitrogen-interstitial	two nitrogen atoms fill one original site

ductile. If however, the first crack is initiated prior to plastic flow, the crack propagates at high velocities and that material is considered to be brittle. Due to the high density of strong atomic bonds and the strongly directional nature of the bonding, diamond has a marked resistance to plastic flow and is therefore traditionally considered to be inherently brittle in behaviour. Indentation hardness, friction and wear are all anisotropic and can be explained in terms of basic crystallographic characteristics.

Plastic deformation.

The nature of plastic deformation of crystalline materials is dictated by shear along certain planes in specific directions. This deformation corresponds to a net relative movement of a large number of atoms in response to an applied stress. Interatomic bonds are ruptured and then reformed and this occurs by the motion of dislocations.

In the diamond cubic structure the slip systems are $\{111\}\langle 110\rangle$, with twelve slip systems in total, as for face centred cubic metals. Slip occurs between the closest packed planes i.e. the $\{111\}$ planes, and the direction of slip is along the shortest lattice vector, the $\langle 110\rangle$ direction, of magnitude $a/2\sqrt{2}$, where a is the edge of the cubic unit cell.

A single crystal under an applied stress will be subjected to shear components of that stress, with the exception of directions parallel or perpendicular to the stress direction. The resolved shear stresses depends on the applied stress and on the orientation of both the slip plane and the slip direction to that applied stress. Slip in a single crystal will occur on the most favourably oriented slip system when the resolved shear stress reaches a critical value. This is the *critical resolved shear stress*, τ_c, or the minimum shear stress to initiate slip and is a basic property of the crystal which, for diamond, will be considered in detail in Chapter 3.

In the diamond cubic crystal structure it is important to distinguish between shear along the closely stacked glide planes, aB in Figure 1.4, or along shuffle planes, Aa. In general, dislocations move on the glide set rather than the shuffle set and dissociate forming partial dislocations with a lattice vector $a/6\ \langle 112\rangle$.

Plastic deformation can also occur by twinning. Slip and twinning differ from one another in several respects. The crystallographic orientation above and below the slip

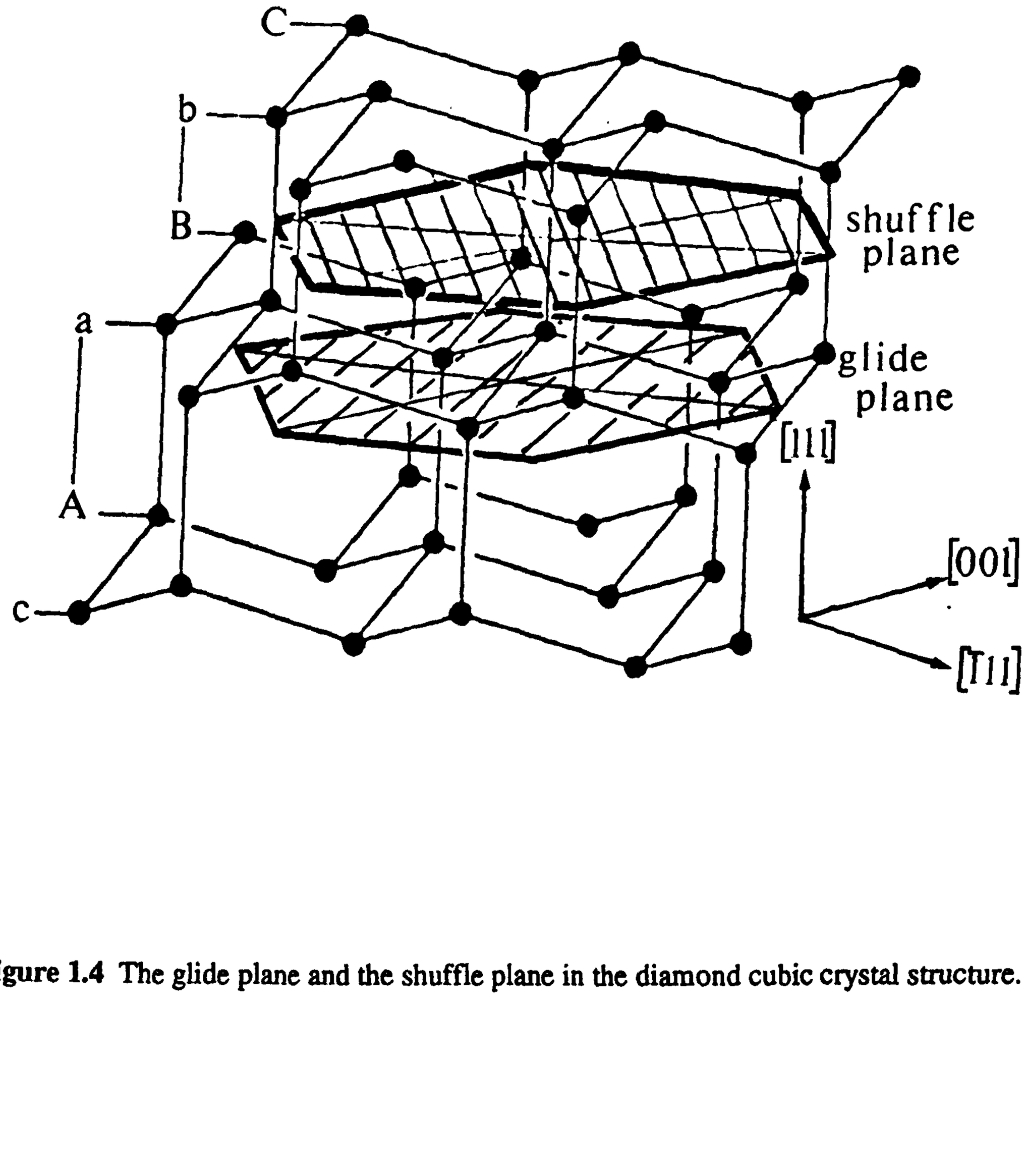

Figure 1.4 The glide plane and the shuffle plane in the diamond cubic crystal structure.

plane is the same both prior to and following deformation, whereas in the case of a twin there will be a re-orientation across the twin plane. Slip occurs in multiples of the atomic spacing, but the atomic displacement for twins is less than the interatomic separation. Twinning tends to be favoured in a crystal where there are a limited number of slip systems and when the orientation of the crystal with respect to the stress axis is unfavourable for slip. The amount of bulk plastic deformation from twinning is usually small by comparison with that resulting from slip. Twinning, however, may be a prerequisite to deformation by slip, since it enables crystallographic reorientation with respect to the stress axis to permit further bulk plastic deformation by slip.

Evans and Wild (1965) showed that bulk plastic deformation occurred when diamond plates were stressed in three-point bending experiments, at temperatures above 1500°C. Under these experimental conditions, diamonds containing a low density of dislocations and a high density of platelets required higher stresses to deform them plastically than diamonds with virtually no nitrogen but a high density of dislocations.

Mao and Bell (1978) reported plastic deformation when two diamond anvils were subjected to 172 GPa in a high pressure diamond cell. They also observed that the flow was a minimum in a diamond with a very high concentration of impurity nitrogen atoms and a high concentration of platelets.

DeVries (1975) deformed both natural and synthetic diamond crystals, $\approx$ 1mm in size, at high pressure and temperature, and observed "deformation lamellae" of increased abrasion resistance, possibly twins. Confirmation of this by Lee *et al* (1984) led the authors to suggest that twins are the predominant mechanism of deformation and that the formation of twin bands create conditions favouring the formation of secondary cross twins in some of the primary twin bands. Slip bands were also observed, and in some instances dense dislocation forests, however twins and dislocations were not observed together.

The question of whether plastic deformation occurs at room temperature in diamond has been more controversial. Howes and Tolansky (1955) suggested that the raised surface outside the contact area of indentations made in diamond at room temperature by a 0.39 mm diamond ball, was due to plastic flow. The observation of dislocations produced beneath room temperature indentations in diamond (Humble and Hannink, 1978) suggests

that if there is sufficient constraint to eliminate tensile fracture significant plastic deformation will occur at room temperature.

Fracture.

Viewed from certain directions, the crystal structure model of diamond atoms can be seen to be layered. These directions are the cubic, ⟨100⟩, octahedral, ⟨111⟩ and the dodecahedral, ⟨110⟩ directions. The density of the bonds between atoms is higher in certain directions, for example in the octahedral direction. However, it can also be seen that alternate layers are less strongly bonded. When fractured, diamond splits between closely bonded layers, breaking only one bond in each tetrahedral group, resulting in a 'perfect' new surface. Such fracture occurs along definite crystal planes, commonly referred to as cleavage planes, a feature of diamond so expertly exploited over the centuries by both industrialist and gemmologist.

Predominantly, diamond cleaves along the (111) plane, having an experimental cleavage energy of 5.50 ± 0.15 Jm^{-2} for that plane (Field and Freeman, 1981). Calculations of the ideal fracture strengths of most materials have been shown to be several orders of magnitude greater than the experimental values but are based on potential models which assume a perfect atomic lattice. In reality, strength is dependent on the internal lattice defects and other stress concentrators, such as cracks. However, this result is remarkably close to the theoretical value of 5.3 Jm^{-2} suggesting that little if any dislocation movement occurs in the stress field at the crack tip. The fracture energy for (110) cleavage is measured as 7.1 ± 1.0 Jm^{-2} (Field and Freeman, 1981) and compares with 6.5 Jm^{-2} for theoretical cleavage. Silicon and germanium do not cleave as readily as diamond.

The critical stress intensity factor K_{IC} is related to the cleavage energy, γ, and the fracture surface energy G by:

$$K_{IC}^2 = 2E\gamma = EG$$

where E is Young's modulus. Novikov and Dub (1991) measured the fracture toughness of diamond from the length of the radial cracks initiated from the corners of Vickers indentations. Aligning the indenter diagonal with the ⟨110⟩ direction produced penny

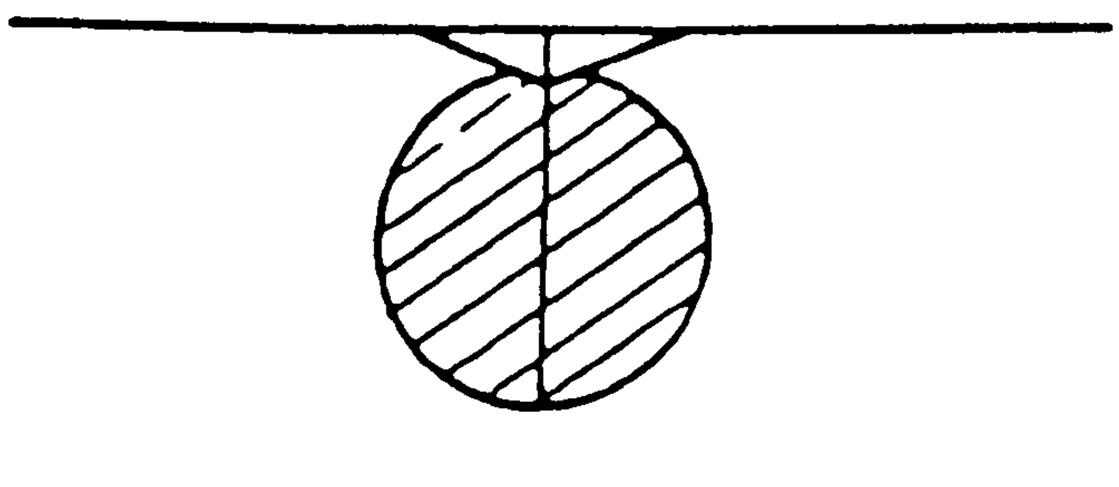

(a)

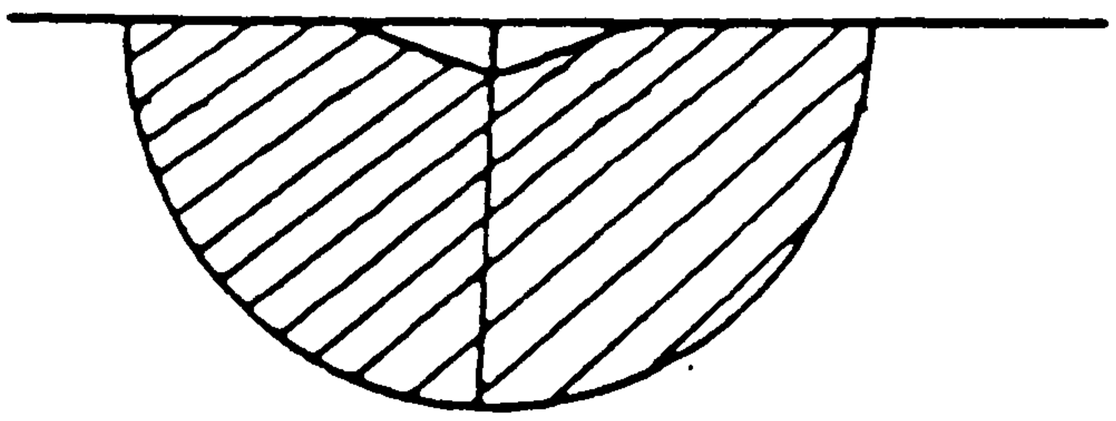

(b)

(c)

Figure 1.5 Cracks beneath a Vickers indentation, after Novikov and Dub (1991): (a) penny shaped cracks; (b) half - penny shaped cracks; (c) Palmqvist cracks.

shaped cracks beneath the indentation along {110} planes in <110> directions, Figure 1.5(a). These cracks were formed under a 2 N load. Increasing the load caused crack growth within the crystal and the eventual removal of the load propagated the cracks to the surface, forming half-penny cracks, Figure 1.5(b). Alignment of the indenter diagonals with the ⟨100⟩ direction also produced penny cracks but these did not emerge onto the surface. Some cracks did develop along the (111) planes in both cases. If the load did not exceed 2 N, cracking occurred during unloading forming Palmqvist cracks, Figure 1.5(c). A fracture toughness of 5 MN $m^{-3/2}$ was measured at room temperature for the ⟨110⟩ direction on a (001) plane for both natural and synthetic diamond. The fracture toughness was significantly anisotropic, in that it was measured as 13.5 MN $m^{-3/2}$ for the ⟨100⟩ direction on the (001) plane.

1.4. Some mechanical properties of diamond.

Hardness of diamond.

The hardness scale devised by the mineralogist Mohs, is a scratch test based on the ability of one mineral to scratch another mineral. On a numbered scale of 1 to 10 any mineral will scratch those of lower numbers and in turn be scratched by those of higher numbers. The difference in hardness between 1 (talc) and 9 (corundum) is significantly less than that between 9 and 10 (diamond). There are no natural minerals between 9 and 10, only manufactured hard materials, such as the carbides of boron, silicon and tungsten. The Mohs scale is not infallible and indeed a scratch may be made on a crystal by another material whose Mohs number is two units lower on that scale (Kelly, 1966). Recent work (Brookes *et al*, 1987) has established that plastic deformation and wear of diamond can occur even when the difference in hardness between the diamond and the indent material is a factor of ten.

Hardness tests are influenced by the anisotropy of the material, i.e. the variation of measured hardness as the orientation of the indent changes with respect to the crystallographic plane of the specimen. A review of the hardness of diamond in 1971 by

Brookes indicated a lack of reproducibility in the values of hardness, ranging from 65 GPa (Knoop *et al*, 1939) to 525 GPa (Berkovich, 1951). A definition of optimum conditions was necessary, so that comparisons might be made with other crystalline solids.

More recent measurements, taking into account orientation, diamond type, impurity content, type and shape of the indent and the magnitude of the normal load, have been made (Brookes, 1979). The results for type Ia and type IIa diamond are summarised in Table 1.5.

Table 1.5 Knoop hardness (GPa) of diamond at room temperature.

	(001)		(110)		(111)	
	<100>	<110>	<100>	<110>	<110>	<211>
type I	93	83	108	88	56	63
type II	103	91	115	94	76	110

load = 1 kgf, room temperature, mechanically polished surfaces.

Although the processes of slip and fracture are competitive they are not mutually exclusive. However, catastrophic brittle failure is frequently the dominant mechanism in a standard hardness test where dislocation mobility is limited. The Knoop indenter appears to induce less cracking than other indenters, therefore encouraging plastic deformation, and best reflects the intrinsic anisotropy of crystals. The nature of anisotropy is such that it is more dependent on crystallographic direction than on the plane of indentation and this is observed in diamond where the ⟨100⟩ direction is the hardest direction, whichever the plane of indentation. As with other hard materials, cracking is less extensive for indentations in the hard directions. Nevertheless, the high degree of correlation between markedly anisotropic Knoop hardness and the model proposed by Brookes *et al* (1971) based on resolved shear stresses on active slip systems (outlined in Chapter 2), lends

support to the suggestion that limited dislocation movement can influence and even control the mechanical behaviour of ceramic crystals, including diamond at low homologous temperatures (T/T_m).

Knoop indentations on a (11$\bar{1}$) surface of a type II diamond (Harrison, 1973) and Berkovich indentations on (111) surfaces of type I diamonds (Trefilov *et al*, 1975) showed a linear H:T relationship at temperatures close to room temperature, with a sharp decrease in hardness at approximately 1450°C (0.43 T_m). The activation energy and the activation volume were found to be 2.6 ± 0.2 eV and 20 x 10^{-24} cm^3 respectively (Trefilov *et al*, 1975).

The three point bend test.

The critical resolved shear stress for plastic flow in diamond has proved difficult to evaluate, due to the experimental difficulties in deforming diamond crystals under uniaxial stress conditions and the three point bend test has yielded the most significant information to date. Evans and Wild (1965) found that type II diamonds deform plastically at 1800°C, but the critical resolved shear stress was significantly lower for type IIa diamond than for type I diamond, i.e. approximately 0.48 GPa and 1.2 GPa respectively. These authors further measured a critical resolved shear stress of 0.63 GPa for type II diamond at 1700°C and estimated the ductile-brittle transition temperature as 1700°C for type II diamond and 1750°C for type I diamond.

Trefilov *et al* (1988) also measured the strength of diamond in three point bend tests, over a wider temperature range, and presented their data as a plot of activation volume versus the yield point. From these results they estimated the brittle-ductile transition temperature to be 1300°C (0.39 T_m) and derived values of 0.2 - 0.1 GPa for the critical resolved shear stress in the temperature range 1300 - 1750°C. For comparison, the critical resolved shear stress of covalent materials is in the region of 10^{-2} G (G = 553 GPa for diamond), whereas the critical resolved shear stress for face centred cubic metals is of the order of 10^{-5} G.

Friction.

Diamond surfaces tend to be associated with low frictional forces and high wear resistance. The frictional force developed between sliding surfaces is known to consist of two components, one due to deformational ploughing and the other due to adhesion. The coefficient of friction, μ, for diamond on diamond is usually between 0.05 and 0.10 in air, and when the contacting surfaces are relatively blunt there is no deformational ploughing. However, if sharp diamond indenters slide on flat (001) or (110) surfaces in air, μ varies with the normal load, the crystallographic direction of sliding and the sharpness of the slider. Then, the coefficient of friction for a 60° cone on a (001) surface may be closer to 0.1 when sliding in a [100] direction, and 0.4 when sliding in a [110] direction (Bowden and Brookes, 1966). Similarly, marked anisotropy for sliding friction has been observed by Enomoto and Tabor (1980), but a complete explanation of the phenomenon has not yet emerged. However, most of the experimental evidence indicates that it is the deformation component of the frictional force rather than the adhesion component, which determines the nature of the anisotropy. In contrast, the adhesion component can be of greater significance when diamond surfaces are cleaned. For example, when the adsorbed layers are removed by repeated sliding in a high vacuum, the coefficient of friction approaches unity and wear is greatly accelerated.

Abrasion and wear.

The abrasion resistance and wear properties of diamond, using a rotating wheel charged with diamond on the flat specimen surface, have been evaluated (Wilks and Wilks, 1991) and it is clear that (i) there is a great dependence on the orientation of the surface and the direction of abrasion (ii) there are sharp changes in the magnitude of wear near certain planes and directions and (iii) if the direction of traverse is reversed, the rate of wear may be quite different.

Abrasive wear is essentially a brittle process and attempts have been made to explain it using an original model of Tolkowsky (1920) based on micro-cleavage and cleavage on the {111} planes (Wilks and Wilks, 1965, 1972). The order of increasing relative abrasion resistance of different planes in different directions is summarised as follows:

1. dodecahedron (011) parallel to the [100] direction
2. cube (001) parallel to the [100] direction
3. octahedron (111) parallel to the $[11\bar{2}]$ direction
4. octahedron (111) parallel to the $[\bar{1}\bar{1}2]$ direction
5. dodecahedron (011) parallel to the [110] direction
6. cube (001) parallel to the [110] direction

The abrasion resistance under these conditions varies by two orders of magnitude and these observations correlate well with practical grinding and polishing in that the fastest removal of material corresponds to the conditions of 1 and 2 in the above list. It should be noted, however, that the hard and soft planes in abrasion resistance measurements are not the hard and soft planes and directions for indentation hardness.

1.5 Summary.

The range of defects in diamond, all with the potential to influence the mechanical properties, is shown to be diverse. Many of them have been well characterised but relationships between the nature of those defects and the mechanical properties of diamond have not yet been established convincingly. This is probably because such defects are more likely to influence plastic properties, rather than fracture, and these properties are difficult to quantify in this particular material, using conventional techniques. The principal aim of this work has been to extend the soft indenter technique so as to demonstrate its potential to increase our understanding of the way in which these defects influence the plasticity of diamond.

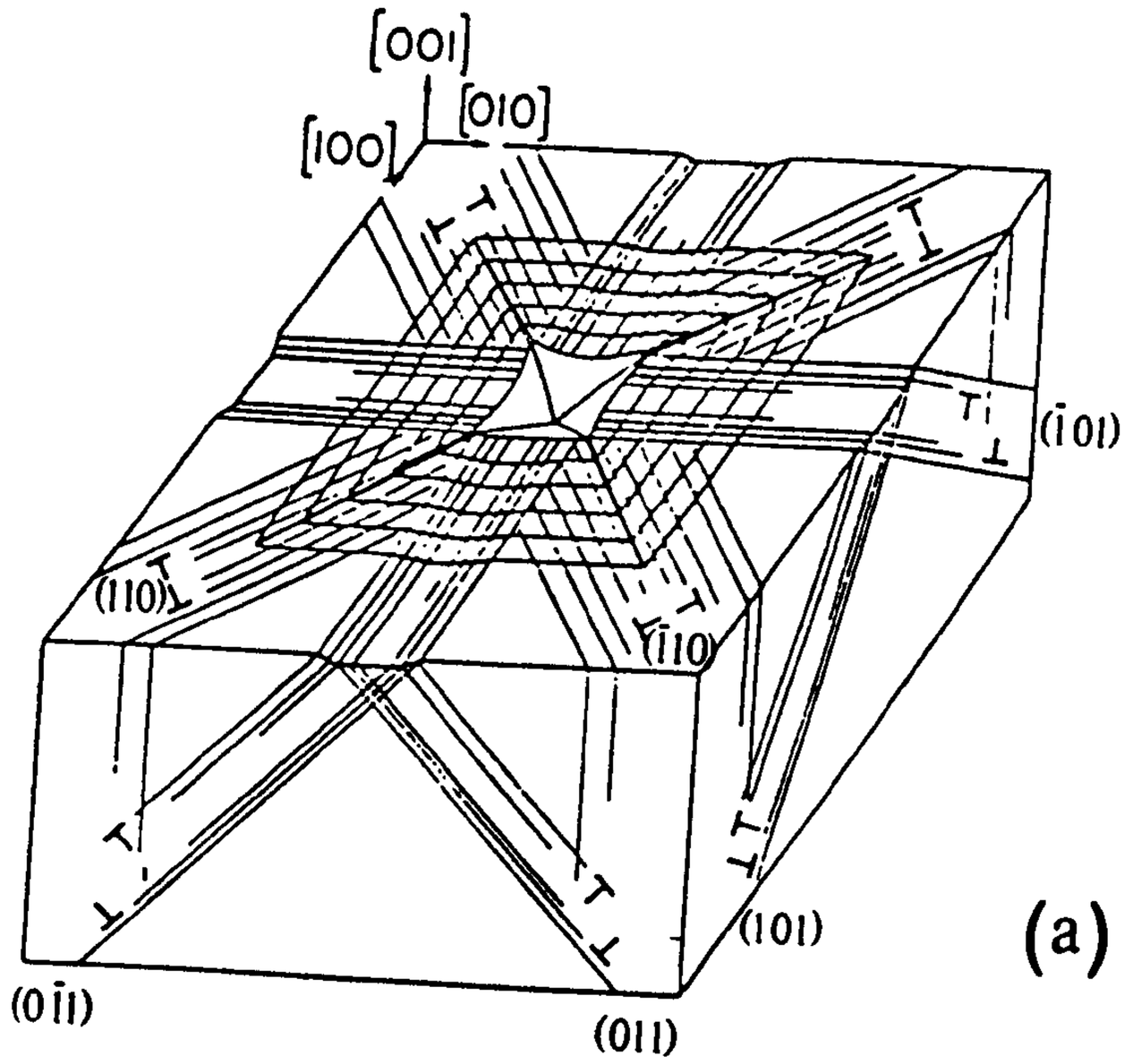

(a)

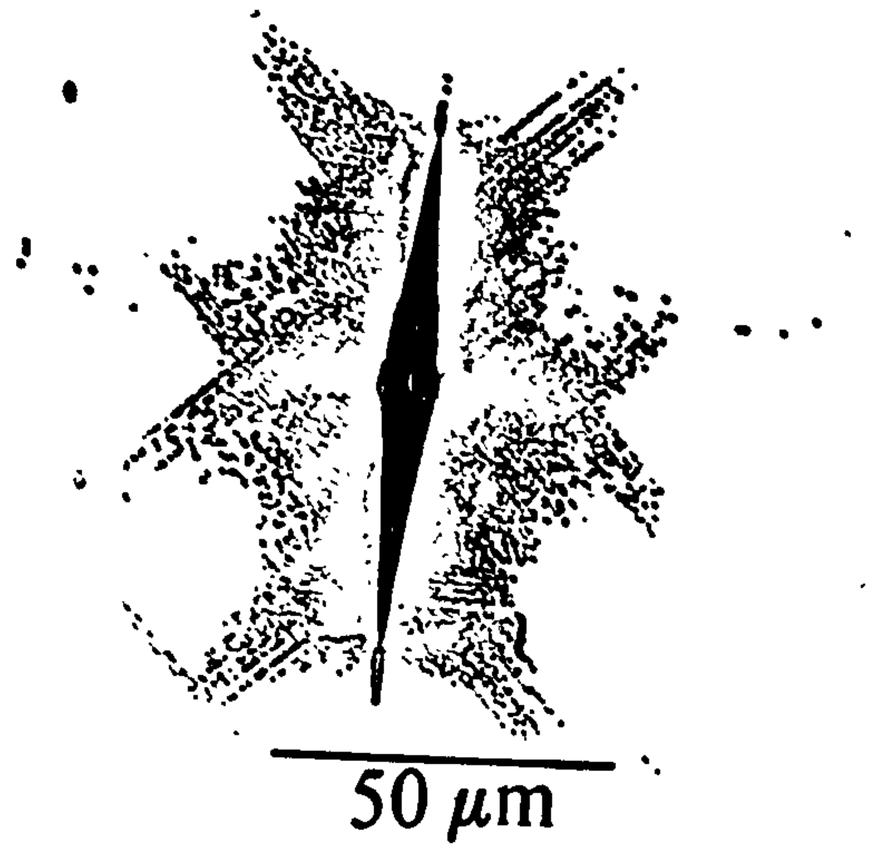

(b)

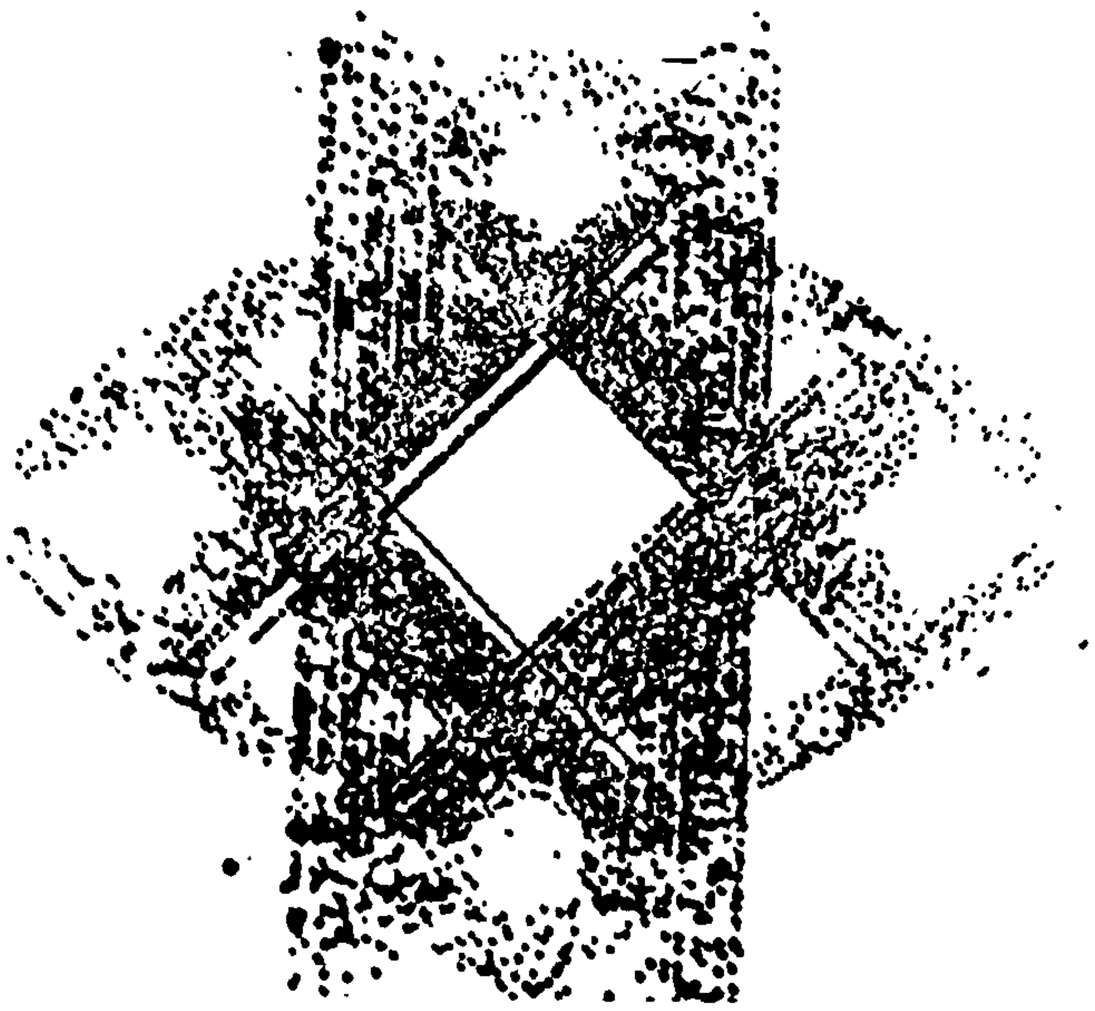

(c)

Figure 2.2 (a) the primary slip planes activated by a diamond pyramidal indentation on a (001) surface of MgO, (b) an etched Knoop indentation in a (001) surface of MgO where the etched rosette reveals that slip has occurred on all six slip planes, (c) the dislocation distribution 45 μm below the original surface.

Chapter 2. Indentations and Impressions - Modelling.

2.1 Indentation Hardness.

The topic of indentation hardness of metals and ceramics is concerned primarily with their plastic properties and only to a limited extent with their elastic properties. The hardness test is utilised to determine hardness, yield strength, fracture toughness, and creep properties of an extremely wide range of materials, including diamond. The advantages of such tests include small sample dimensions, simple preparation techniques and a relative non-destructive nature. In this work the static indentation method was employed to study the deformation involved in forming permanent impressions in diamond.

The relationship between the indentation process, conventional stress : strain data and work-hardening.

In general, the indentation hardness test involves the application of a known normal load to a natural or polished surface, using an indenter with a hardness considerably greater than the material being tested. Three different types of test are commonly employed to determine hardness values:

(i) *The Brinell test* uses a 10 mm steel or tungsten carbide ball, and a load of between 500 and 3000 gf which is maintained constant for a specified time. The Brinell hardness, H_B, is a function of both the magnitude of the load and the diameter of the resulting indentation and is expressed as:

$$H_B = \frac{2P}{\pi D\left[D - \sqrt{D^2 - d^2}\right]}$$

where P is the applied load, D is the diameter of the ball and d is the mean diameter of the indentation. The hardness is calculated from the **contact** area not the **projected** area in the plane of the surface. In materials which undergo significant work-hardening during the indentation process, the measured hardness increases with increasing normal load for a given indenter diameter, D. This is because the average level of plastic strain within the

volume that is deformed increases in proportion to the ratio of d / D. In practise the d / D ratio is kept between 0.25 and 0.5 to minimise this effect and to obtain reproducible and consistent values.

When the hardness is calculated from the **projected** area, this is the Meyer hardness, H_M expressed as:

$$H_M = \frac{4P}{\pi d^2}$$

This represents a mean contact pressure, which is more directly comparable with the method used in this work than H_B.

(ii) *The Rockwell test* utilises a small indenter, usually a small diameter tungsten carbide ball or a rounded tipped cone. The hardness number, H_R, is determined by the difference in penetration depth resulting from the application of a minor load followed by a larger major load. Several different scales are used, based on the indenter size and the applied load, permitting the testing of almost the entire hardness range, but not diamond.

(iii) Other testing techniques use diamond pyramidal indenters, the most commonly used being the *Vickers* indenter with an included angle of 136° between the faces. With this type of indenter the indentations are geometrically similar, regardless of load, and therefore a very light load may be used to sample a microscopic area. The hardness, H_V, is calculated as the load divided by the **contact** area of the indentation, and is:

$$H_V = \frac{1.854\ P}{d^2}$$

where d is the mean diagonal length.

Two other diamond pyramidal indenters in common use are the *Knoop* and the *Berkovich* indenters. The Knoop indenter produces an indentation which, when projected on to the indented surface, is a parallelogram with the long diagonal seven times longer than the short diagonal. The angle included between the pyramid edges producing the long diagonal is 172°30' and for the short diagonal it is 130°. The hardness measurement, H_K is based on the unrecovered **projected** area and not the contact area, as in the Vickers hardness measurement, and as such is not directly comparable. The Knoop indenter

penetrates the specimen about half as deep as the Vickers indenter for a given normal load so that it is more sensitive than the Vickers indenter to surface effects. The hardness value is again a measure of mean pressure. The *Berkovich* indenter is a triangular based diamond indenter with an angle of 65° between its axis and each facet. The hardness is calculated as the load divided by the surface area of the impression. Its major advantage is that polishing three convergent planes, rather than four as in other common indenters, must result in a sharp point rather then a chisel edge. For this reason, nanoindentation apparatus invariably uses a Berkovich indenter.

These and other hardness standards differ somewhat in the means of producing and measuring plastic deformation, but they all provide a measure of resistance to plastic deformation over a range of strain which is simply related to the geometry of the indentation.

Tabor (1951) established that hardness is basically a measure of flow stress in compression i.e. the averaged flow stress of polycrystalline material in the work-hardened zone beneath the indentation. The work-hardening leads to the concept of a representative strain where the flow stress, Y, is related to a representative yield stress, Y_R. The yield stress is then related to the Vickers hardness by:

$$H = C\,Y_R$$

where, for a Vickers indenter, C has a value of about 3 for polycrystalline metals. If it is assumed that there is no friction between the face of the indenter and the specimen, the applied pressure is uniform and has a value of ≈ 3 Y for polycrystalline metals. However, if there is appreciable friction between the surfaces, the pressure applied is not uniform, but increases towards the apex of the indenter with a corresponding increase in the mean value of the pressure. The Vickers indenter can be shown to develop a representative or average strain within the deformed volume of 0.08 (8%). This was confirmed by comparing a hardness:representative strain curve with a uniform stress:strain curve for a metal at various stages of deformation. In other words, the indentation hardness is C times the flow stress at this augmented value of strain (8% - Tabor, 1951).

Thus, Tabor's analysis established that indentation hardness is essentially a measure of the yield stress or elastic limit of the material being tested. For polycrystalline metals,

there is some elastic recovery of the indentation when the indenter is removed; the main dimensional change is, however, in the depth rather than in the projected area of the indentation. Therefore the pressure determined from the indentation size is very nearly equal to the effective pressure during the actual formation of the indentation. Calculations using the depth of the indentation, as in the Rockwell test, are complicated by possible elastic recovery and either appreciable 'pile-up' around the indentation or 'sinking in' of the indentation.

The hardness test in any form might be envisaged as a constrained compression test and as such imposes a considerable hydrostatic stress. This is an advantage when testing brittle materials as the hydrostatic component suppresses fracture whilst permitting the application of a stress sufficient to induce plastic deformation. However, although the value of 3 for the constraint factor C has been shown to apply to metals, it can be as large as 35 for alkali halide structures (Westbrook, 1973) and lower than 3 for materials which undergo significant elastic recovery. Applying this relationship to diamond where the average hardness is about 90 GPa, then the flow stress might lie between 3 GPa and 30 GPa. Since the tensile strength of diamond is about 3 GPa (Field, 1979), it is not surprising that brittle fracture might precede plastic deformation.

Cracking

Whilst largely incidental to the process of indentation, and often formed after the event, cracking and fracture around indentations can affect the accuracy of hardness measurements. However, the extent of indentation cracking can be usefully related to the fracture toughness of a material, (Palmqvist, 1962), and sharp indenters are often used to study crack generation and propagation.

Brittle fracture is usually analysed in terms of cohesive bonds rupturing at the tip of a growing crack. In general, fracture occurs when the applied stress level exceeds some critical value at a stress concentrator. This is described by the Griffiths criterion:

$$\sigma_c = \left(\frac{2\,E\,\gamma_e}{\pi\,a}\right)^{\frac{1}{2}}$$

where E = modulus of elasticity, γ_s = specific surface energy and a = the depth of a surface crack or half the length of an internal crack or stress concentrator. The fracture toughness of a material is generally expressed in the form:

$$K_{IC} = Y \sigma \sqrt{\pi a}$$

where Y is a dimensionless parameter that depends on specimen and crack geometries.

The stress required to propagate a crack, therefore, varies inversely with the dimension of the stress concentrator. When the stress intensity factor for fracture, K_{IC}, is achieved before the necessary shear stress for dislocation movement, then the material behaves in a brittle fashion.

Whether or not a crack propagates in a material is, to a greater or lesser extent, dependent on the mobility of dislocations in that material. Initially, the stress concentration at the tip of a newly formed crack may be accommodated by plastic strain and some degree of plasticity may precede the fracture, with microcracks forming during or as a result of slip or twinning. If dislocations are emitted from the crack tip, local conditions are modified and either (a) dislocations emitted from a crack exert a back stress on the crack, effectively reducing the local stress intensity factor, i.e. crack tip shielding, or (b) the crack tip is modified by either edge character dislocations which will blunt the crack tip, or screw dislocations which will jog the crack tip, i.e. crack-tip blunting. Dislocations may be nucleated in the material near the crack tip by other sources but would be strongly repelled by the crack tip.

There are essentially three different types of crack commonly associated with indentations and they are shown in Figure 2.1.

1. Hertzian cone cracks, Figure 2.1(a), occur by contact of a curved indenter on a flat sample surface. When a normal load is applied to a spherical indenter on the surface of a material, both the indenter and the material deform elastically according to the classical equations of Hertz. Removal of the normal load permits elastic recovery of both indenter and indented material. Analysis of the stresses generated across the circle of contact shows that they are not uniform and ring cracks may form around the periphery of the area of contact at sufficiently high loads. The critical normal load, P_C, required to produce ring cracks is proportional to the radius of the indenter, R, through which the

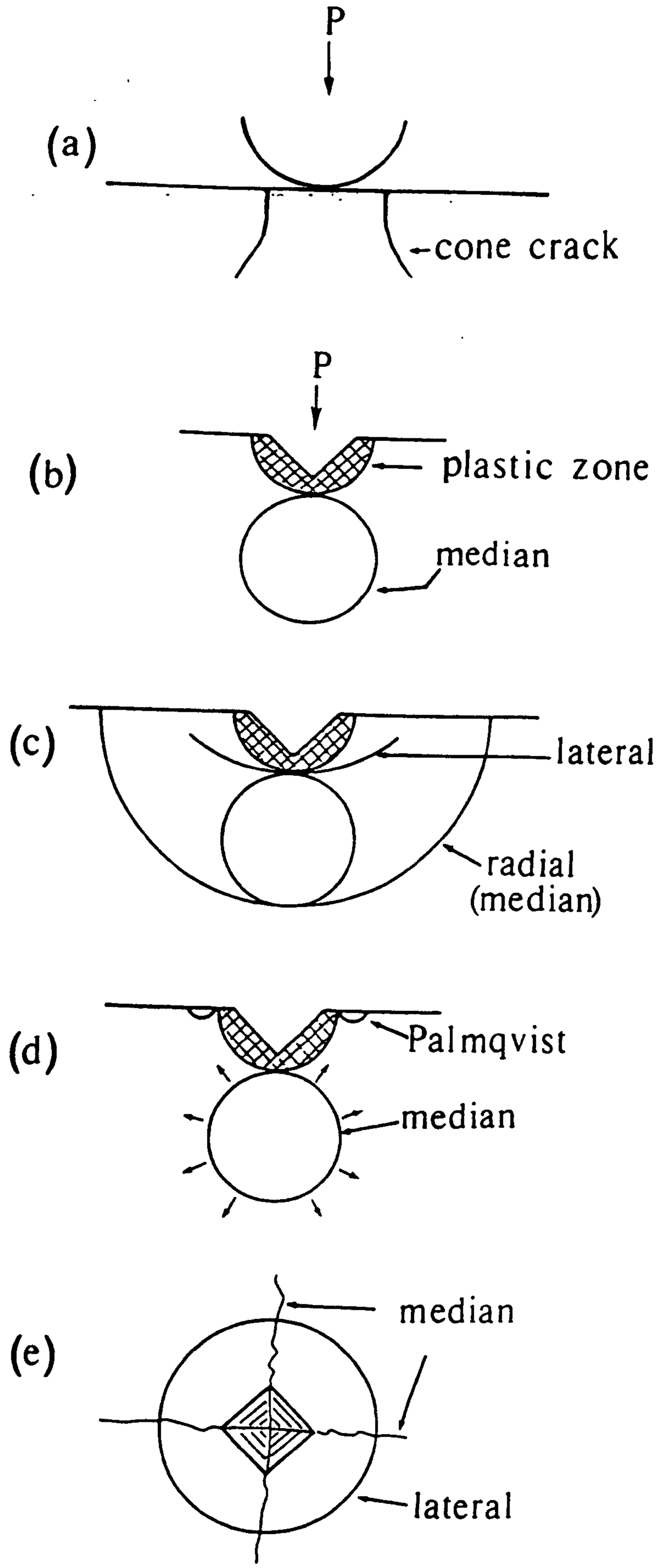

Figure 2.1 The different types of cracks commonly associated with indentations, (a) Hertzian cone cracks, (b) median cracks, (c) lateral cracks, (d) Palmqvist cracks (e) a Vickers indentation with associated cracks.

normal load is applied. This is the Auerbach relationship, i.e. the critical load/indenter radius is a constant. Such Hertzian cracks are particularly readily formed in covalently bonded structures during the indentation process (Howes and Tolansky, 1965). In their work on diamond, Howes and Tolansky (1965) noted a decreasing strength as the indenter radius increases and Seal (1958) found a linear relationship between the critical load for cracking during sliding on (110) planes of diamond and the radius of the slider.

2. *Median cracks*, Figure 2.1(b), formed on loading, are deep penny and halfpenny (or radial) cracks, at right angles to the surface. Sometimes Lomer-Cottrell locks act as nuclei for the initiation of median cracks beneath the indentation and these cracks form on planes of maximum stress. On the application of the load, the stress reaches a value high enough to nucleate a crack in the interface between plastically deformed material and material which is elastically strained and that crack propagates into the bulk of the material. On removal of the load the residual stress may be sufficient to drive the penny crack to the surface transforming it into a halfpenny crack, Figure 2.1(c).

3. *Lateral cracks*, Figure 2.1(c), which form on unloading, tend to be on fracture planes approximately parallel to the surface. Lateral cracking is formed as a result of elastic/plastic mismatch stresses. The crack nucleates at the high stress boundary between the zone of plastically deformed material and the elasticaly deformed region outside. As the indenter is removed and the material relaxes, stresses at this boundary reach a high enough value to form a flaw, or to activate an existing flaw, and the crack propagates towards the surface. As these cracks tend to propagate at a small angle to the surface of the indented material, the result can be the removal of small chips. Lateral cracks extend with positive crack opening displacement on unloading and tend to close with reloading. Very brittle materials form lateral cracks whereas materials with some degree of plasticity tend to form median cracks.

Palmqvist cracks, Figure 2.1(d), are shallow radial surface cracks extending out from the corners of an indentation. When the penny median crack propagates through to the surface, the Palmqvist crack becomes part of the median / radial crack system.

Despite the large number of slip systems available, the strength and directionality of the covalent bond structure in diamond cubic solids reduces the probability of plastic flow

in the high stress field at the tip of a crack, with the result that diamond behaves in a brittle fashion under most experimental conditions at temperatures below half the melting point.

2.2 Microplasticity and the indentation size effect.

Microhardness testing has been established as a simple method for determining the slip systems of single crystals and evaluating dislocation mobilities. Much of the original basic work on deformation under point loading has been carried out on magnesium oxide, due to the availability of a reliable dislocation etchant and a chemical polish, and the simple slip system geometry. There are six slip planes in the rocksalt crystal structure, with one slip direction in each plane, eg (110) [110]. However, on each pair of mutually orthogonal slip planes, eg (110) and ($\bar{1}$10), the resolved shear stress is always the same, as the angle λ for one of the slip systems is the angle ϕ for the other and vice versa (see the Schmid:Boas equation in the following section of this chapter). With respect to the (001) surface, two of the {110} planes are normal to that surface, i.e. (110) and ($\bar{1}$10), and these will be referred to as $\{110\}_{90}$ slip systems. The other four planes are at 45° to that surface, i.e. (011), (0$\bar{1}$1), (101) and ($\bar{1}$01), and these will be referred to as the $\{110\}_{45}$ slip systems. Figure 2.2(a) illustrates these slip planes with respect to the (001) surface.

Edge components of dislocation lines which emerge at a free surface form slip steps. The other dislocation lines which intersect the surface can also be identified at that point by etch pitting. The combined technique of etch pitting the distribution of dislocations around the microindentation revealing the so-called dislocation rosette, Figure 2.2(b), followed by the removal of surface layers by chemical polishing and re-etching, Figure 2.2(c), has provided much information on the extent of dislocation activity generated by the indentation stress, particularly in ionic solids, such as magnesium oxide, and covalent materials, such as silicon and germanium. Rosette development depends on the experimental temperature, and in silicon and germanium it has been established that the size of the rosette at a given temperature depends on the level of doping, (Roberts *et al*, 1985). These authors contend that doping affects the basic dislocation velocity and thus the brittle:ductile transition temperature. Such techniques have greatly increased our

knowledge and understanding of the nature of microplasticity which accompanies indentations.

Geometric similarity implies that, for pyramidal indenters, the hardness of a crystal should be independent of the normal load because the strain is constant. However, it is well established that under otherwise identical experimental conditions, the measured indentation hardness increases with a decrease in the normal load, and furthermore, the greater the intrinsic hardness the more marked this effect becomes. This phenomenon is now generally referred to as the *indentation size effect* (ISE) and has been confirmed in a number of materials including cubic boron nitride (cBN), silicon carbide, silicon, germanium, magnesium oxide and aluminium oxide. The ISE effect is often analysed by the relationship:

$$P = A\, d^n$$

where P is the load, d is the diagonal length of the impression, A is a constant and n, the stress exponent ≤ 2.

An explanation, based on finer slip with decreasing loads, was offered by Burnand (1974) as a result of observations made on a wide range of ceramic single crystals. He concluded that the spacing between active slip planes was not constant, but tended to decrease with reducing normal loads. The observation of geometric similarity between the dislocated zone and the decreasing size of the indentation was also established. He concluded that this produced a greater degree of strain and work-hardening within the dislocated zone with a correspondingly increased hardness.

Li and Bradt (1991) have subsequently related the effect to the multiplicity of slip systems and the work-hardening characteristics, and suggest a modified Meyer's law. Their normalised form of Meyer's Law provides a definition of a critical indentation test load and a characteristic indentation size. They further propose that ISE is due to the existence of "Newtonian-like *proportional specimen resistance*" which is composed of two components: (a) the elastic resistance of the test specimen, and (b) the friction at the indenter:specimen interface. The externally applied load is reduced by the indenter facet:specimen friction resulting in an overestimation of the effective test load and therefore an apparent reduction in the hardness.

For ideal plastic materials, the yielding beneath the indenter is often assumed to be perfectly homogeneous and continuous but this clearly cannot be so for single crystals because of the crystallographic constraints. Moreover, Bull *et al*, (1989) propose that the yielding is neither perfectly continuous nor uniform under the contact area and that this accounts for the ISE effect. They suggest that, ahead of the indenter, discrete bands of concentrated slip are initiated sequentially during the process of indentation. Their observation of visible lines at an average spacing, δ, formed by yielding or cracking at intervals, is characteristic of the material, grain size and surface finish. As the contact area grows under the increasing applied load, "yielding occurs at the outer edges of the contact area where the tensile stresses of the elastic field combine with the stretching imposed by the sloping faces of the indenter". On yielding, the local tension will be at least partly relieved and the contact area supported elastically. Further critical build - up of stress will eventually result in further yielding. On unloading, recovery of the elastic component of deformation associated with each of the slip bands reduces the final size of the indentation and hence gives rise to the apparent increase in hardness. They propose a quantitative model where the difference between the ideal diagonal length d_i and the recovered diagonal d_m is thought to be a function of the distance between these slip bands, δ. Their model results in the following equation:

$$H_m = H_0 \left(1 + \frac{\delta}{d_m}\right)$$

where H_m is the measured hardness at a given load, H_o is the hardness of the material at loads sufficiently high as to be outside the range of this effect i.e $d_m \gg \delta$, and is defined as $H_0 = k P d_i^{-2}$ where k is a constant (1854.4 for a Vickers indenter) and P is the applied load. The fit of their experimental results to this equation is impressive and the measured values of 1 to 10 μm spacing between the slip bands for several ceramic single crystals compare well with the derived values of δ. These concentrated slip bands may be directly comparable to features, termed *laths*, observed beneath impressions in diamond, and this is discussed in Chapter 4.

2.3 Modelling indentations in single crystals.

The Knoop indentation technique is particularly sensitive to small variations in hardness and has been used to establish the basic anisotropy of hardness of single crystals. The availability of suitable slip systems and the constraints imposed by the facets of the indenter on slip plane rotation are of some significance in the hardness measurement and a number of models have been developed to explain the anisotropy.

One of the first attempts was by Daniels and Dunn (1949) based on the equation of Schmid and Boas i.e. $\tau_c = P/A \cos\lambda \cos\phi$, where τ_c is the critical stress to initiate dislocation movement, $\cos\lambda$ is the angle between the stress axis and the slip direction and $\cos\phi$ is the angle between the stress axis and the slip plane normal. Daniels and Dunn (1949) selected a tensile stress axis parallel to the steepest slope of each indenter facet and modified the Schmid-Boas equation by including a constraint term, $\cos\psi$, to allow for the restricted rotation of slip planes during indentation. However, the predictions using this model were not always consistent with the results.

Brookes, O'Neill and Redfern (1971) concluded that the maximum constraint on slip plane rotation was not only defined by the axis of rotation being perpendicular to an indenter facet $(\cos\psi = 0)$, but also by the slip direction being parallel to the line of intersection of the indenter facet with the indented surface. They further modelled the process on the concept of a simple uniaxial tension parallel to the line of greatest slope in an indenter facet, or a line of compression perpendicular to it. The modifying function which reduces the effective resolved shear stress, due to rotational constraint, is $1/2\ (\cos\psi + \cos\gamma)$. The complete form of the effective resolved shear stress equation, ERSS, is:

$$\tau_c = (P/A)\cos\lambda\cos\phi\ \left[1/2\ (\cos\psi + \cos\gamma)\right]$$

where $\cos\psi$ is the angle between the indenter facet and the axis of rotation and $\cos\gamma$ represents the angle between the slip direction and a horizontal axis lying parallel to the

indenter face. The relationship between the angles involved in this model are reproduced in Figure 2.3. When resolved on to the available slip systems for each of the four indenter facets, the mean ERSS curve, as a function of indenter orientation, can be obtained from the maximum ERSS values for each of the four facets.

The mean ERSS curve predicts the nature of the anisotropy only, and a direct correlation between these values and the hardness number at a given orientation cannot be made. Nevertheless, the variation of 1/ERSS with indenter angle was found to correspond well with the variation in observed Knoop hardness in both metallic and non-metallic single crystals, including the hardness anisotropy of diamond, for a wide range of homologous temperatures, (Brookes, 1971).

The Brookes, O'Neil, Redfern or BONR model considers slip at the elastic:plastic boundary remote from the indenter facets. Roberts (1986) made a study of the 'extended' stress field produced by the indenter, in the form of a long flat punch, by resolving the elastic stress field onto the available slip systems. Results of this analysis are produced in the form of a list of resolved shear stresses on each slip system at regularly spaced points plus (i) a plot of the calculated resolved shear stress values for all the slip systems as a function of indenter angle on a single crystal plane and, (ii) a map of the most highly stressed slip systems in the crystal bulk under and around the indenter, with contours of resolved shear stress values. The slip patterns predicted by this model correspond well to those observed experimentally in cubic semiconductors.

2.4 The soft indenter technique.

The study of macroscopic dislocation movement in hard materials, such as MgO and TiC, has recently been extended by the use of softer indenter materials (Brookes *et al*, 1988). When the tip of a softer conical indenter is pressed against a harder surface, the resultant circular blunted contact area will grow until it is large enough to support the applied load elastically. Microdeformation of the harder material can occur when contact pressures are developed which are 10 - 100 times lower than the nominal hardness values. Control over the magnitude of the resultant mean contact pressure, P_m, can be exercised by using different materials for the indenter. Resolving a mean pressure, the *threshold*

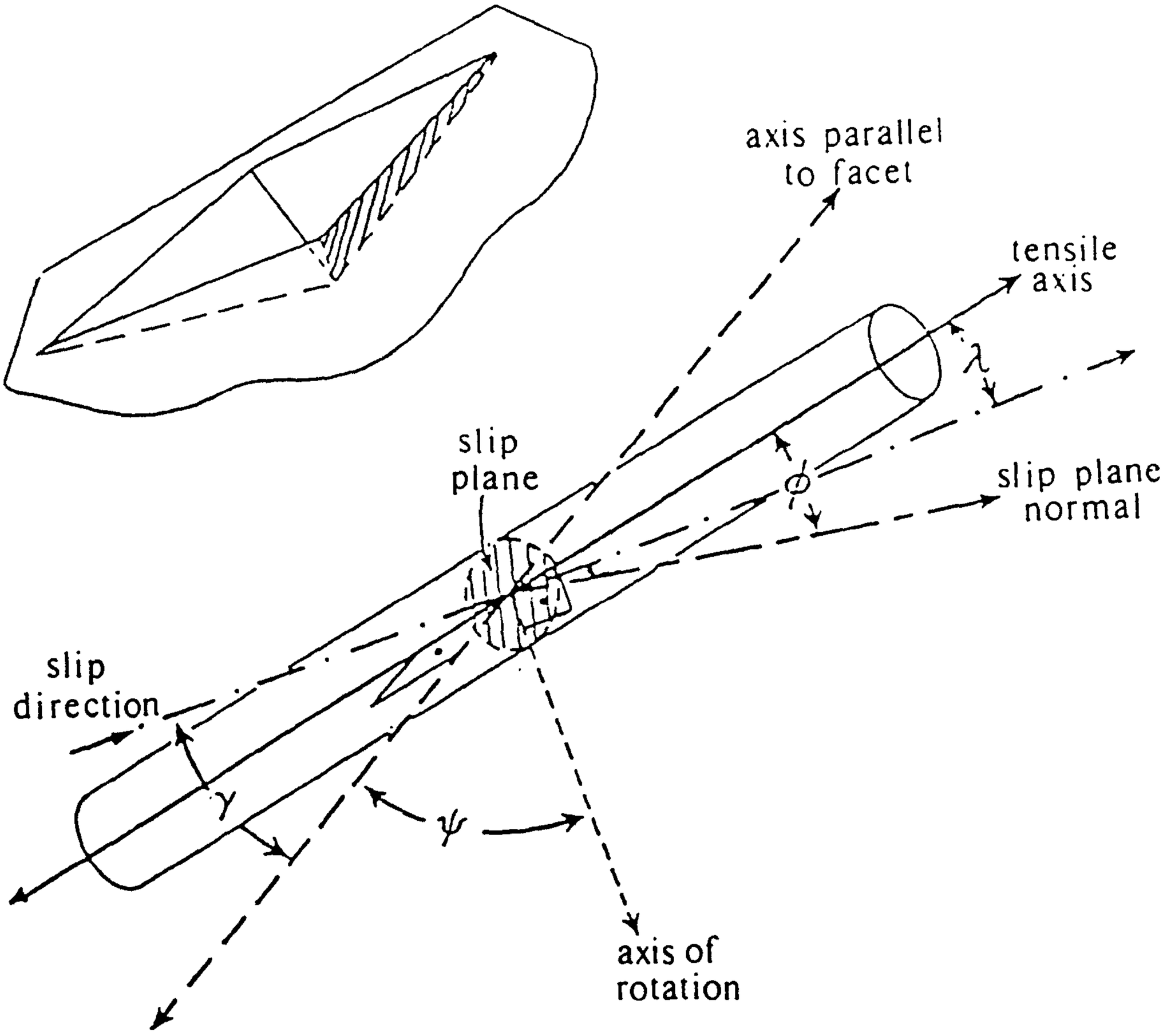

Figure 2.3 Schematic drawing to illustrate the Brookes, O'Neil, Redfern model, (Brookes *et al*, 1971).

pressure, P_m, which is only just sufficient to move a few dislocations on the active slip system will yield an estimate of the critical resolved shear stress for a particular crystal (see Chapter 3). Indenter materials producing higher levels of P_m, i.e. indenters made from materials of greater hardness, will move an increasing number of dislocations and produce a higher level of strain within the dislocated zone beneath the indenter.

Comparison of the room temperature (0.1 T_m) dislocation behaviour in response to a diamond indenter, and a copper indenter under otherwise directly comparable experimental conditions, was made by Brookes *et al*, (1987), on (001) MgO surfaces. The copper cones blunted as a result of the indentation process and no apparent damage was evident on the surface of the MgO. However, subsequent dislocation etching of the surface revealed some etch pits, although not sufficient to form a rosette. The dislocation configuration beneath a copper cone is shown in Figure 2.4(a) and can be compared with a steel cone, Figure 2.4(b), where the mean pressures were 0.7 and 4.5 GPa respectively. Note that dislocations lie predominantly on $\{110\}_{45}$ planes for the lower mean pressure and on both these and the $\{110\}_{90}$ planes at the higher pressure.

Subsequent serial polishing confirmed that the extent of the dislocation movement beneath a rigid diamond indenter was comparable to that beneath the 'soft' copper indenter. The dislocated volume formed beneath a point contact was shown to be directly related to the magnitude of the applied load but was independent of the mean pressure (Brookes and Green, 1972). The density of the dislocations within that volume, and therefore the effective, average or representative strain increased with the hardness of the indenter material until, approaching the hardness of conventional rigid indenters, cracks were initiated (Shaw and Brookes, 1989). The effective strain can also be increased if the normal load is repeatedly applied, leading to work-hardening, fatigue and fragmentation as in reciprocating sliding experiments.(Brookes *et al*, 1987).

The dislocated volume developed beneath both conventional rigid and soft indenters increases with dwell time so as to preserve geometrical similarity. With a continuously flattening 'soft' cone, and therefore a continuously decreasing mean pressure, the average level of plastic strain in the dislocated volume will decrease. It has been shown that this form of time dependent plastic flow continues in MgO whilst the mean pressure exceeds the threshold pressure. (Brookes *et al*, 1991).

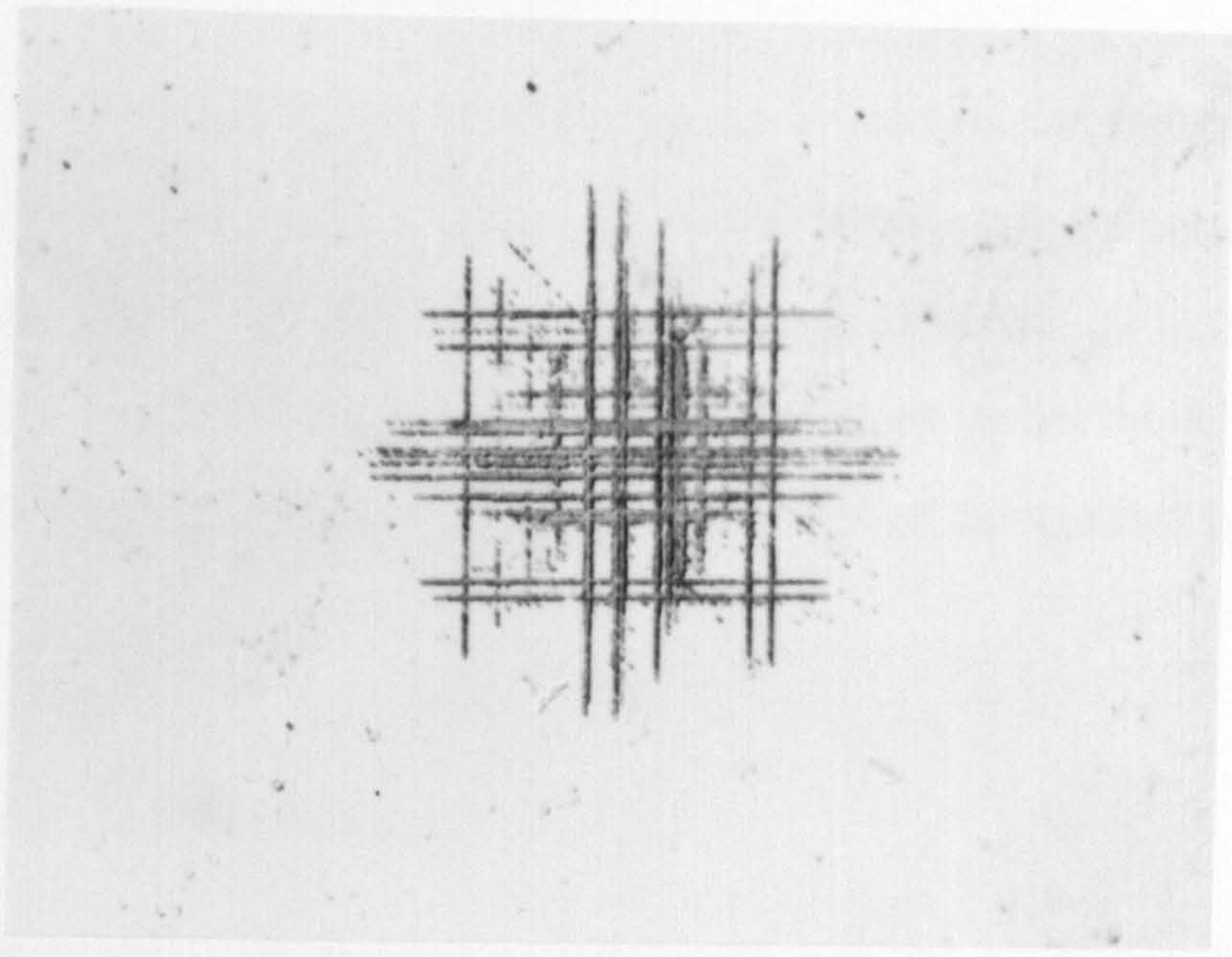

(a)

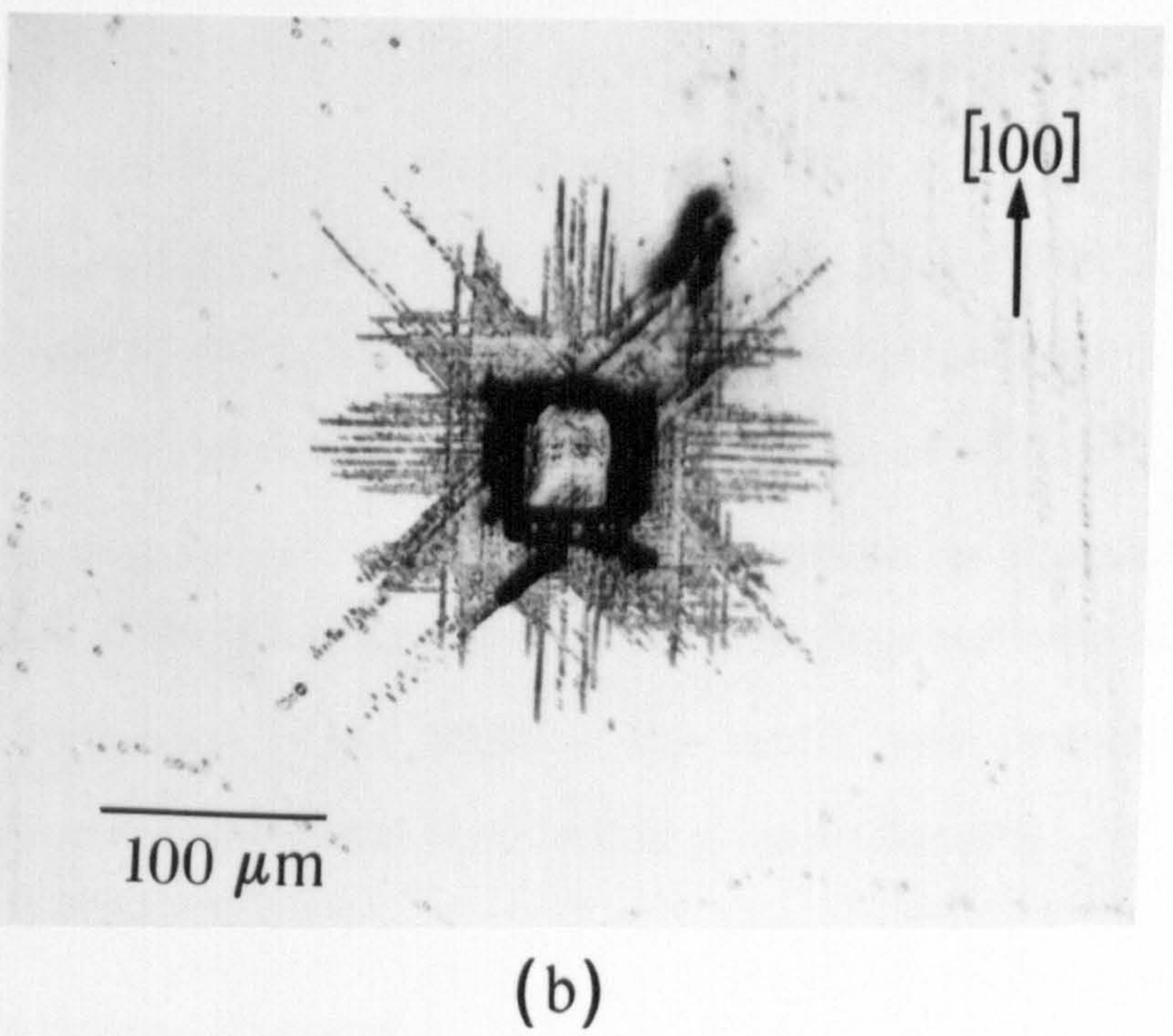

(b)

Figure 2.4 Etched dislocations produced on a (001) MgO surface at room temperature by: (a) a copper cone; (b) a mild steel cone.

2.5 Modelling the soft indentation technique.

Whilst most models of the indentation process indicate that the magnitude of the maximum resolved shear stress is about one third of the contact pressure, (Kelly, 1966), the most suitable model for soft indenters is that due to Roberts (1988). This will be discussed briefly for {110} ⟨110⟩ slip systems, in the light of earlier work on MgO, and in more detail for {111} ⟨110⟩ slip systems, in anticipation of the results presented later for diamond.

{110} ⟨110⟩ slip systems - eg MgO.

The predictions of the Roberts model for the case for a (001) surface of a single crystal with a {110}⟨110⟩ slip system is shown in Figure 2.5. Sections are taken normal to the surface and on the (010) plane, viewed in the [100] direction, Figure 2.5(a), and on the ($\bar{1}$10) plane, viewed in the [110] direction, Figure 2.5(b). The model predicts a maximum resolved shear stress, RSS, at a position beneath the surface at a depth of ≈ 0.60 of the contact radius, a, and 0.348 of the nominal pressure, P_m, for the (010) section, and at a depth of 0.65a and 0.345 P_m for the ($\bar{1}$10) section. Within the marked boundary, the maximum stresses are compressive and distributed equally on all $\{110\}_{45}$ slip systems. Outside this boundary the maximum resolved shear stresses are developed on the two $\{110\}_{90}$ slip planes. This is consistent with the radial displacement away from the contact area. Further verification of the details of this model, with particular reference to experimental evidence obtained with MgO, will be given in Chapter 3.

{111} ⟨110⟩ slip sytems - diamond.

Earlier work on diamond confirmed a simple method of introducing and controlling dislocations at low homologous temperatures (Brookes *et al*, 1988). Multiple slip was seen to occur as a result of the pressure transmitted using a cubic boron nitride (Amborite) cone of included angle 120°, at experimental temperatures of 1000°C, on the (001) face of a type Ia diamond. The cone flattened after a loading time of 300 seconds such that the

1. (1 1 0) [1 $\bar{1}$ 0]

2. (1 0 1) [1 0 $\bar{1}$]

3. (0 1 1) [0 1 $\bar{1}$]

4. ($\bar{1}$ 1 0) [1 1 0]

5. ($\bar{1}$ 0 1) [$\bar{1}$ 0 $\bar{1}$]

6. (0 $\bar{1}$ 1) [0 $\bar{1}$ $\bar{1}$]

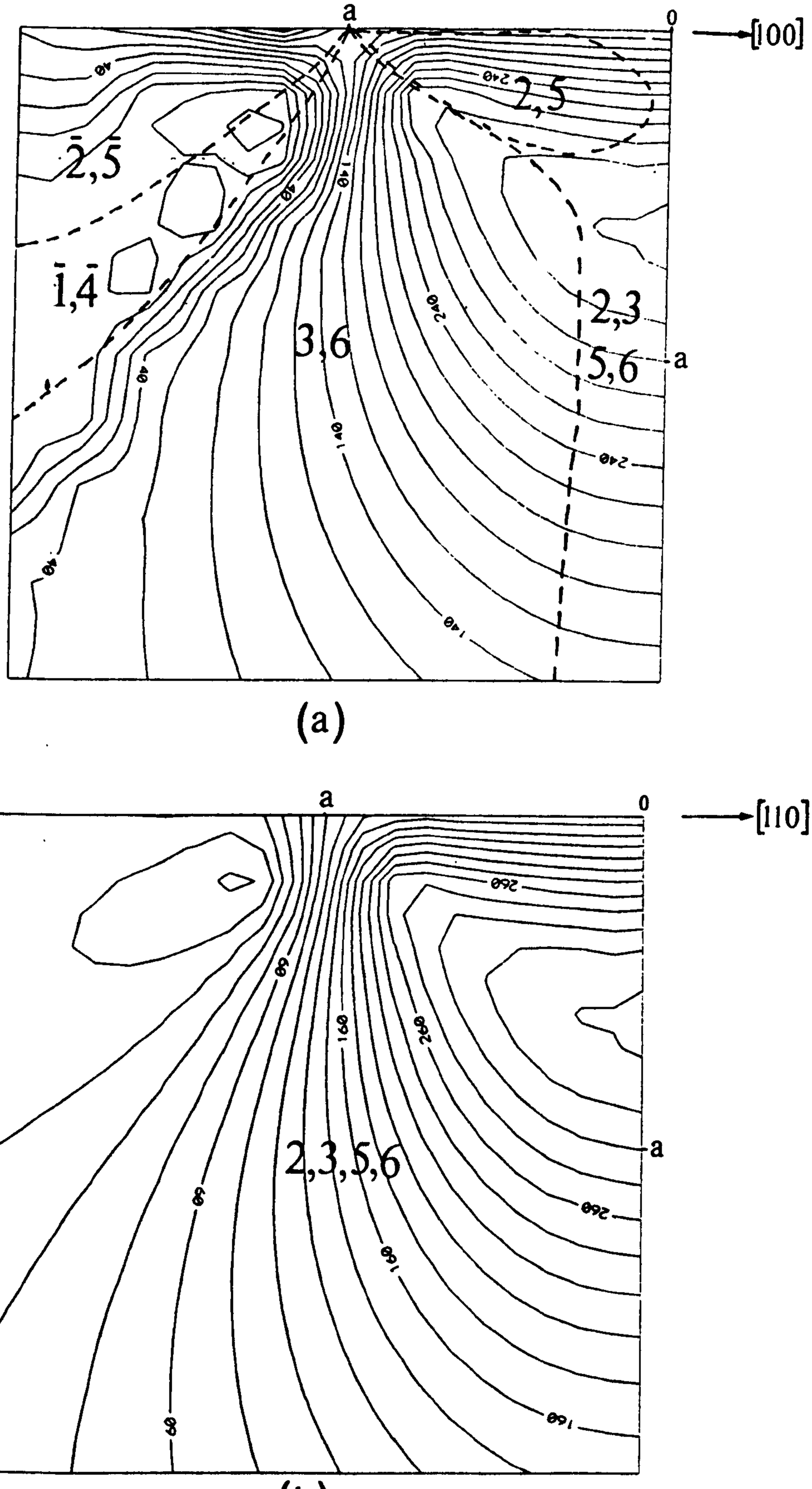

Figure 2.5 Resolved shear stress maps for (a) [100] section , (b) [110] section through a (001) surface for a crystal with {110} <1$\bar{1}$0> slip systems. Note, it is predominantly the $\{110\}_{45}$ slip systems which are activated.

applied pressure was ≈ 10 GPa. This pressure was sufficient to develop a large number of slip lines within the area of contact, directly comparable with those developed in MgO and consistent with multiple slip on the {111} ⟨110⟩ slip systems in this case. No fracture occurred under these experimental conditions.

The Robert's model for a uniformly loaded circular contact on a (001) surface of diamond, and resolved onto the twelve slip systems of the {111} ⟨110⟩ type, is reproduced in Figure 2.6. A plane section is taken normal to the indented surface passing through the centre of contact and is divided into regions where different slip systems are the most highly stressed. These are labelled and the negative values of RSS are indicated by a bar over the number. Roberts applied a simple convention for the labelling of slip planes where the positive side of the slip plane is always upwards with respect to the indented surface and the positive sense is always downwards. Therefore, a positive sense of RSS indicating shear is such that the top side of the slip plane should slip into the crystal and a negative sense will indicate that the underside of the slip plane will slip into the crystal. The contours shown are of the highest resolved shear stress RSS, irrespective of the slip system. The sections shown in Figure 2.6 are for (010) [100] and ($\bar{1}$10) [110] respectively The peak resolved shear stress in the (110) section is at x = 0.52a, z = 0.5a, with RSS = 0.30 P_m. For the (100) section, the peak is at x = 0.58a, z = 0.54a, with a RSS = 0.316 P_m.

It is worth noting here that the values of RSS immediately below the surface in the contact area are low, equal to 0.102 P_m, over the entire contact area. The slip systems with the highest RSS values under the contact area are those on the convergent slip planes, i.e. 11 and 12 in Figure 2.6. Outside the area of contact, at depth, the slip systems with the highest RSS are those with a slip vector parallel to the surface (i.e. 7 and 10), and near to the surface the highest RSS is on divergent planes (i.e 3 and 2). In other words, this model predicts that the maximum stress is ≈ 0.32 P_m for a (001) surface and {111} ⟨110⟩ slip systems and the maximum lies on a loop with a radius of 0.27a below the surface. This contrasts with the singular point of maximum RSS for the {110} ⟨110⟩ slip system shown in Figure 2.5 and this reflects the greater complexity of the {111} ⟨110⟩ slip systems in diamond.

1. (111) [$\bar{1}$10]
2. (111) [10$\bar{1}$]
3. (111) [01$\bar{1}$]
4. (1$\bar{1}$1) [110]
5. (1$\bar{1}$1) [10$\bar{1}$]
6. (1$\bar{1}$1) [0$\bar{1}\bar{1}$]
7. ($\bar{1}$11) [110]
8. ($\bar{1}$11) [$\bar{1}$0$\bar{1}$]
9. ($\bar{1}$11) [01$\bar{1}$]
10. ($\bar{1}\bar{1}$1) [$\bar{1}\bar{1}$0]
11. ($\bar{1}\bar{1}$1) [$\bar{1}$0$\bar{1}$]
12. ($\bar{1}\bar{1}$1) [0$\bar{1}\bar{1}$]

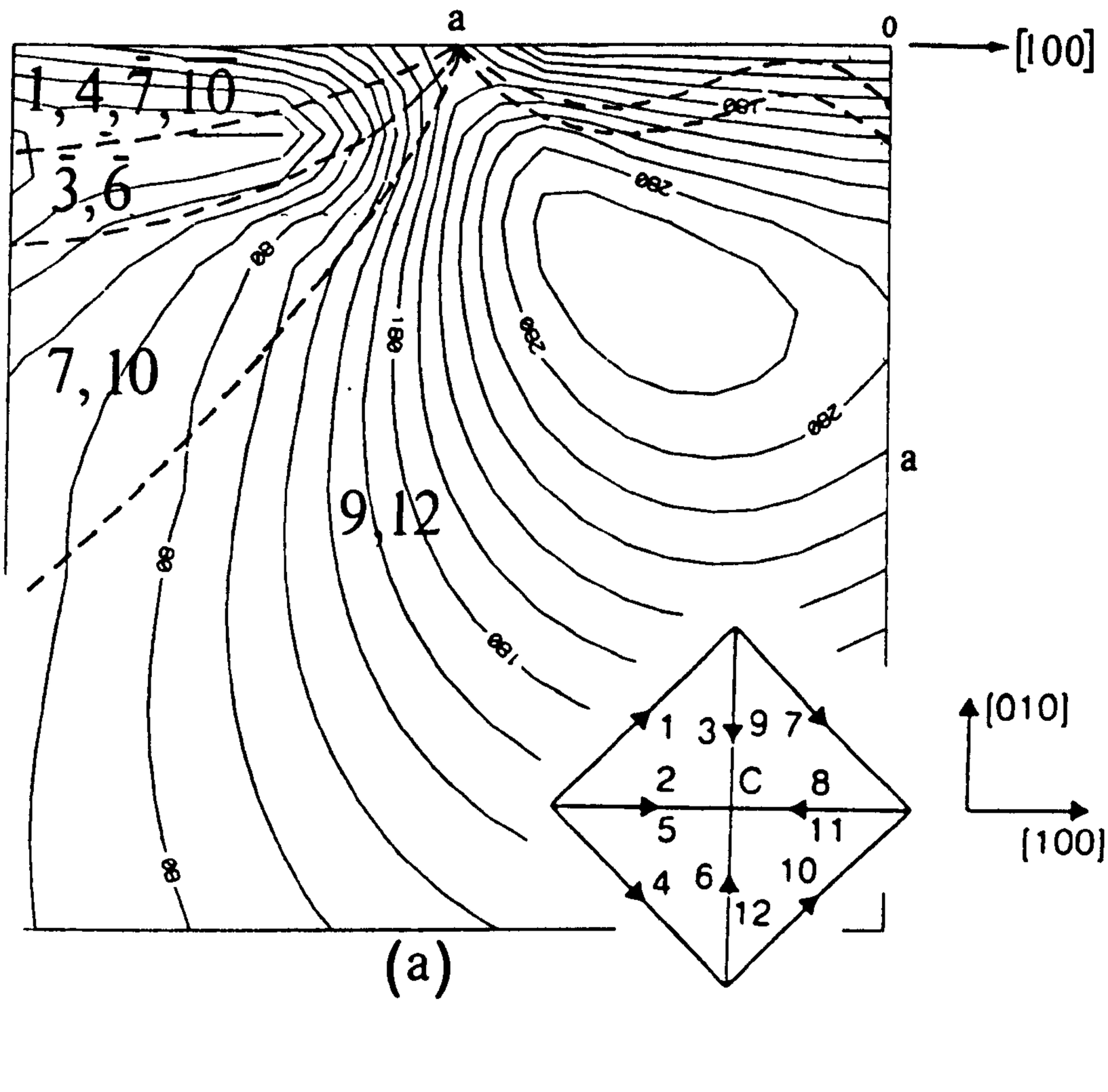

Figure 2.6 Resolved shear stress maps for: (a) [100] section;

(b) [110] section through a crystal with {111} <110> slip systems.

Note, it is predominantly the converging slip systems which are activated.

Clearly, the zone beneath the indented surface of a single crystal with the diamond cubic structure is anisotropic. The relative amounts of activity on the various slip systems will be controlled by internal stresses within the plastic zone as well as by the applied stresses. Nevertheless, the applied indenter stress patterns should provide a reasonable indication of the initial dislocation activity in a crystalline solid.

A family of {111} planes with dislocations having Burgers vectors of a/2 ⟨110⟩ describe a tetrahedron, therefore there are two tetrahedra relative to the indented plane of, say {111}, Figure 2.7(a). The slip plane tetrahedra are mirror images i.e. the triangular base of the tetrahedron may be (i) (111), with the apex of the tetrahedron below the surface, or (ii) $(\bar{1}\bar{1}\bar{1})$, with the base of the tetrahedron below the surface. The significance of these two tetrahedra of slip planes is that relative to an indenter penetrating the surface, dislocations move on either converging planes, A, diverging planes, B, or on planes parallel to the surface, shown in Figure 2.7(b). It can be seen from Robert's model that slip will occur on convergent {111} planes in the highly stressed region beneath the indenter and that slip will occur on divergent {111} planes in the region outside the area of indenter contact. Dislocation mobility on convergent planes will be limited by the formation of Lomer-Cottrell locks and will lead to a high rate of work-hardening, whereas dislocation mobility on divergent planes will be determined by the intrinsic lattice friction stress. Outside the indentation area there is a small region where slip systems containing dislocations with Burgers vectors parallel to the surface will have a slightly higher resolved shear stress than either converging or diverging slip systems and rosette slip will dominate in those particular regions.

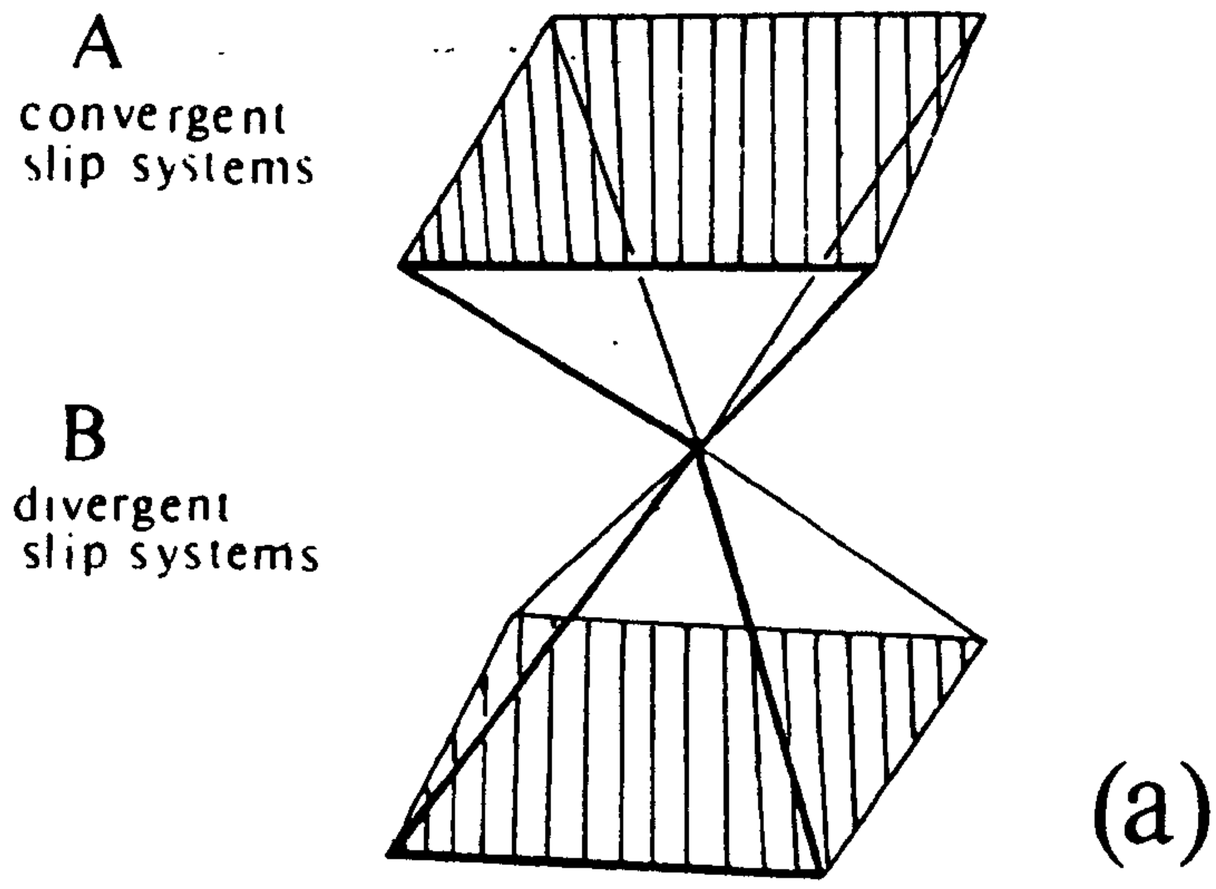

Figure 2.7 Resolved shear stress map for a [100] section through the (001) plane for the diamond cubic structure (given in Figure 2.6 (a)).

(a) the formation of tetrahedra by A - converging slip and B - diverging slip;

(b) schematic of the active slip systems beneath and adjacent to the contact area.

2.5 Summary

It has been shown that the response of crystals to the indentation process is primarily determined by their plasticity. A number of models based on resolved shear stress criteria have been established, and are reviewed in this chapter. The success of this approach is used to justify the relationship between the critical resolved shear stress and the hardness of a given material. However, with conventional rigid indenters, scope for developing a better understanding of plasticity is limited by a tendency to brittle fracture due to a high level of representative strain.

Similar modelling of the soft indenter technique, in which the representative strain can be controlled through selection of indenter materials, enables further information to be derived, eg estimates of the critical resolved shear stress.

Chapter 3. The critical resolved shear stress in diamond.

3.1 General considerations.

When conditions are such that cracks form, dislocation movement is pre-empted. Conversely, cracks are frequently initiated as a consequence of plastic flow and often as a result of dislocation interactions. The greater the difference between the flow stress and the fracture stress, the greater the possibility that plastic deformation will dominate in response to the applied stress. An indication of this can be obtained from the ratio of theoretical cleavage strength to the theoretical shear strength. This ratio is 1.69 for diamond compared with 2.34 for silicon, 4.55 for iron and 20.83 for copper (Kelly, 1966). The fact that the measured value of the cleavage energy is only slightly greater than the theoretical value for diamond suggests that little, if any, dislocation movement occurs in the stress field at the crack tip. The actual fracture strength of diamond is dependent on defect size and even good quality diamonds have sharp ended defects of about 0.5 μm long (Field, 1984).

For a plastically isotropic solid, the onset of plastic flow will occur at a point within the specimen where the principal shear stress is highest. An ideally plastic solid will not work harden and there will be no difference between the yield stress and the flow stress at increasing levels of strain. However, plastic behaviour in single crystals is highly anisotropic; work-hardening is likely; and the stresses around an indentation are extremely complex such that the Tabor relationship is not a reliable guide to the yield strength. The hardness of single crystals is greatly affected by the constraints imposed by the limited number of slip planes and a *critical resolved shear stress* criterion, namely the stress required to activate dislocation sources on the most favourably oriented slip plane.

In a single crystal, the hardness, H, will be related to the resolved flow shear stress, τ_f, by $H = C\,\tau_f$, where C is a constant dependent on the indenter geometry, orientation and the crystallography of the indented material. τ_f represents the sum of the critical resolved shear stress at yield τ_c, and the stress needed to overcome the work-hardening due to enforced dislocation motion on intersecting slip planes during deformation.

Westbrook (1973) determined that for many single crystals there is a large discrepency between the average hardness and the yield stress and that the ratio H / Y is of the order of 35 rather than 3 as in polycrystalline materials. Analysis of the work-hardening process suggests that the material property most likely to influence the critical resolved shear stress is the shear modulus, G, (Gerk, 1977). Data for hardness, τ_c and the shear modulus of various materials is given in Table 3.1.

Tensile or compressive stress:strain curves for well annealed single crystal metals have a simple form. Yield occurs at relatively low stresses (10-4 G) and, for favourable orientations, shear occurs on parallel slip planes leading to a low rate of work-hardening (Stage I). At increased levels of strain, more slip planes become available with an accompanying increase in dislocation activity, intersecting slip and the shear stress increases almost linearly with strain - Stage II work-hardening. In the indentation process, the onset of Stage II dominates the behaviour and Stage I will be almost non-existent for all orientations. With materials such as f.c.c. metals and alkali halides:

$$\tau = \frac{G}{250}$$

A plot of hardness against G for a number of single crystals is given in Figure 3.1 and it can be seen that for f.c.c metals and alkali halide crystals:

$$H \approx 10^{-2} G$$

but for covalent solids:

$$H \approx 10^{-1} G$$

The high H / G ratios for covalent crystals indicate that pressures approaching the theoretical shear strength are developed beneath the indenter and dislocation sources might well be created rather than existing dislocations propagated. Such homogeneous nucleation of dislocations normally occurs at about 3 x 10-2 G, which corresponds to a resolved shear stress of about 16.8 GPa for diamond. In silicon and germanium, where τ_c can be measured, dislocation movement occurs at about 3 x 10-4 G, about 0.017 GPa. Slip has been observed in diamond at elevated temperatures, at a similar fraction of the shear modulus, G, indicating the possibility of significant dislocation movement at those

Table 3.1. Ratios of shear modulus, G, hardness, H, and critical resolved shear stress, τ_c.

crystal	H / G	H / τ_c	τ_c / G x 10^{-4}
diamond	0.16	26 (0.35Tm)	46
Si	0.16	117 (0.6Tm)	2.3
Ge	0.14	113 (0.6Tm)	2.3
SiC	0.14	200 (0.5Tm)	3.9
TiC	0.12	30 (0.35Tm)	7.5
MgO	0.07	117 (0.1Tm)	6.0
LiF	0.03	500 (0.2Tm)	0.6
Cu	0.013	400 (0.22Tm)	0.3
Ag	0.015	300 (0.22Tm)	0.5
Al	0.008	200 (0.31Tm)	0.4
Pb	0.01	167 (0.49Tm)	0.6

(G for diamond is 545 GPa at 273K)

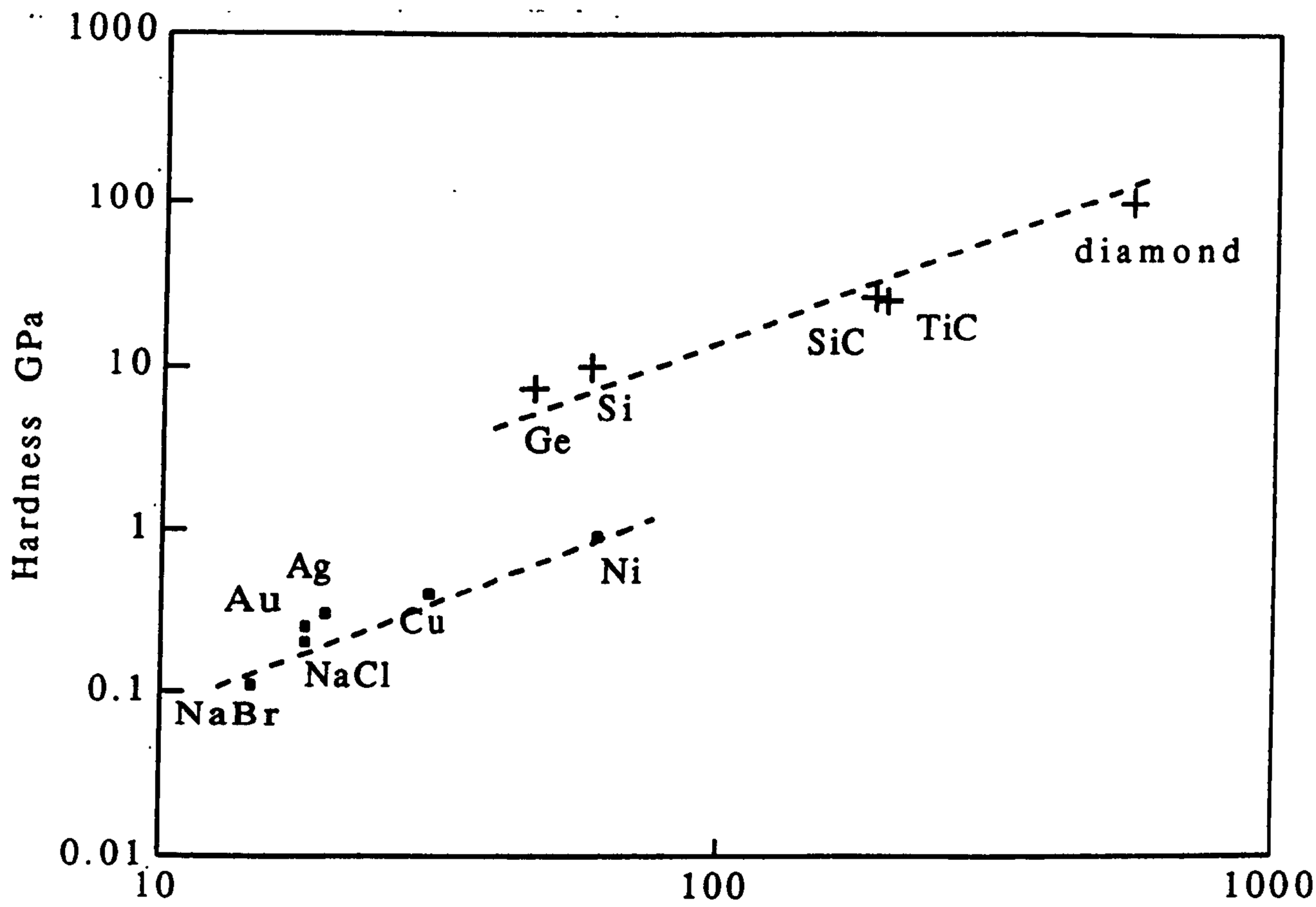

Figure 3.1 - Hardness vs shear modulus for different materials.

temperatures. However, the high τ_c / G ratio suggests that dislocation movement will be difficult. Low values of the H / τ_c ratio (resolved shear stress structure factor) for covalent crystals may indicate that, compared with metals and ionic solids, τ_c may play a more important role in the determination of the hardness than the associated degree of work-hardening.

The τ_c in covalent solids tends to decrease exponentially with temperature (Kelly, 1966), whereas the fracture stress is basically independent of temperature. Traditionally, τ_c is evaluated from uniaxial stress:strain curves or bending experiments but such methods are not well suited to the study of diamond. Indentation techniques have been used to identify the temperature at which the stress required for plasticity becomes less than for fracture i.e. the brittle ductile transition temperature (Hirsch *et al*, 1989), but the hardness test in its standard form does not permit the evaluation of a critical resolved shear stress. However, the soft indenter approach can be adapted for such purposes as demonstrated by the work of Brookes *et al* (1988).

The main advantages of this technique may be summarised:-

1. Soft indenters ensure that stress concentrations are not developed at the tip of sharp indenters or in the peripheral contact of rigid spherical indenters, such as to produce cracking.

2. The maximum resolved shear stress is developed beneath the surface, minimizing the effect of surface defects, under essentially compressive forces.

3. Data can be obtained from small specimens and volumes, reducing the probability of a few random but effective stress concentrators dominating the behaviour.

4. Where available, etch pitting techniques may be used as a very sensitive indicator of the onset of dislocation mobility.

The main disadvantages of applying the technique to diamond is that there is no suitable dislocation etchant available. Consequently, the onset of plastic deformation has to be identified through the development of visible slip steps on the deformed surface. Therefore, estimates of the critical resolved shear stress based on this approach are likely to be somewhat high.

The application of the soft indenter technique for the determination of the critical resolved shear stress in MgO.

A demonstration of the application of this technique is best given by the experimental work on MgO single crystals reported by Shaw and Brookes (1989). There, the mean contact pressure necessary to produce localised plastic flow, without fracture, was directly related to the critical resolved shear stress of MgO. A dislocation etchant was used to reveal the distribution and density of dislocations produced by initially sharp indenters of softer materials. The degree to which the indenters flattened under load was found to be inversely proportional to the nominal hardness of the indenter material. In those tests, cadmium produced a few dislocations, indicating that the threshold mean pressure for dislocation nucleation was close to the value of the mean pressure developed by that material. Dislocations were consistently produced by all of the harder materials used i.e. zinc, aluminium, copper, 70/30 brass and EN33 steel. The dislocations developed by all the materials except the steel were confined to a small number of discrete {011} planes, all inclined at 45° to the (001) surface, and directly below the contact area, with no region of high dislocation density. The steel indenter also induced slip on the $\{110\}_{90}$ in addition to slip on the $\{110\}_{45}$ planes. The dislocations on the $\{110\}_{90}$ slip planes did not penetrate into the crystal to the same depth as dislocations on the $\{110\}_{45}$ slip planes. Additionally, the depth of the dislocations developed beneath the contact area was considered to be only very slightly dependent on the hardness of the cone material and the extent of dislocation movement was determined by the normal load - rather than the mean pressure developed.

The critical resolved shear stress in MgO was known to be between 0.049 and 0.069 GPa for deformation in uniaxial compression at room temperature (Groves and Kelly, 1964). The Roberts model predicts a maximum resolved shear stress of 0.35 P_m for a (001) surface with a {110} ⟨110⟩ slip system, shown in Figure 2.5, and this maximum is located at 0.33 of the radius of the contact area beneath the surface. In the work by Shaw and Brookes (1989), the threshold mean pressure developed by cadmium was 0.17 GPa,

giving a τ_c of 0.060 GPa, which is in good agreement with the experimental value of Groves and Kelly. Mean contact pressures of $\approx$0.17 GPa, obtained beneath blunt cones made from even softer cones, did not initiate dislocation movement.

A variation of this method, to determine the threshold contact pressure and hence estimate τ_c for MgO, was undertaken. Increasing the dwell time, for a given normal load, caused a reduction in P_m due to time dependent plastic deformation of the indenter material. Brookes *et al,* (1991) monitored the increase in contact area with dwell time using a pure aluminium cone to deform a (001) surface of MgO. The initial blunting developed a mean pressure of 0.25 GPa with a normal load of 1 kgf and a dwell time of 300 seconds. The dwell time was then increased to enable creep of the aluminium so as to reduce the mean contact pressure continuously. The crystal was etched at regular intervals, and the mean contact pressure was determined to confirm that it was still sufficient to move dislocations. New dislocations were observed whilst the contact pressure was above 0.20 GPa but, after 10^5 seconds, the aluminium cone developed a mean contact pressure of 0.15 GPa and further expansion of the dislocated region stopped. No dislocations were evident in the contact region when this particular flattened cone was then used on an undeformed part of the crystal surface. Clearly the threshold pressure to initiate dislocation movement in magnesium oxide at room temperature was between 0.2 and 0.15 GPa, consistent with the earlier work. This demonstration is of particular relevance to the study of diamond, using the soft indenter technique, since the range of candidate cone material is especially restricted.

3.2 Experimental procedure for measurements on diamond.

These experiments were carried out in the apparatus which is illustrated in Figure 3.2. The diamond specimens were mounted on a graphite anvil such that the horizontal flat surface was uppermost and could be deformed by an indenter located in the turret. The bottom of the graphite anvil was secured in a water-cooled copper hearth and the top of the graphite anvil was situated within a radio-frequency induction coil. Translation of the hearth along both the *x* and the *y* direction, and rotation of the turret, allowed numerous indentations to be made under controlled experimental conditions. The apparatus was

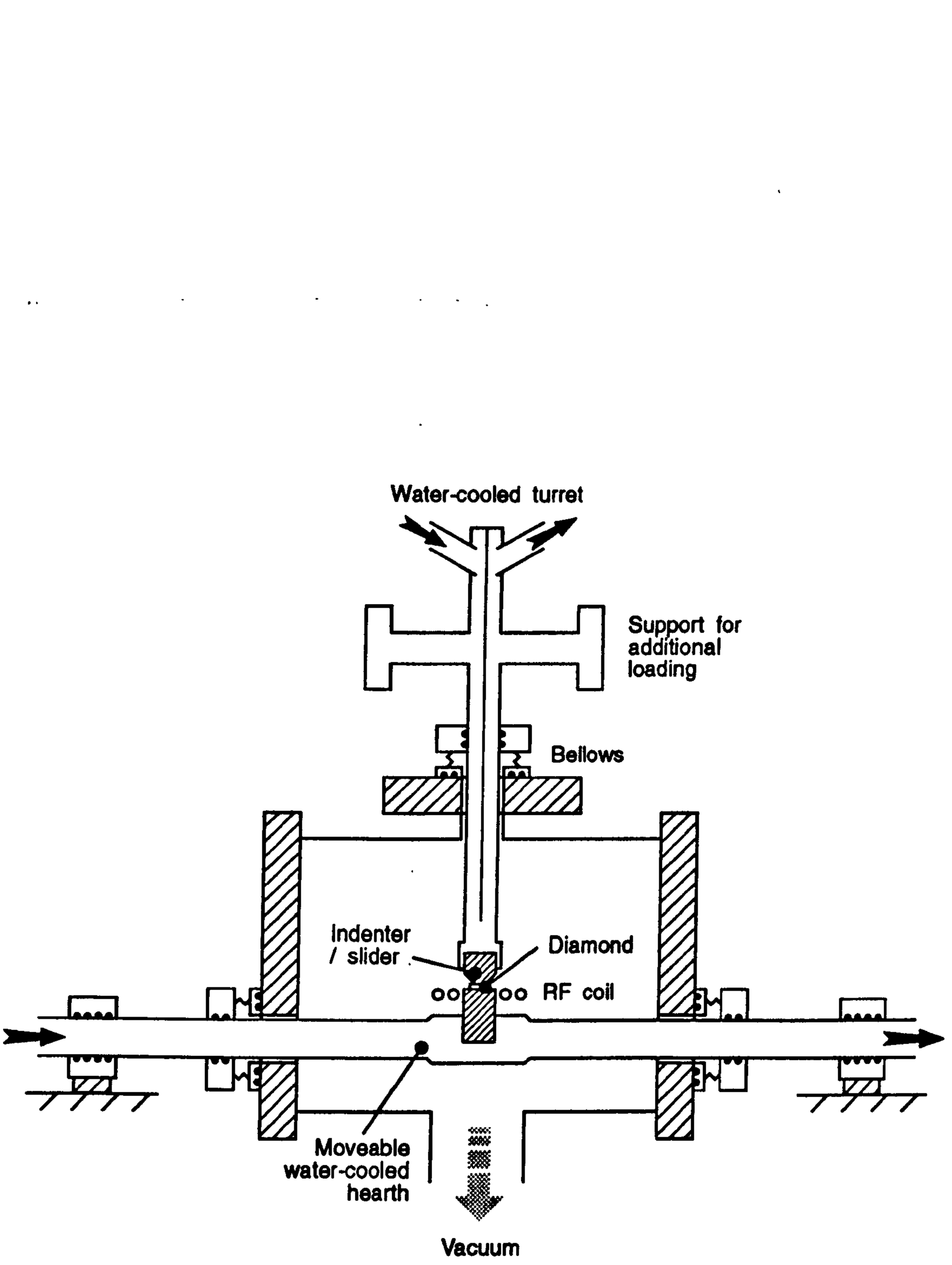

Figure 3.2 Schematic of high-temperature apparatus

contained within a chamber which was evacuated, typically to 10-5 mbar, and the graphite anvil directly heated by the radio frequency induction coil, using a 30 kW, 450 kHz generator. The surface temperature of the specimen was monitored using an optical pyrometer and an accuracy of ± 25° C was established by comparison with a direct contact thermocouple.

Depending on which chamber was used, when the constraint on the turret was removed, a normal load of 100 N or 115 N was developed between the cone and the flat specimen, due to the difference between atmospheric pressure and the vacuum within the chamber. This was monitored by substituting a load cell for the specimen and a flat plate for the cone. The normal load was increased by the addition of weights directly onto the frame of the turret, or decreased by partially counterbalancing the weight of the turret with extra weights.

The pressure developed between indenter and specimen was evaluated from measurements of the contact area on the diamond and the flat developed on the tip of the indenter, using standard optical microscopy techniques. Direct phase detecting interferometry was used to measure the change in surface topography as a result of an applied mean pressure, with the result that both the area of deformation and the displaced volume of diamond, for a given set of experimental conditions, could be measured.

The diamonds used in this work were supplied by De Beers with the exception of the isotopically enriched diamond made by General Electric, discussed in Chapter 6. Most of the diamonds had been polished with some parallel surfaces. This provides the optimum geometry for producing a round flat on the end of the indenter and a symmetrical impression. Most of the impressions, unless otherwise stated, were made on (001) surfaces. This is one of the easier planes for the diamond polisher to produce and the emergent slip line pattern, the result of the intersection of the four planes of the {111} ⟨110⟩ tetrahedron with the surface, is both symmetrical and useful. The quality of the polished surface varied from specimen to specimen however, and this is apparent in the micrographs. Whilst the degree of surface roughness might well affect the friction and adhesion between the indenter and the specimen surface, this does not significantly affect the plasticity.

Basic errors will have arisen from several sources. Random errors will have occurred largely through sample variation, and systematic errors, inherent in the instrumentation or as a result of the way in which the instruments were used, will always be present. The significant errors in this study include:

(i) The temperature measurement. The optical pyrometer can measure a temperature to an accuracy of 5°C, but the sight glass may decrease the measured temperature by up to 20° C. The overall uncertainty was estimated to be 2.5% at 1000° C.

(ii) The normal load. The sensitivity of the load cell used in the calibration of the applied load was ± 0.3 in 100 N, whereas the change in applied load due to pressure variation as a result of a change in vacuum, of 10^{-4} to 10^{-7} mbar, was determined to be less than 0.1 N over the pressure range.

(iii) The observation of the precise area of contact and the method of determining that contact area. Measurements of contact areas were originally taken from photographs by "square counting". However, direct measurement on the Nikon Optiphot microscope, where an accuracy of ± 0.3 μm was possible, was eventually selected as the standard procedure. The deviation between the two methods was determined to be insignificant, but it was considered that a routine for direct, self consistent measurement would be more reliable, than developing and printing photographs, where operator errors could be considerable.

(iv) Different observers may vary in their individual hardness measurements, however Ross (1985) has shown that a scatter of less than ± 6% is typical for experienced observers.

The combined errors for pressure measurement are estimated to be about 6%, and for the temperature measurement at about 2.5%.

3.3 Results

A limited range of ceramics were available from which to make 'soft' cones for use as indenters in the investigation into the deformation of the three different types of diamond, namely type IaAB, synthetic type Ib and type IIa. Table 3.2 lists those materials, with the corresponding mean contact pressures, and their respective indentation hardness

values, at the experimental temperature of 1000°C. In general, indenters made from ceramic materials with a nominal hardness greater than 20 GPa at room temperature will develop a mean pressure sufficient to exceed the critical resolved shear stress of diamond at experimental temperatures above which dislocations move easily through the lattice. Oxides and metals likely to form carbides were not considered as suitable indenter materials for this study.

The Knoop hardness of diamond at 1000° C is ≈70 GPa (Harrison, 1973, Trefilov *et al*, 1975) and hence all the indenter materials used are considerably softer than diamond over the experimental temperature range.

Impressions were made in all three types of diamond in the temperature range 20 to 1600° C, using cones made from the materials listed in Table 3.2.

Between room temperature and 450°C, the contact pressure developed by the cubic boron nitride cones on (001) surfaces of all the types of diamond decreased from about 20 to 11 GPa. Spiral ring cracking was produced, with no evidence of slip lines. Above 450° C, ring cracks were no longer formed, but there was still no evidence of slip lines. Frequently, however, the appearance of the indented area was 'dimpled' and could be seen quite clearly. Dislocation movement cannot be ruled out in this temperature and applied pressure range, but no macroscopic evidence was found.

The minimum temperature at which visible slip lines were observed was 770° C in type Ib synthetic diamond using a cBN cone, P_m = 12 GPa. This so-called brittle-ductile transition temperature was established as 950° C for type IaAB diamond, with a P_m = 9.5 GPa, and 1100° C for type IIa diamond, with a P_m = 5.5 GPa. These then are the conditions for the onset of macroscopic slip, i.e. the mean contact pressure necessary at the minimum temperature. Cones made from other ceramic materials also induced plastic deformation in diamond. The mean contact pressures developed by some of the materials used in the temperature range 750 - 1300° C are summarised in Table 3.3. for the three type of diamond studied. The crosses in the table indicate that the pressures developed by that particular indenter material were insufficient to cause macroscopic plastic deformation.

Figure 3.3 shows the variation in mean pressure with temperature, for cBN, Si_3N_4 and TiB_2. The range of mean pressures using a cBN indenter was achieved by permitting

Table 3.2 The mean pressures developed by various materials under an applied load of 100N and their hardness values, at 1000°C.

	Pm (GPa)	**HK** (GPa)
cBN	9.0 GPa	18 GPa
B4C	6.5 GPa	
Si3N4	5.7 GPa	10 GPa
TiB2	4.2 GPa	5 GPa
TiC	2.6 GPa	6 GPa
Ir	1.5 GPa	

Table 3.3 The mean pressures, GPa, and temperatures to develop plastic deformation in type Ib, type Ia and type IIa diamond.

temp. °C	**770**	**950**	**1000**	**1100**	**1200**	**1300**
type Ib:						
cBN	12	10	8.5	7.3	6.7	5.1
B4C	x		7.5	6.0	5.0	4.3
Si3N4	x	x	4.0		3.7	3.4
TiB2	x	x	3.7	3.8	3.0	3.0
TiC	x	x	2.6			
type Ia:						
cBN	x	9.5	8.5	7.4	6.6	5.1
B4C	x	x	6.5	5.5	5.0	4.3
Si3N4	x	x	5.7		3.7	3.4
TiB2	x	x	x	3.8	3.0	3.0
TiC	x	x	x	x		
type IIa:						
cBN	x	x	x	7.0	6.5	4.8
B4C	x	x	x	5.5	5.0	4.0
Si3N4	x	x	x		3.7	
TiB2	x	x	x	x		3.0
TiC	x	x	x	x		

x - indicates no slip was observed.

indicate no experiment.

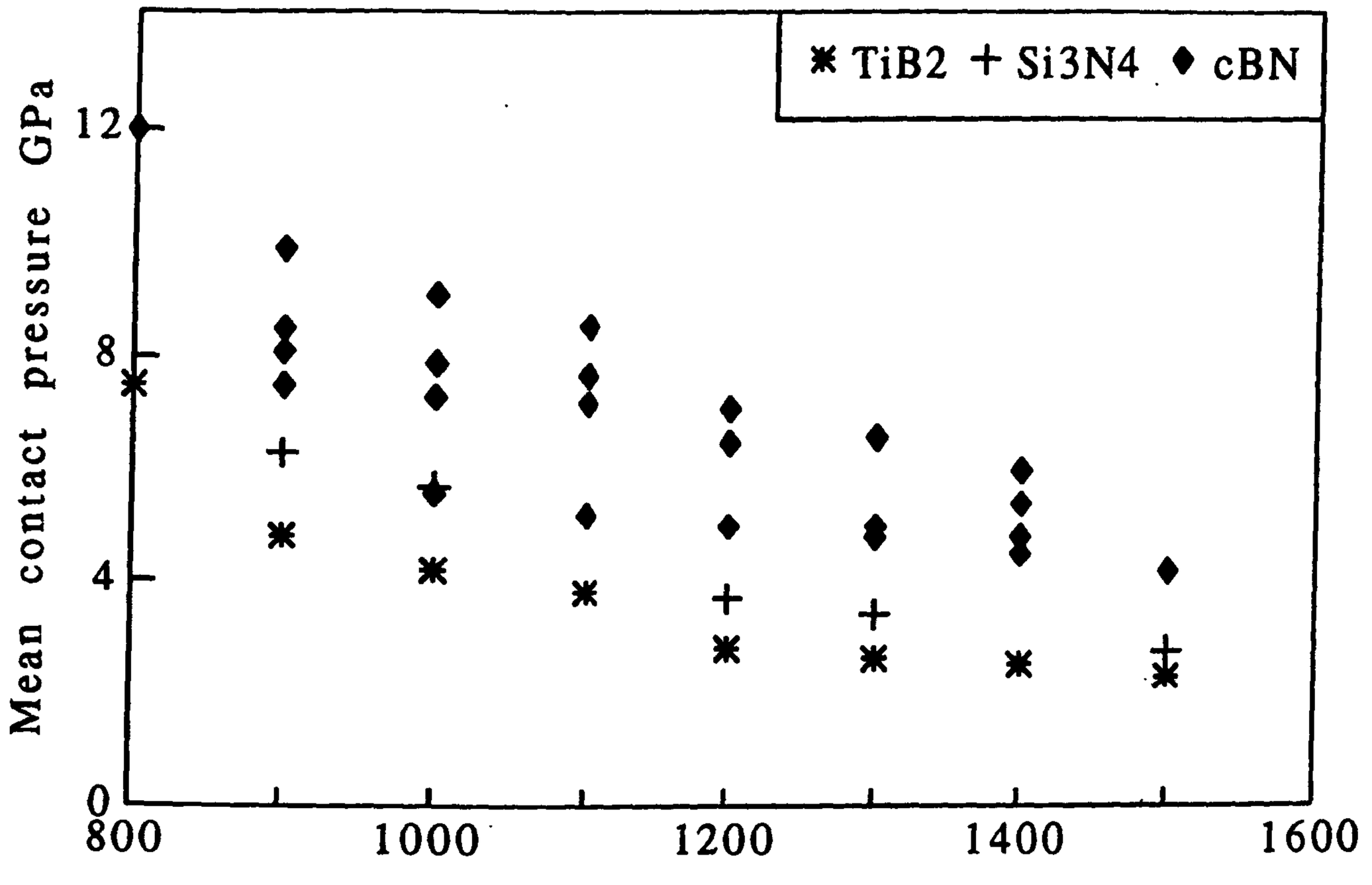

Figure 3.3 - The mean pressure for different indenter materials. The range is obtained by different dwell times.

the indenter to deform due to creep processes. By using a deliberately flattened indenter instead of a sharpened cone, an increased range of mean pressures is available to investigate the onset of plastic deformation at a given temperature. An alternative method for producing a flat indenter with an increased contact area and therefore a reduced contact pressure, is to flatten the indenter at an temperature up to 200° C higher than the experimental temperature. By utilising both of these flattening methods a comprehensive range of mean contact pressures was achieved.

The 'softest' material used in this study to produce a plastically deformed impression in diamond, was TiC, on type Ib diamond. The mean pressure developed using this indenter was 2.6 GPa at 1000° C. However, slip was not observed in type Ia or type IIa diamond under otherwise exactly the same experimental conditions.

A cone made from iridium developed a mean contact pressure of 1.5 GPa, and this was found to be too low to produce plastic deformation in any form of diamond, in the temperature range 900 - 1200° C. As a result of this experiment, a minimum mean contact pressure was established within that temperature range.

Mean pressure against temperature, for the three different types of diamond studied, is given in Figure 3.4 for type Ib, Figure 3.5 for type Ia and Figure 3.6 for type IIa diamond. The points on curve A represent contact pressures where slip lines were not visible. Therefore, below curve A macroscopic plastic deformation in diamond was not observed. The points on curve B represent the contact pressures where slip was visible and above which multiple slip was observed. The area between the curves represents a region of uncertainty within which the threshold mean pressure, P_m, for the onset of macroscopic plastic deformation lies.

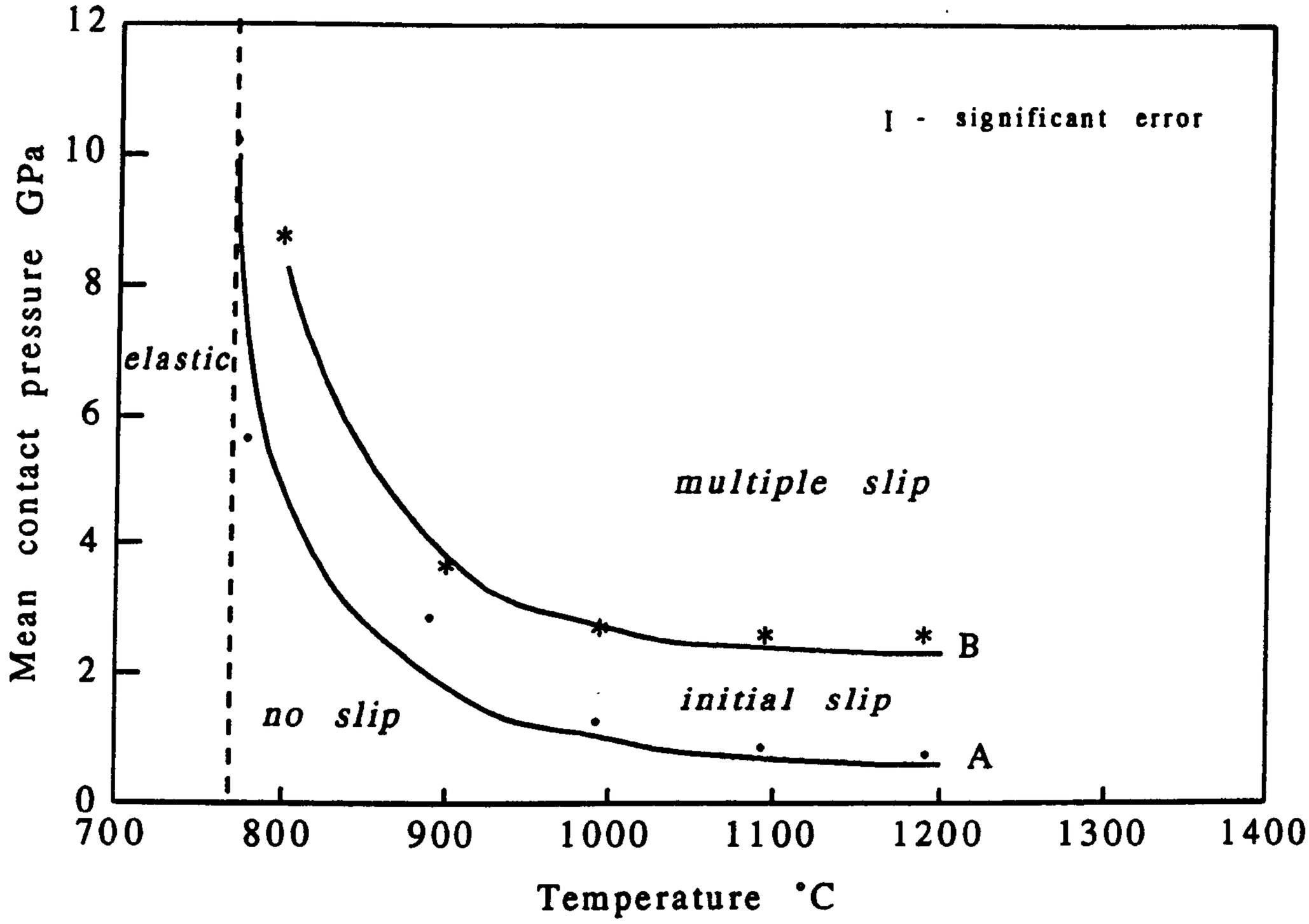

Figure 3.4 - Illustrating the pressure range within which slip is initiated in type Ib synthetic diamond.

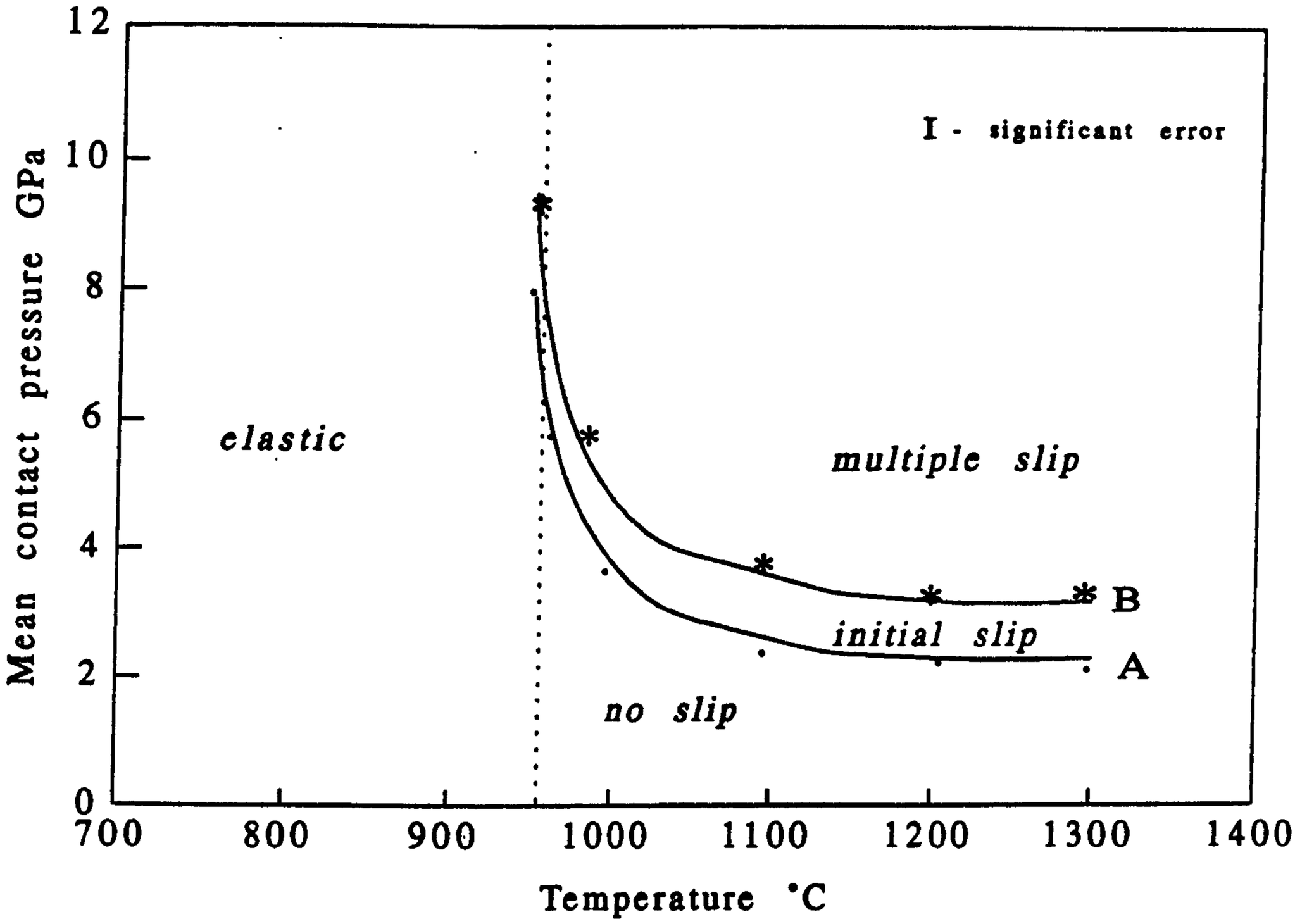

Figure 3.5 - Illustrating the pressure range within which slip is initiated in type Ia natural diamond.

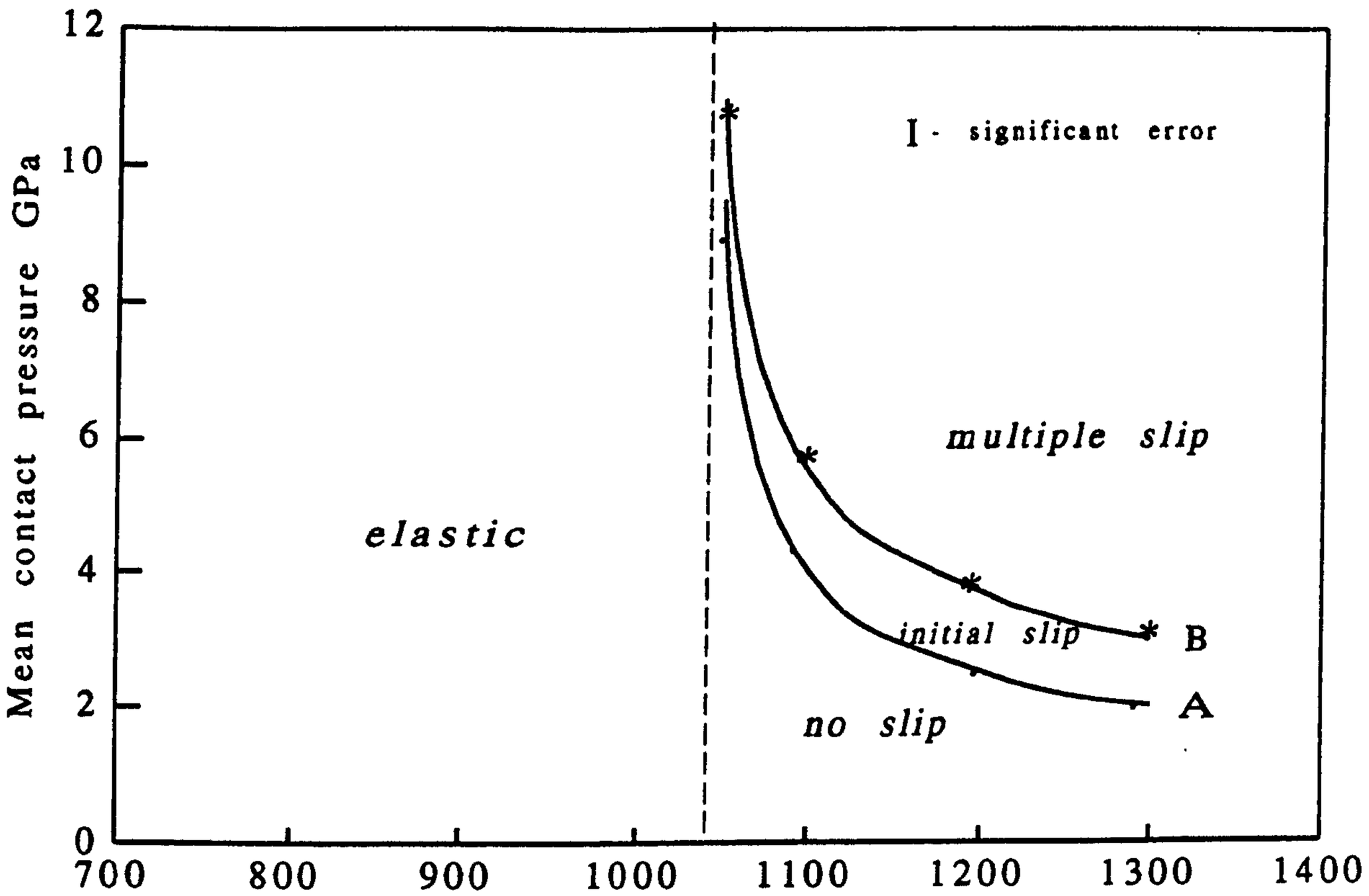

Figure 3.6 - Illustrating the pressure range within which slip is initiated in type IIa natural diamond.

3.4 Discussion.

Categorically, on the basis of these results, certain conclusions can be made concerning the plastic deformation of different types of diamond. Firstly, it is clear that the movement of dislocations is first initiated at different temperatures:

type Ib: at 770°C, $P_m = 12$ GPa;

type Ia: at 950°C, $P_m = 9.5$ GPa;

type IIa: at 1100°C, $P_m = 5.5$ GPa.

Secondly, that there is a rapid decrease in the threshold pressure, P_m, which occurs at increasing temperatures:

type Ib → type Ia → type IIa.

Finally, at a given temperature at which plastic deformation occurs readily in all types, the magnitude of P_m increases in the same order, eg at 1100°C:

type Ib: $\tau_c = 1.0 - 4.1$ GPa

type Ia: $\tau_c = 2.6 - 5.0$ GPa

type IIa: $\tau_c = 5.0 - 10.3$ GPa

Using these measurements of P_m in conjunction with the Roberts model (Figure 2.6) the critical resolved shear stress can be estimated and the corresponding values of τ_c are summarised in Table 3.4. The results for type Ia diamond, from 1000 - 1400° C are shown in Figure 3.7 and can be compared with those due to Trefilov *et al* (1988) which were based on measurements in the temperature range 1600 - 2000° C using three point bend tests. The correspondence in the results of these independent studies is convincing. In contrast, values of critical resolved shear stress for diamond at 1800°C of $\tau_c = 1.2$ GPa for type I and 0.48 GPa for type IIa diamond, reported by Evans and Wild (1965), are significantly higher than those obtained in this work or by the Russian workers.

However, it should be noted that the mechanical behaviour of covalent solids is highly strain rate dependent. Trefilov *et al* (1988) determined that, for three point bending, loading rates in excess of 0.25 GPa s^{-1} resulted in brittle failure whereas slower

Table 3.4 Estimates of the critical resolved shear stress (GPa) between 700° and 1400°C.

°C	type Ib	type Ia	type IIa
770	3.8		
950	1.30 - 2.4	3.0	
1000	0.32 - 1.3	2.30 - 3.5	
1100	0.32 - 1.3	0.64 - 1.6	1.60 - 3.70
1200	0.32 *	0.32 - 1.0	0.95 - 2.56
1300	0.32 *	0.32 *	0.64 - 1.44
1400	0.32 *	0.32 *	0.32 - 1.30

* - indeterminate due to the constraint on the availability of softer indenter materials, but not greater than 1.3 GPa.

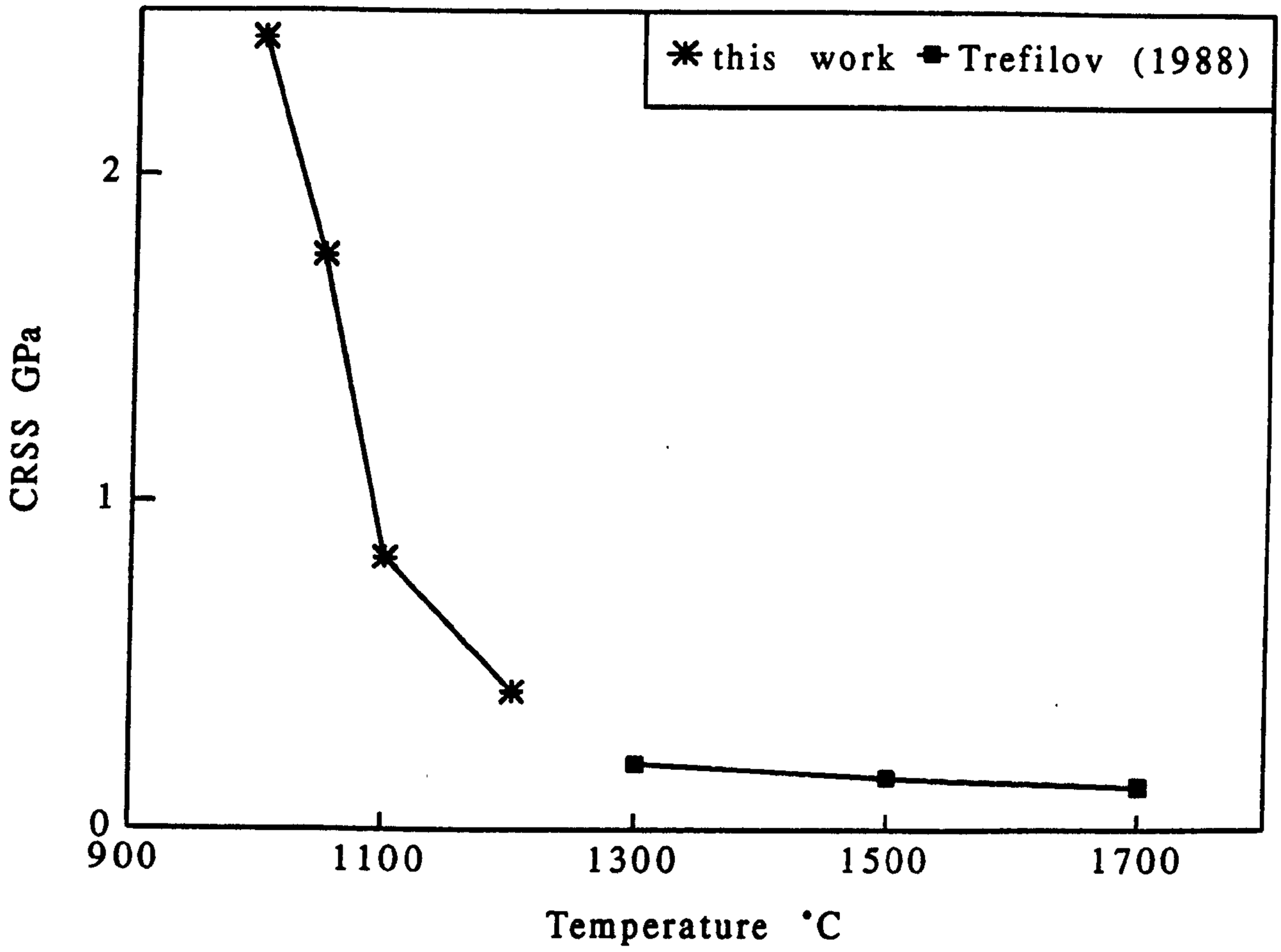

Figure 3.7 Estimate of the critical resolved shear stress vs temperature for type Ia diamond.

loading rates resulted in plastic deformation and a bent diamond. Trefilov *et al* (1988) applied a strain rate of $\approx 2 \times 10^{-6}$ in the three point bend tests, whereas the conventional indentation test is estimated to produce a strain rate of $\approx 10^{-4}$ (Hutchings, 1980). Whilst the softer indenter technique will undoubtedly have a lower strain rate than the conventional indentation method, the comparison of the estimated τ_c with those of the Russian workers indicates that the sensitivity of diamond to this effect is not marked.

An Arrhenius plot of τ_c versus temperature has been used to analyse the behaviour of other single crystal materials, e.g. Si (Rabier e*t al,* 1983); SiC (Fujita *et al,* 1987); and TiC (Williams, 1964). This exercise yields activation energies, deduced by a least squares fit using all the data, for Si = 1.6 eV; SiC = 3.4 eV and TiC = 1.5 eV (low temperature regime) and 3 eV (high temperature regime). A similar plot for type Ia and type IIa diamond, using the results given in Figure 3.7, is shown in Figure 3.8 and the relevant activation energies are 5.7 eV (17 RT_m) for type Ia and 4 eV (11.6 RT_m) for type IIa. Plotting the results from the work of Trefilov e*t al* (1988) gives an activation energy of 2.6 eV (7.5 RTm).

Williams (1963) has analysed his compression data for TiC in a similar manner and observed that there are at least two distinct temperature regimes. In the higher temperature regime, the activation energy was 3 eV (9.9 RT_m) and that is the same energy as required for creep mechanisms in TiC. In the lower temperature regime, the corresponding activation energy was 1.5 eV (4.9 RT_m). The transition temperature was 0.4 T_m, and it is interesting to observe that extrapolation of the linear relationship between log τ_c and homologous temperature, in the lower temperature regime, would indicate a critical resolved shear stress, at room temperature, of 12 GPa. Williams considered this to be improbably high and speculated on the existence of a third regime at lower homologous temperatures. A similar extrapolation of the data for diamond also predicts a value for the critical resolved shear stress at room temperature which is improbably high. However, Brookes *et al* (1987), on the basis of localised plasticity and work-hardening of TiC by softer sliders, estimated that the τ_c of this material was 0.5 GPa at room temperature. It may well be that there are similar temperature dependent regimes for diamond but further work is required to confirm this.

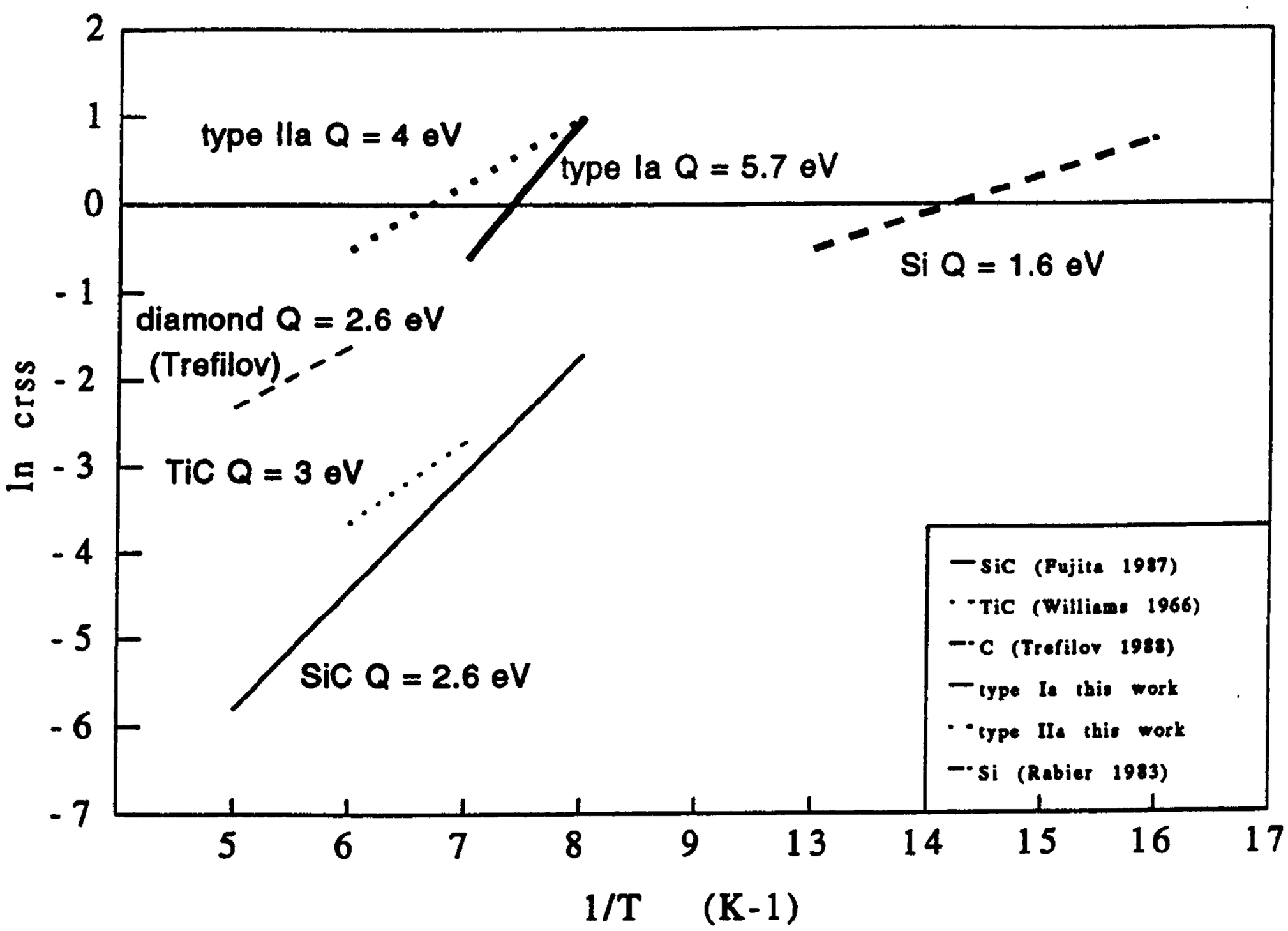

Figure 3.8 - Critical resolved shear stress vs reciprocal temperature for some covalent crystals.

Whatever, τ_c decreases rapidly with increasing temperature over a limited temperature range and the exact nature of this behaviour is dependent on the diamond type. In Figure 3.9, τ_c values are plotted for type Ia diamond, SiC, and TiC, normalised with respect to the shear modulus, as a function of homologous temperature. The normalised τ_c for diamond appears to decrease more rapidly than that for SiC. Because of the high value of the shear modulus for diamond, the normalised value of τ_c for SiC appears to be much higher than that for diamond at temperatures in the region of half the melting point. The normalised τ_c values for TiC, measured at the same homologous temperatures, are very similar to those of diamond above 0.35 T_m.

3.5 Summary.

It has been shown that materials which are considerably softer than diamond at a given temperature, are capable of producing permanent plastic deformation during static indentation. The pressures developed, when resolved onto the active slip systems, are controlled so that the appropriate critical resolved shear stress is exceeded, with the result that slip steps are formed on the surface and a dislocated volume is generated beneath the contact area. The results presented here enable a sound estimate to be made of the critical resolved shear stress for three types of diamond over a range of temperatures all below half the melting point. These results reinforce earlier work which indicated that a greater applied stress is required to plastically deform type IIa diamond than type Ia diamond and that type Ib synthetic diamond is more easily deformed plastically than natural diamond.

Thus it is shown that, at temperatures likely to be produced during many metal forming processes, plastic deformation is possible in diamond at mean contact pressures an order of magnitude less than the corresponding indentation hardness. It can be concluded that the range of softer materials capable of plastically deforming diamond at temperatures well below half the melting point is significantly greater than might have been anticipated from previous work and that further investigation is likely to confirm that cumulative

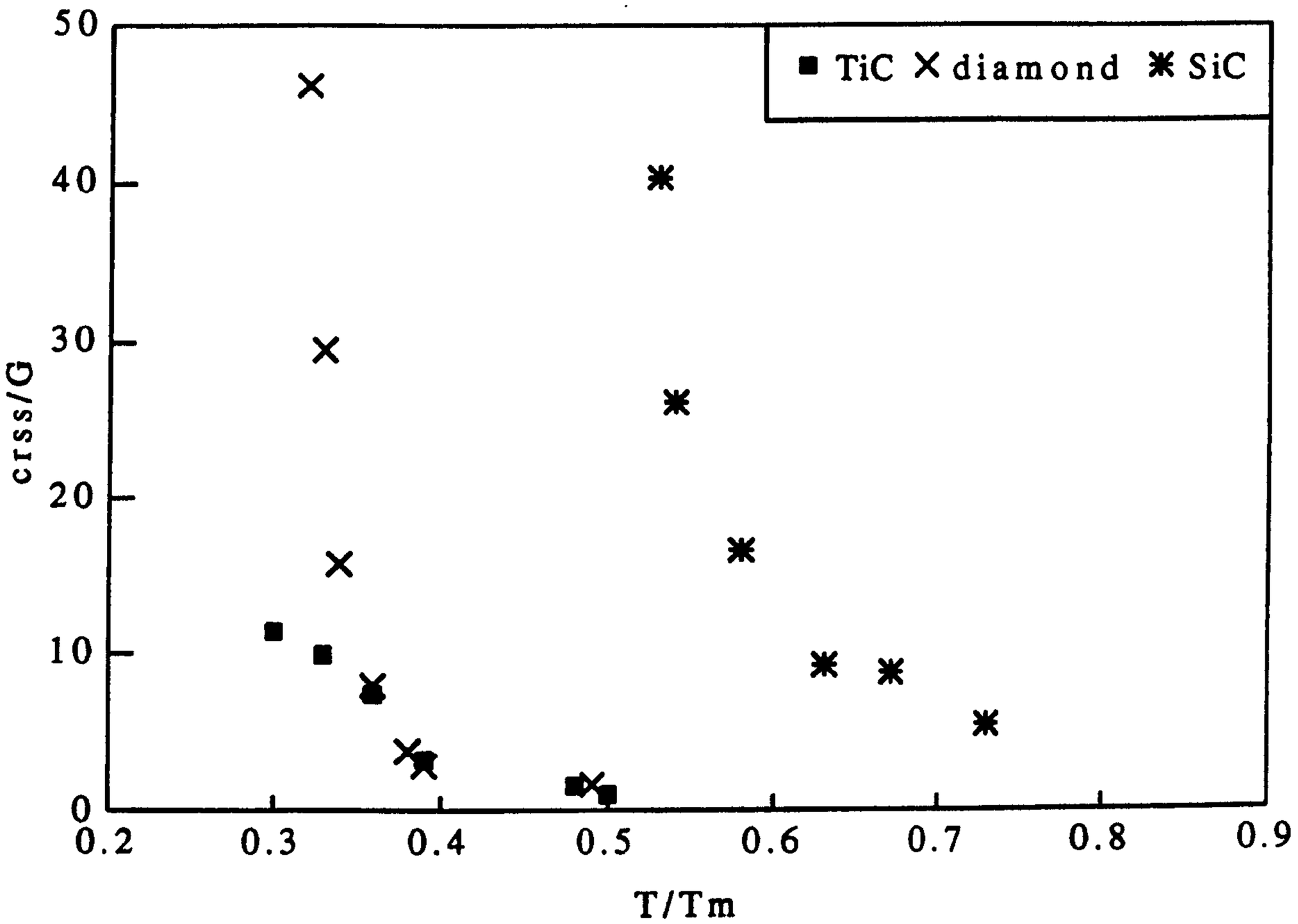

Figure 3.9 Estimate of the critical resolved shear stress / shear modulus vs homologous temperature for covalent materials.

deformation based on this principle is an important consideration in such applications as the wear of cutting tools.

Finally, it is shown that plastic deformation of diamond may be relatively easier than in silicon carbide, over the temperature range 0.3 - 0.5 T_m, on the basis of the relevant ratio of critical resolved shear stress : shear modulus.

Chapter 4. Aspects of plasticity and fracture in diamond.

4.1 Indentations formed by plastic deformation in crystalline solids.

One approach to understanding the mechanisms of deformation during the formation of an indentation by pyramidal indenters, is to imagine that it is formed by the radial compression of concentric hemispherical shells. The centres of these shells may be considered to be located at the tip of the indenter and the magnitude of the strain decreases progressively outwards towards the elastic-plastic boundary. In this inner central region the magnitude of the plastic deformation is fairly large and it might be regarded as a plug of work-hardened material which advances into the crystal as the indenter penetrates further. The surface of the indentation can be considered to be the original surface folding downwards progressively. However, the surface area must be larger than the pre-indented area, if only due to the emergence of slip steps onto the surface.

A significant amount of elastic recovery occurs in the specimen during unloading, producing an up-lifted region of the surface immediately adjacent to the impression. This recovery of elastic strain is incomplete and is suppressed by the plastically deformed zone in the region of the impression, i.e. a condition of residual stress exists around the unloaded permanent impression.

Residual stress can give rise to reversed plastic flow on unloading of the indenter and was first reported by Ablova (1962), who observed step-like protuberances on the surfaces adjacent to, and also within, the indentations in germanium single crystals. He suggested that these features were slip traces caused by secondary yielding resulting from non-uniform and residual elastic strains.

Hirsch *et al* (1986) observed slip line formation adjacent to indentations made on the (111) planes of GaAs. They deduced that with the removal of the external load, the internal stresses were relieved by an upward displacement of that part of the crystal in the immediate vicinity of the indentation and that this recovery process occurred up to 60 seconds after removing the applied load.

Brookes and Ross (1986) distinguished between dislocations produced during the loading cycle and those which emerged at the surface after the removal of the normal load in MgO using a Vickers indenter. The crystals were etched whilst under load, flushed clean, and the load removed. The resultant surface revealed a density of dislocation etch pits surrounding the indentation but also some slip steps bordering the indentation, the so-called *picture frame*. Further etching revealed new etch pits, and this overall dislocation pattern was consistent with the usual rosette pattern, Figure 2.2(b). These authors concluded that the picture frame was formed either whilst the normal load was being removed or immediately after that event. An example of the picture frame in diamond is shown in Figure 4.4.

The question of whether plastic deformation of diamond occurs in any form at room temperature has been addressed by a number of workers in the past two decades. The nature of anisotropy of hardness of crystalline materials has been explained on the basis of resolved shear stress models for a wide range of metallic and ceramic material and the modelling implies that the phenomenon of hardness anisotropy at room temperature in diamond can be explained, at least in part, by mechanisms of plastic flow. Further evidence for plastic flow was reported by Humble and Hannink (1978), who indented diamond specimens with a Knoop indenter at room temperature, thinned the diamonds and observed the deformed region using transmission electron microscopy. They confirmed that dislocations, with Burgers vectors b along $\langle 110 \rangle$ directions, were associated with the indentations and concluded that limited plastic deformation of diamond occurs at room temperature under these specific conditions.

4.2 Characteristics of deformation zones associated with impressions in diamond.

As discussed in the previous chapter, the soft indentation technique, when applied to diamond at elevated temperatures, produces plastic deformation visible as slip lines on (001) polished surfaces of diamond, and extensive slip creates deep impressions. The hydrostatic nature of stress beneath the indenter enhances the plastic contribution whilst inhibiting the formation of cracks, whereas the rigid pyramidal indenter produces a relatively high level of strain which induces median and radial cracks during the recovery of the material whilst the normal load is being removed. The tip of the soft cone flattens under the applied load so that its area can support the load elastically and the growth of that area occurs due to the continued deformation of the indenter. The downward displacement of the indenter is therefore due to the *elastic* and *plastic* deformation of the indenter, as well as the displaced volume of the impression as a result of both *elastic* and *plastic* deformation of the diamond.

A feature of the soft indenter technique is that the deformed surface of the *harder* diamond single crystal is replicated on the blunt tip of the *softer* cone. The exact nature of the replication is shown in Figure 4.1 where a blunted cone of TiB_2 was loaded for 3000 seconds on the polished {001} face of a type Ia diamond. The slip lines have been faithfully replicated on the flat of the indenter, which established that the slip lines formed whilst under load.

Diamond does not readily lend itself to the classical serial strip polish and dislocation etch technique employed to reveal the extent of the plastic deformation associated with impressions made in MgO and silicon and germanium. Therefore, in this study a Nikon Optiphot light microscope was used to determine the onset of slip and extent of plastic deformation. This was reinforced by using both transmitted polarised light in birefringent mode and interferometry techniques. The latter is described in Chapter 5.

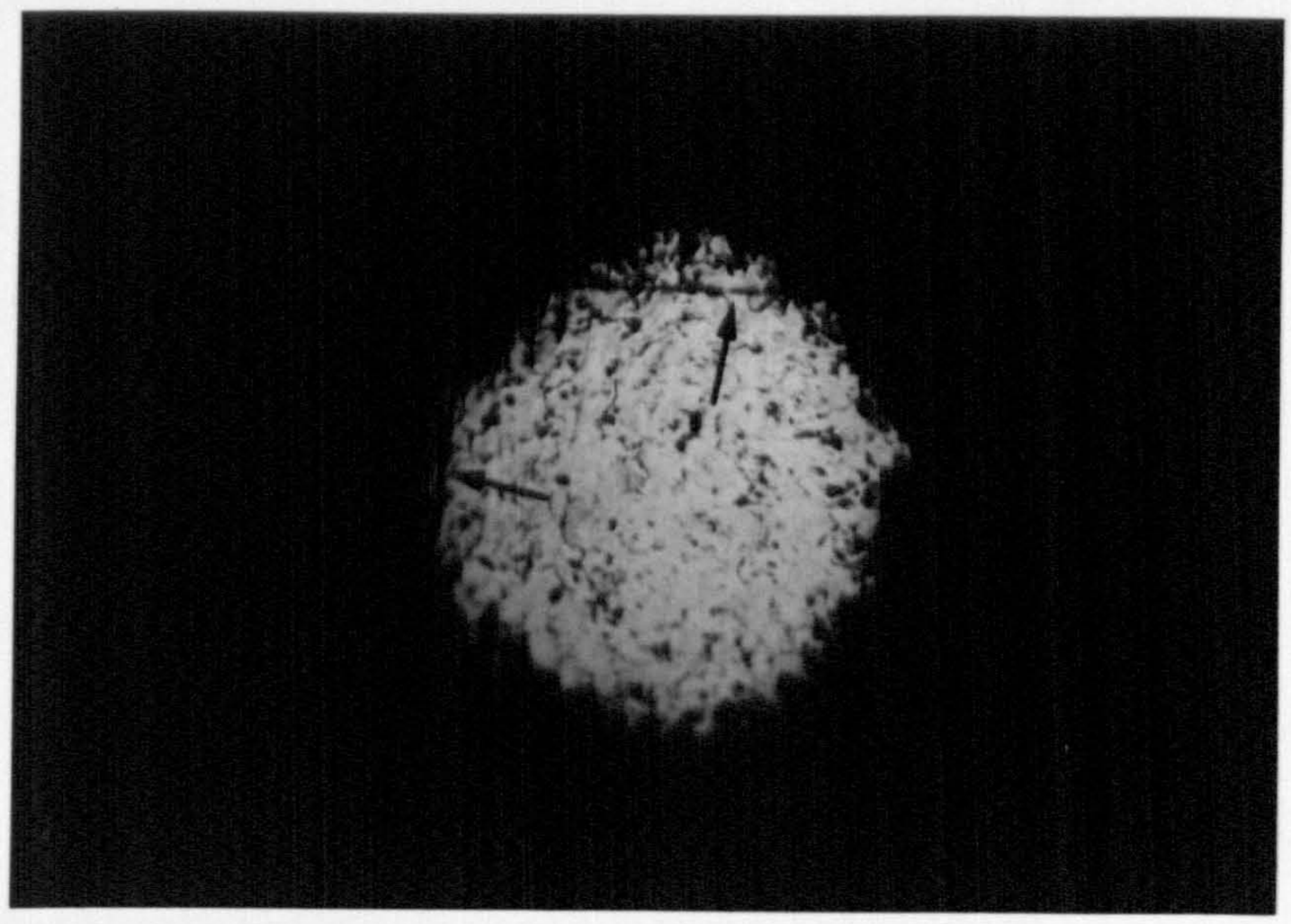

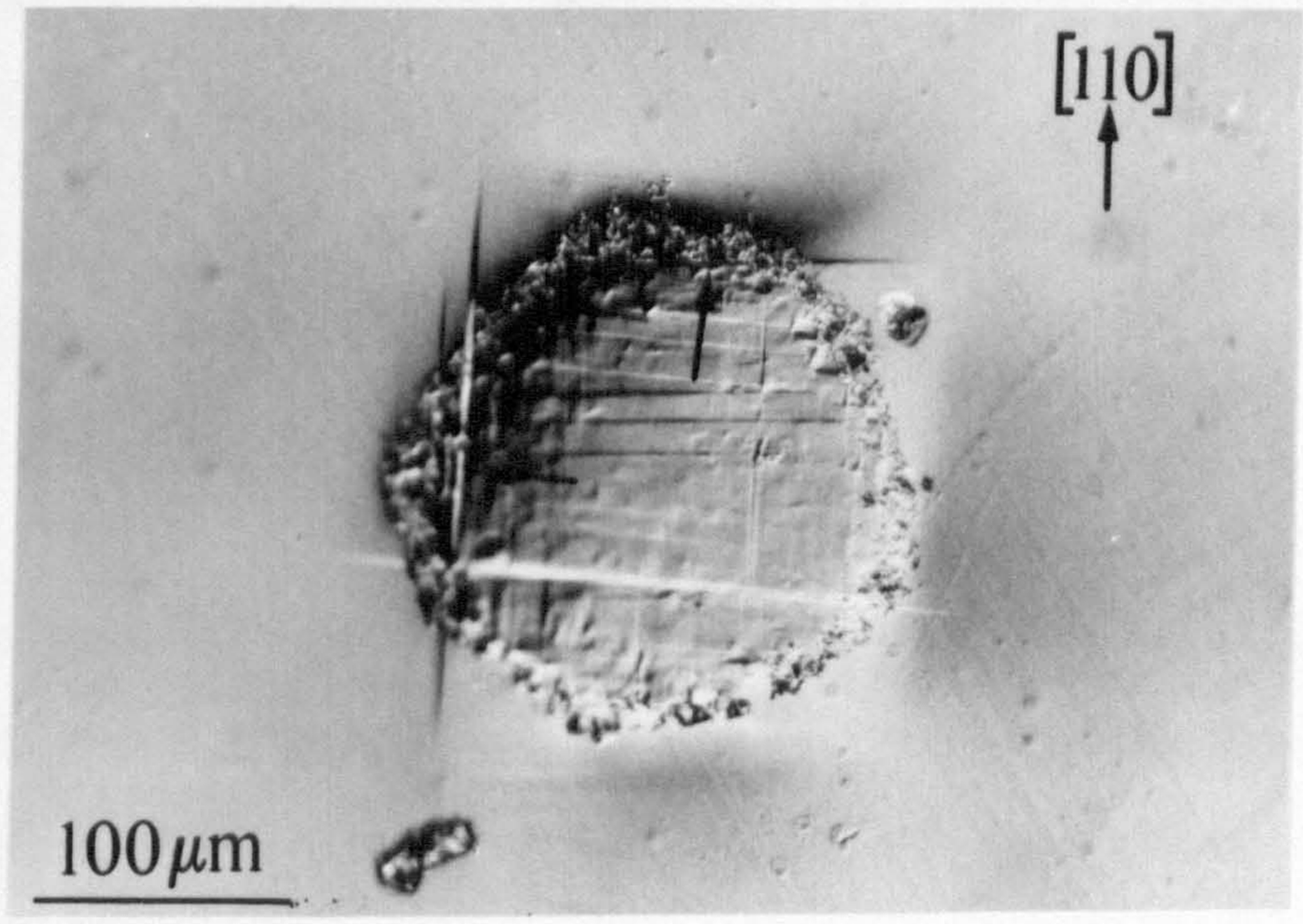

Figure 4.1 To illustrate the replication of features on the blunted indenter tip, **above**, and produced during the formation of the impression, **below**.

The dislocated volume.

By looking through the edge of a crystal, the deformation directly associated with an impression can be viewed. Here, suitable 'windows' must be provided by polished low index planes at 90° to the original surface, i.e. (010) or (011) planes and the closer the impressions are to the window surface, the sharper the image will be as defocusing will be kept to a minimum. The optimum definition is obtained in images revealed by polarised transmitted light. Examination of the birefringence reveals the spatial extent of the deformation, so that an assessment of the volume of plastic deformation can be made. It also illuminates the degree of retardation, due to the residual strain in the diamond, and thus gives an indication of the level of elastic strain. In addition, the onset and nature of cracking beneath the impression can be evaluated in this way.

The initial deformation.

At the lowest temperatures, where there is no significant dislocation movement, classical Hertzian ring cracks may be formed even with softer cones, eg cBN. With increasing experimental temperature, these cracks will not be formed and the deformation becomes plastic. Some workers have called this the brittle-ductile transition.

The onset of plastic deformation at low homologous temperatures (0.3 T_m) with short dwell times of indentation, and a 'low' applied mean pressure produces shallow impressions with dislocations emerging onto the surface directly beneath the area of contact with the indenter. Observations of the first emergent slip steps formed the basis of the measurements in the estimation of the critical resolved shear stress of the different diamond types, described in the preceding chapter, and an example of this is shown in Figure 4.2(a). The degree of strain produced by slightly deeper impressions is low, i.e. that produced by mean contact pressures just greater than the threshold pressure, and there is no associated fracture or uplift outside the contact area. Impressions in type Ia and type Ib diamond are formed by inhomogeneous slip producing coarse intersecting slip steps within, and slightly beyond, the contact area and Figure 4.2(b) shows that the

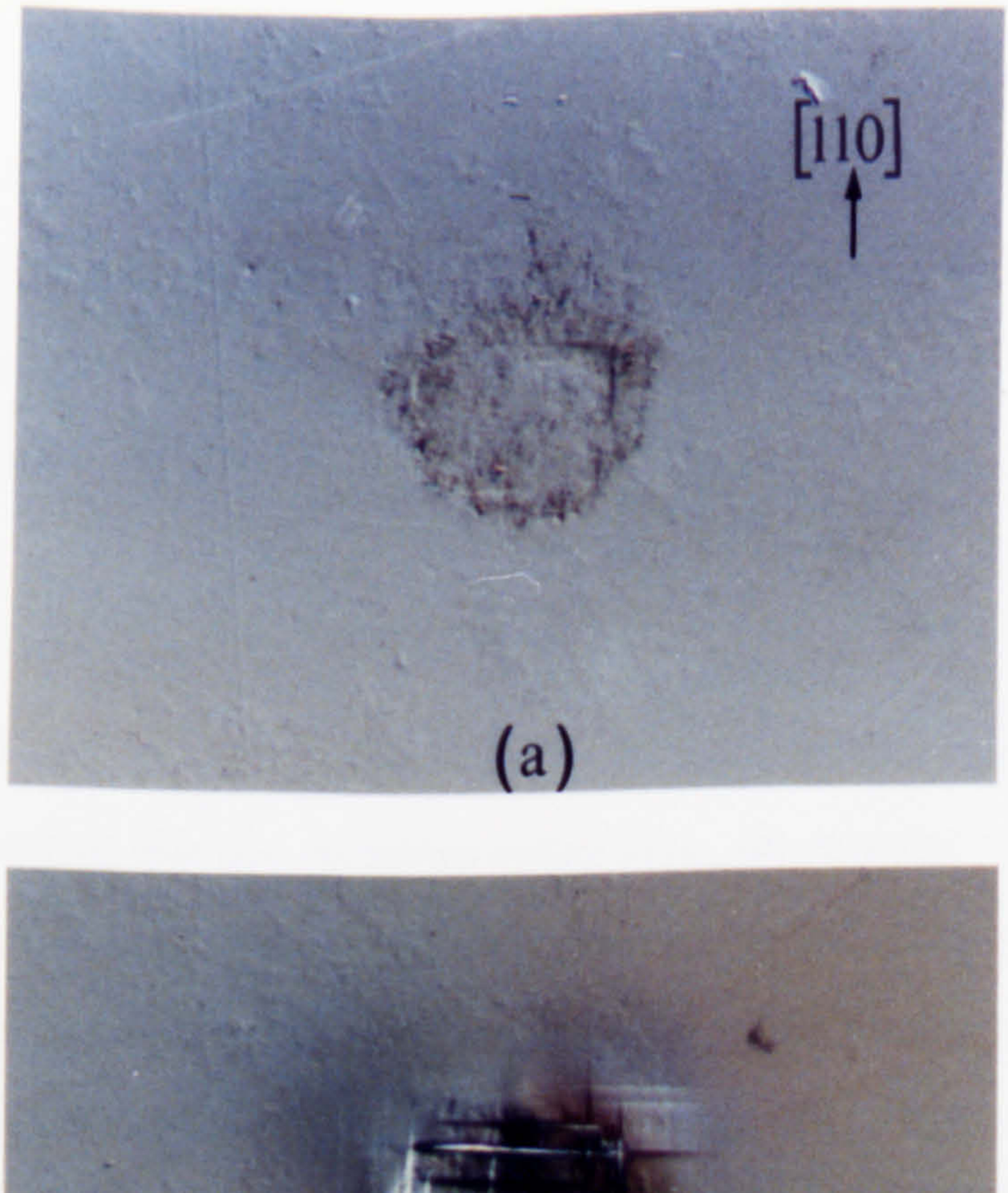

Figure 4.2 Typical impressions formed by the same cBN cone under the following conditions: (a) type Ia, 1000° C, 300 seconds, P_m = 11 GPa, (b) type Ia, 1100° C, 1000 seconds, P_m = 8.5 GPa, (c) type IIa, 1100° C, 1000 seconds, P_m = 8.5 GPa.

typical contact area is circular, the slip pattern is square and the corners of the squares extend beyond the perimeter of the contact circle. In contrast, it is impossible to see the slip steps in type IIa diamonds at the low magnifications available using a light microscope, Figure 4.2(c). This is due to the homogeneity of the slip, i.e. the slip steps are finer and fewer.

Laths.

Once an impression has formed and some degree of birefringence is observable, finer crystallographic features, hereafter called *laths*, are revealed within the plastically deformed volume immediately beneath the impression in type Ia and Ib diamond. Figure 4.3 (a) shows an impression made using a cBN cone in type Ia diamond, focused slightly below the surface to reveal some of these laths. When projected onto the (001) surface the laths appear to lie in both the ⟨110⟩ and ⟨100⟩ directions. Those in the ⟨110⟩ direction are known to lie in the (001) planes because they remain in focus, at a given distance below the original (001) surface, along their complete length when viewed with an optical microscope. This also accounts for the clarity of these particular features shown in Figure 4.3. In contrast, those laths aligned along ⟨100⟩ directions can be seen to be inclined to the original (001) surface. The {001} ⟨110⟩ laths correspond to slip systems **1, 4, 7,** and **10,** which outline the base of the tetrahedron described in Chapter 2 and Brookes *et al* (1990). The ⟨100⟩ laths however, are inclined to the (001) plane and lie in (111) planes. These directions correspond to the edges of the tetrahedron forming the internal apex, i.e. slip systems **2, 3, 5, 6, 8, 9, 11,** and **12.** In Figure 4.3(b) the deformation below the impression is viewed through a (110) plane, i.e. through the side of the specimen, with the contact area indicated. The laths make an included angle of 55° with the surface and internally an angle of 72°. The plastically deformed region immediately below the contact area is illustrative of the distinct arrangements of dislocations with {111} plane tetrahedral symmetry, i.e. the tetrahedral cages, hypothesised by Hirsch *et al* (1985) and considered to govern the indentation process in silicon, germanium and gallium arsenide. Also visible in Figure 4.3 is a Hertzian cone

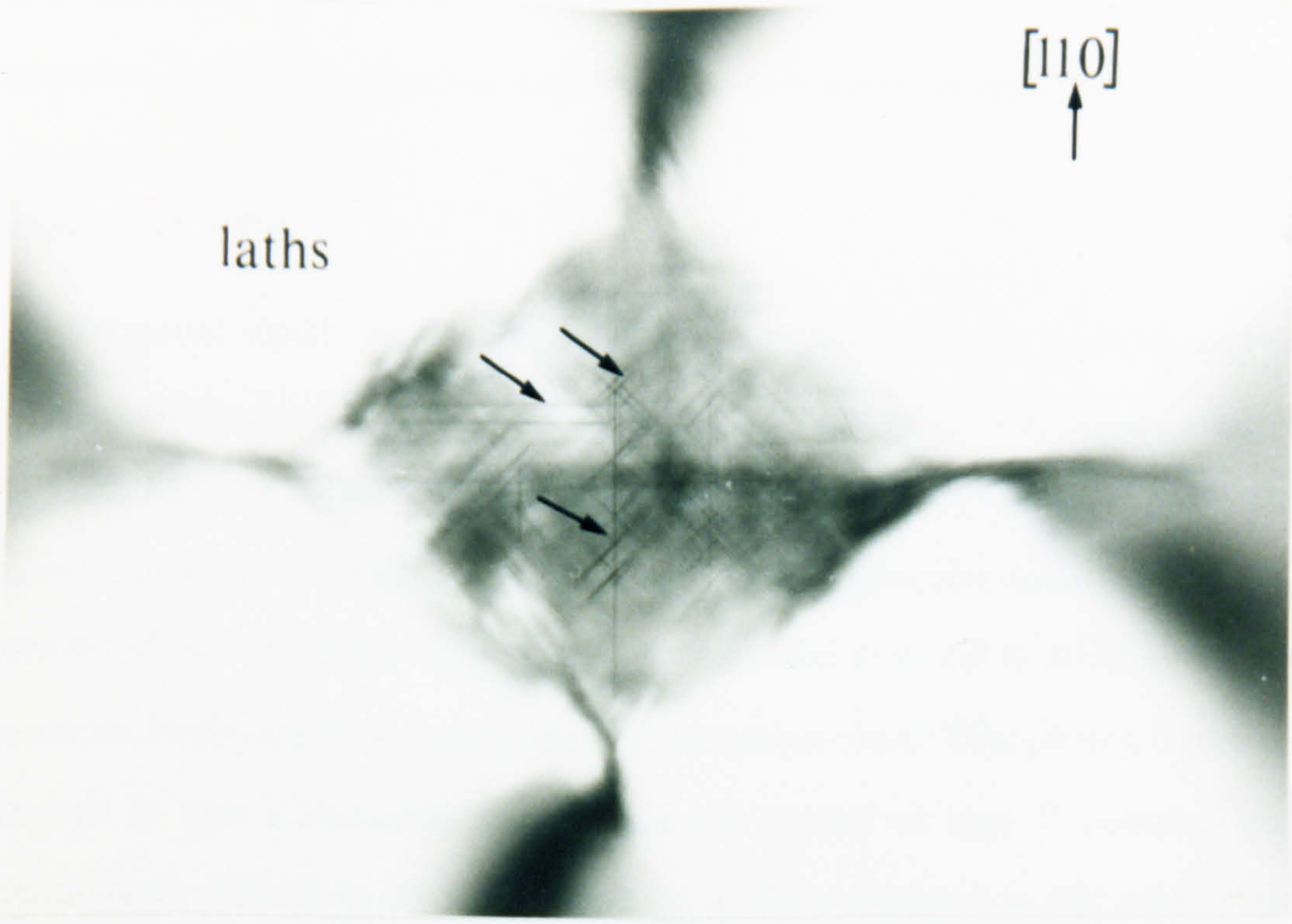

(a)

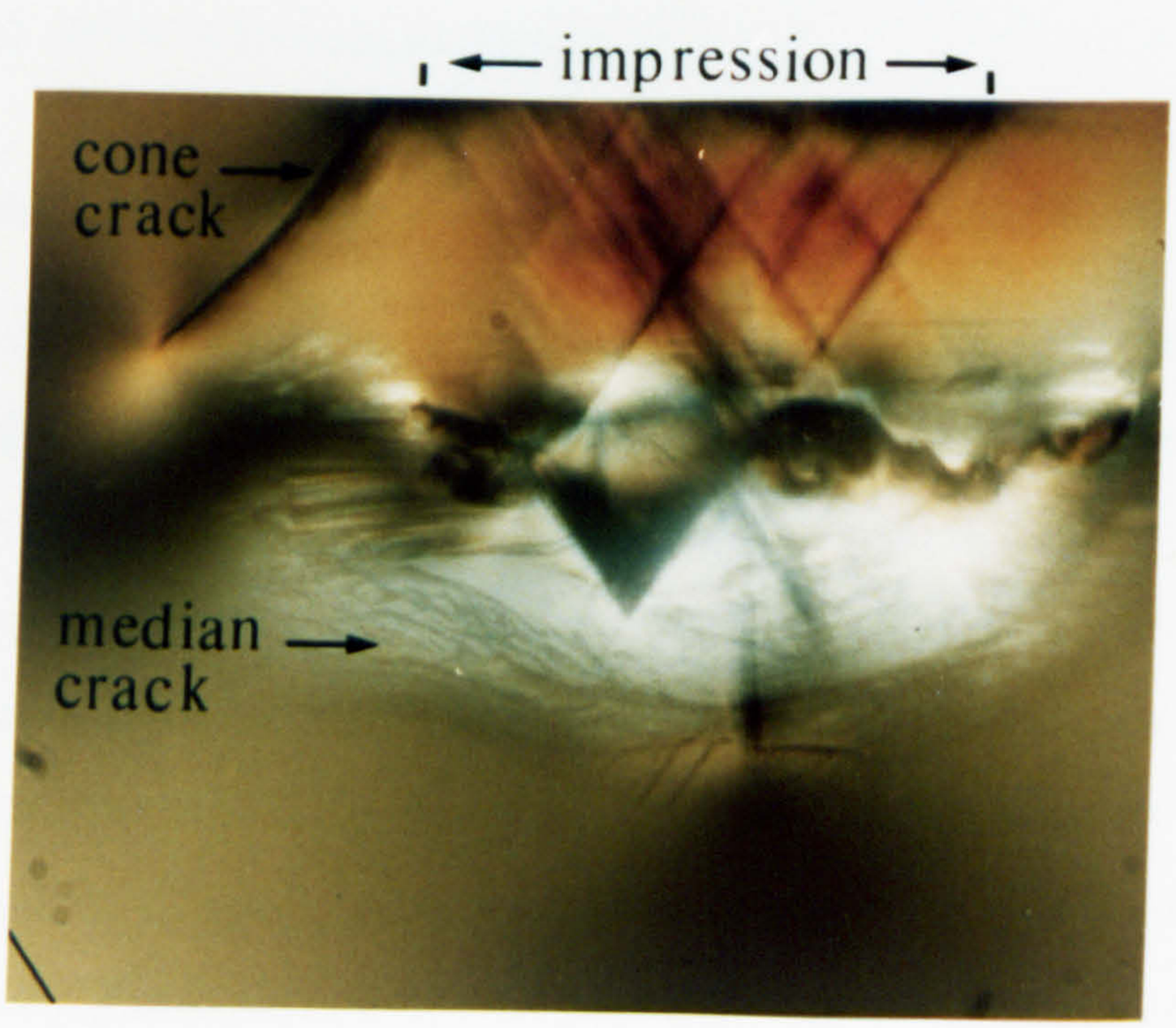

(b)

Figure 4.3 Showing the formation of laths beneath typical impressions, on type I diamonds, which apparently delineate tetrahedral cages, (a) focused through the deformed (001) surface, (b) focused through the side of the crystal giving a section normal to a (110) plane. (transmitted light)

crack and a large median vent which has not been driven to the surface. These laths are a feature of type I diamonds but have never been observed in type IIa diamonds.

Picture frame slip.

Increased dwell times and/or elevated temperatures, for a given applied mean pressure and diamond type, will result in picture frame slip. The square array of (111) ⟨110⟩ slip systems which comprise the impressions made on the (001) plane encourage volume-change by outward displacements. In the impression made by cBN in type Ia diamond shown in Figure 4.4(a), it can be seen that material is raised along the ⟨100⟩ directions, beginning at the outer edge of the contact area. This picture frame is readily observed in type I diamonds but the fine slip typical of type II diamond makes the picture frame difficult to discern. Cracking is often observed in this area in type I but not type II diamonds. In Si and Ge, Hirsch *et al* (1985) observe that picture frame slip actually 'lifts' the impression above the original level of the specimen surface and ascribe this to the effects of reversed plasticity.

Dislocation rosette formation.

Further changes in the experimental conditions to enhance plasticity, either by increasing the experimental temperature or increasing the dwell time of the indenter, produce deeper impressions. Figure 4.4(b), cBN on type Ia diamond at 1250° C, shows long slip lines radiating from the impression, typical of rosette slip formed in fully ductile crystalline materials. The uplift associated with impressions 1500 nm or more deep, occurs along the ⟨110⟩ directions. In other words, the elevation is now at the sides of a predominantly square impression and the shape of the impression is governed by the emergence of dislocations on crystallographically oriented planes at the indented surface, rather than by the original form of the indenter. Impressions approaching a depth of 2 to 3 μm tend to have an associated uplift of 250 nm. Impressions which are twice as deep or ≈6 μm in depth have an increased associated uplift of the same order of magnitude i.e. ≈500 nm.

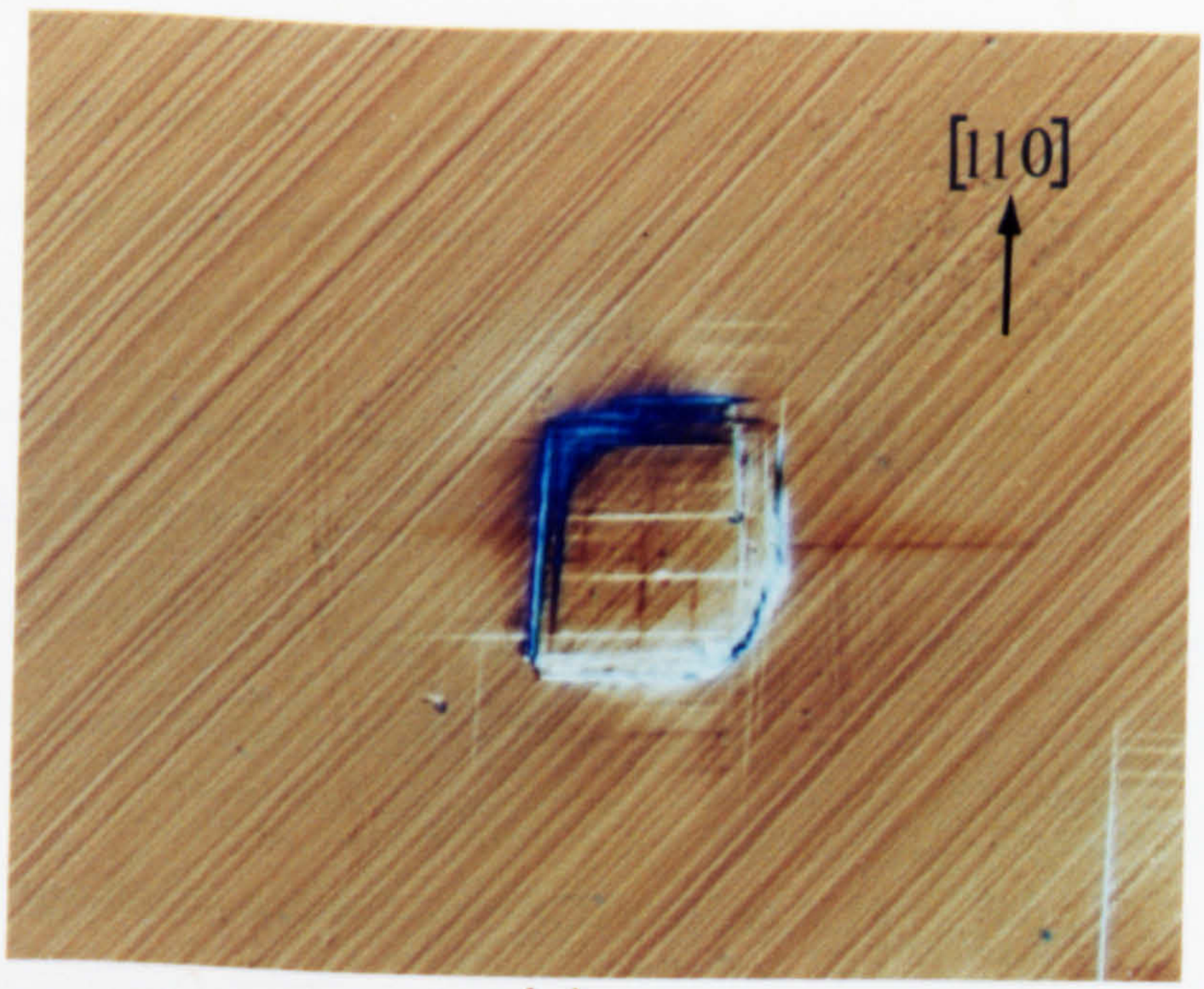

(a)

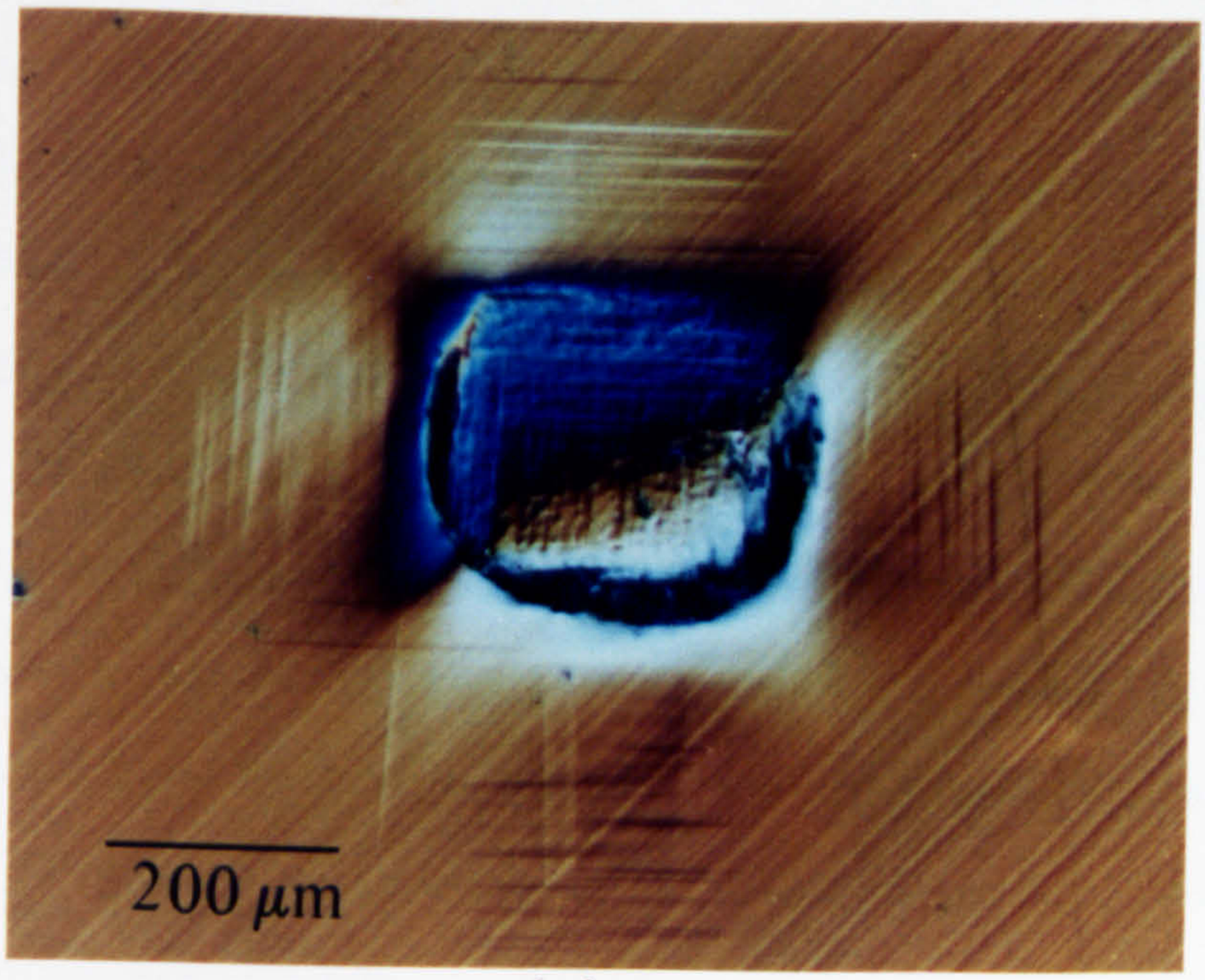

(b)

Figure 4.4 (a) Picture frame slip in type Ia, 1100° C, 300 seconds, P_m = 8 GPa, (b) rosette slip in type Ia, 1250° C 300 seconds, P_m = 6 GPa. (differential interference contrast)

Figure 4.5 shows the effect of decreasing mean pressure with increasing experimental temperature, using a cBN indenter, on a (001) surface of type Ia diamond. As the experimental temperature is increased, the area of contact increases, i.e. the applied mean contact pressure decreases, and both the deformation volume and the strained volume increase significantly. Figure 4.6 shows the result of a similar set of experiments for type IIa diamond. Comparison of Figures 4.5 and 4.6 confirms that the extent of plastic deformation is significantly greater in type Ia diamond than in type IIa diamond for comparable experimental conditions.

Cracking associated with shallow impressions.

The cracks associated with shallow impressions do not always appear to be crystallographically symmetrical but tend to lie along a mixture of ⟨100⟩ or ⟨110⟩ directions emanating from the corners of the picture frame in Figure 4.7(a). The cracks intersect the surface and propagate on {110} planes inclined at 45° to the (001) surface, Figure 4.7(b). Such crack systems are attributed to the reaction of dislocations and in fact are often seen to be deflected at the point of intersection of slip lines i.e. at the corners of the picture frame. This $\{110\}_{45}$ fracture tends to occur with impressions which are between 500 and 1500 nm deep and is most commonly observed as a result of strain induced by impressions in type I diamond made by indenter materials which develop a mean contact pressure in the range 6 - 10 GPa at homologous temperatures of 0.3 - 0.4. The presence of these cracks, therefore, is indicative of either a high mean pressure or some adhesion between the indenter and the diamond. This form of cracking is not observed in type II diamond.

Cracking associated with deep impressions.

Deep impressions, with extensive accompanying plastic flow, often have particularily symmetrical median cracks aligned along the ⟨110⟩ directions on the (001) surface. These cracks originate from beneath the centre of the contact area and bisect the edges of the picture frame and/or rosettes. Transmitted light microscopy reveals the cracks to be on {110} planes normal to the specimen surface. Figure 4.8(a) shows a

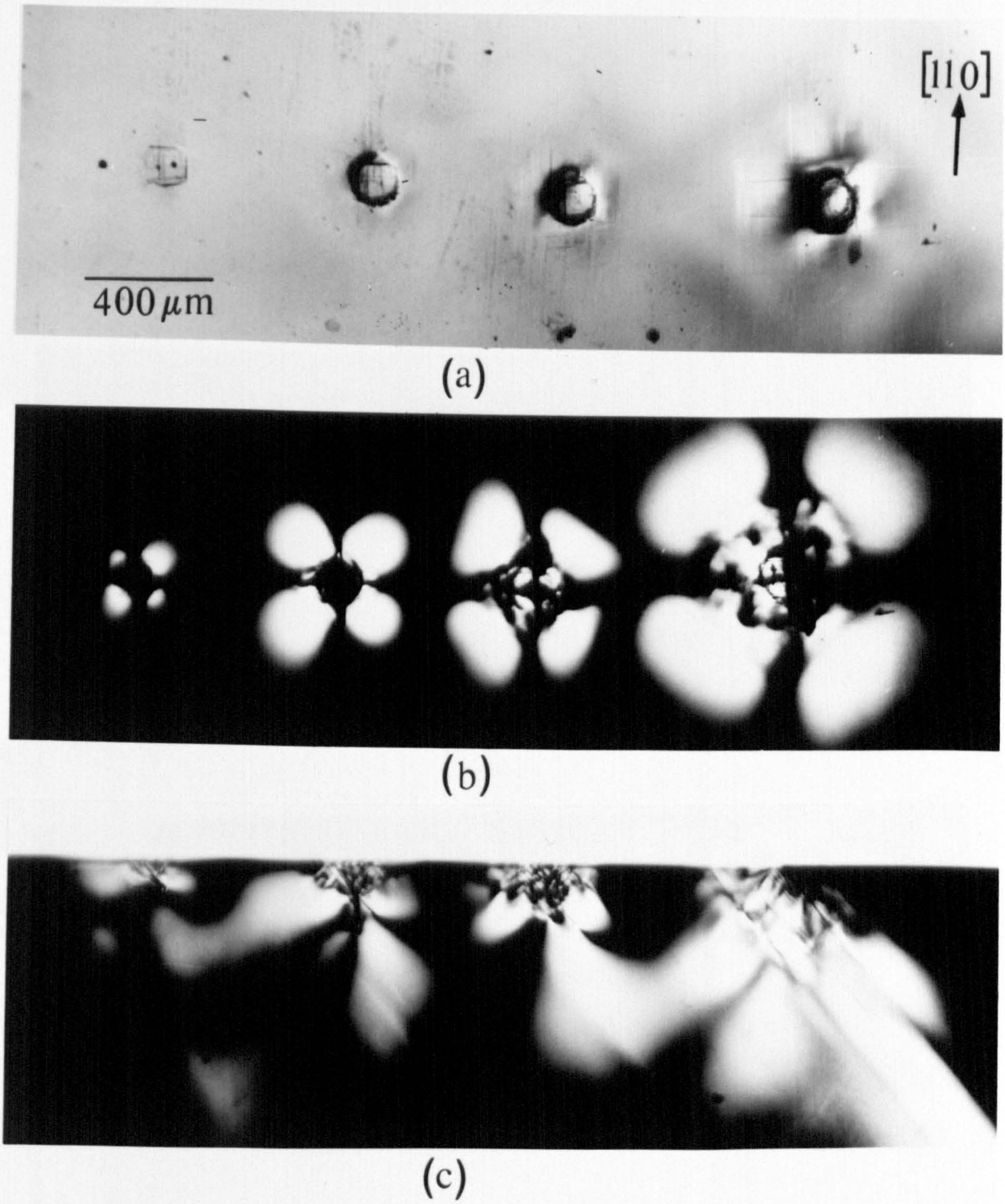

Figure 4.5 The effect of increasing temperature on (001) type Ia diamond using a cBN cone for 300 seconds: (a) differential interference contrast, (b) polarised transmitted light through (001) surface, (c) polarised transmitted light side view through a (110) section.

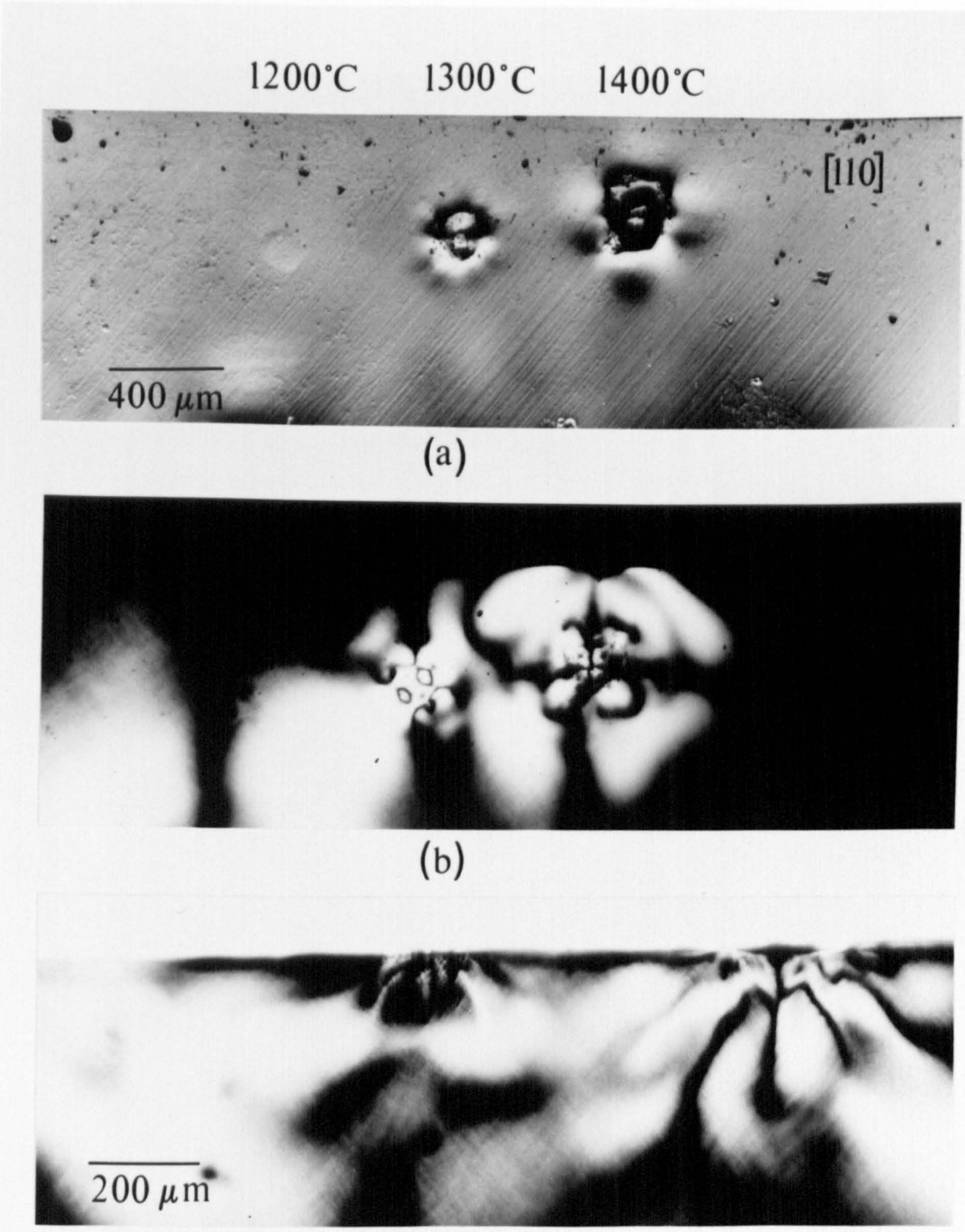

Figure 4.6 The effect of increasing temperature on (001) type IIa diamond using a cBN cone for 300 seconds: (a) differential interference contrast, (b) polarised transmitted light through (001) surface, (c) polarised transmitted light side view through a (110) section.

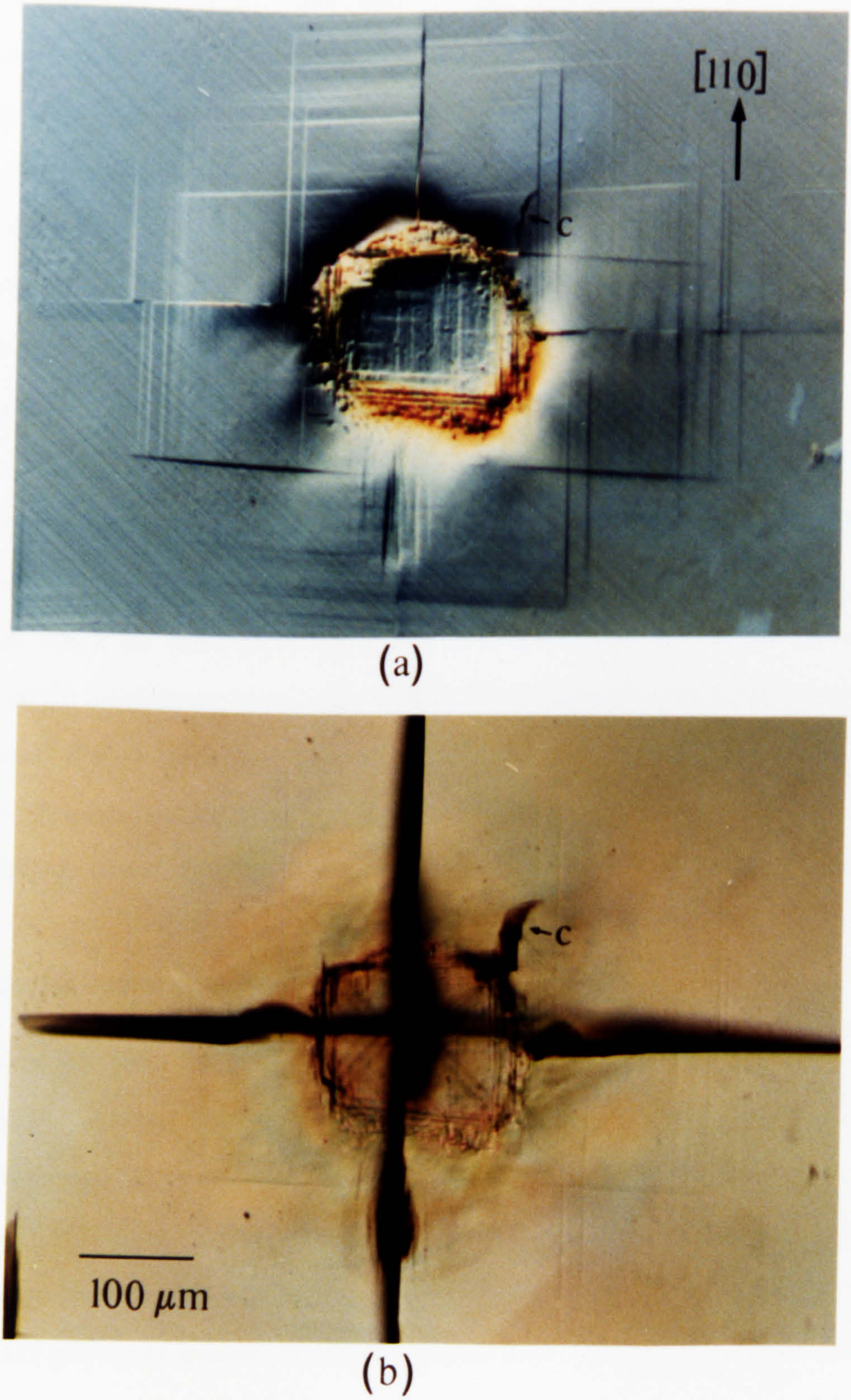

(a)

(b)

Figure 4.7 Impression in (001) plane, type Ia due to a cBN cone at 1400° C for 300 seconds, Pm = 4.5 GPa: (a) rosette formation with (110) median cracks, (differential interference contrast) (b) confirming cracks lying on (110) planes normal to the deformed surface. (transmitted light)

deep impression made with a cBN cone in type Ia diamond at 1250°C. When the impression was made no surface cracking occurred. Figure 4.8(b) shows that median cracks are nucleated beneath the plastically deformed zone and do not always propagate through to the surface (also see Figure 4.3). Propagation of the crack does not always occur at the time of the experiment but may occur some months after the impression was made. Figure 4.8(c) and 4.8(d) show the impression, some months later, and it can be seen that further cracking has occurred, in that (110) cracks have propagated through the rosette arms. In other deep impressions in type Ia diamond the median crack nucleates beneath the deformed zone and propagates around that zone and bisects the rosette arms.

The length of the crack beneath the deformed zone tends to be small, of the order 10 μm; or to extend the entire length of the deformed zone, slightly longer than the area of contact. Once the crack propagates to intersect the surface and bisects the rosette at the edge of the impression, its measured length on the surface tends to be 1.5 to 2 times the diameter of the impression. The uplift associated with these impressions is 500 nm or greater. Impressions made on type Ib diamonds frequently produce surface cracks on {111} cleavage planes, in addition to median cracks produced on the $\{110\}_{90}$ planes.

Strain and geometric similarity.

Figure 4.9 gives an indication of the geometric similarity in type Ia diamond. Here, a Si_3N_4 indenter has been used to make impressions using a dwell time of 300s and 3000s, Figure 4.9(a) and (b) respectively. Interferograms of the impressions, Figure 4.9(c) and 4.9(d) show that the impressions are approximately 1.5 μm and 4 μm deep respectively, (each fringe represents a change in height of 272nm) and that there is considerable pile-up of material outside the contact area. Viewed through the side of the crystal using transmitted polarised light in a {110} direction, Figure 4.9(e), the dislocated zones are apparent through the well defined slip bands. In both cases the depth of this zone is of the same order of magnitude as the diameter of the impression. In other words, time and temperature appear to be interchangeable in terms of geometric similarity of the resultant strain and this is observed in both type I and type II diamonds.

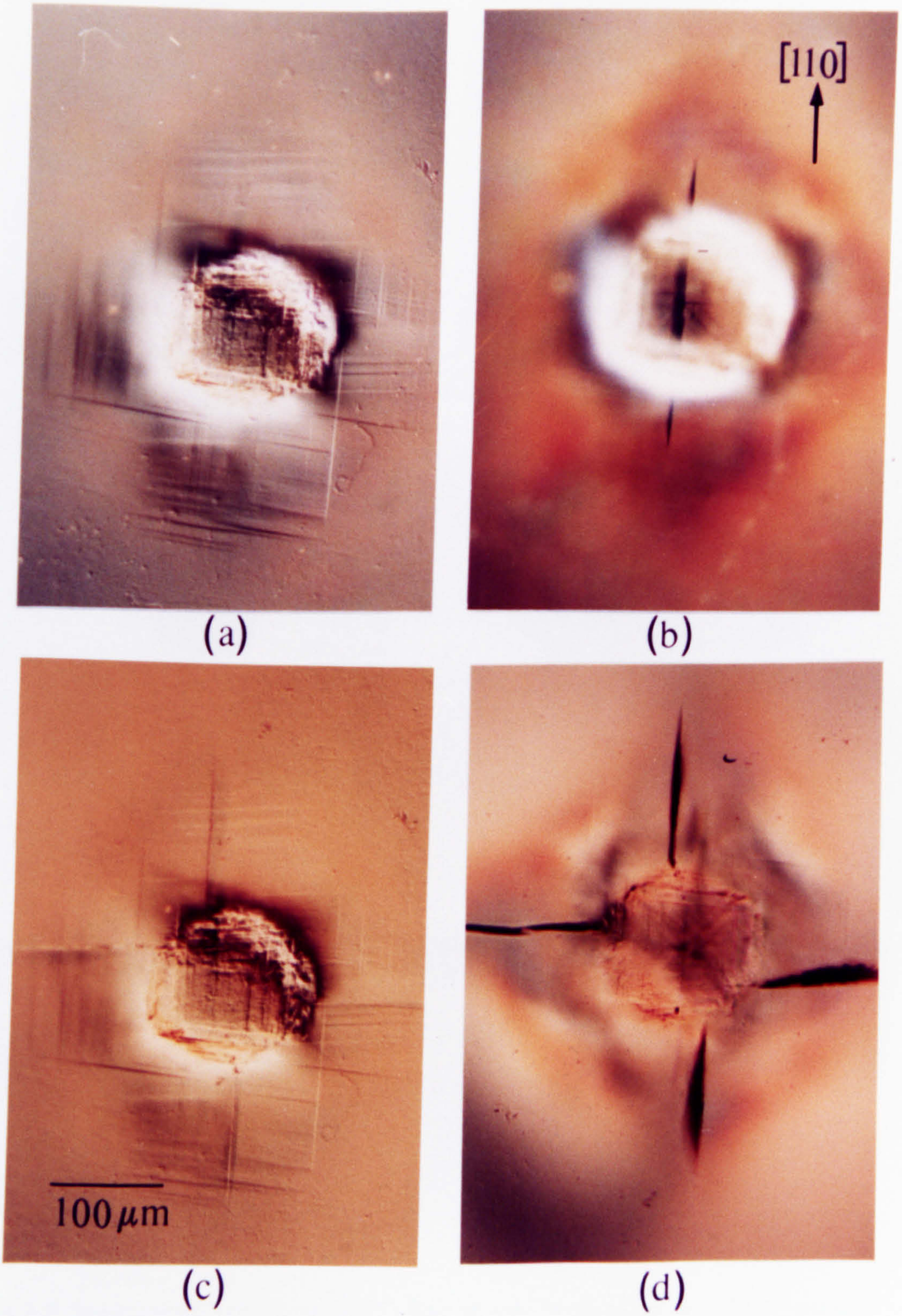

Figure 4.8 Impression in (001) plane of type Ia diamond formed by cBN cone at 1250° C for 300 seconds, P_m = 6 GPa. Illustrating (a) rosette formation and (b) subsurface cracks immediately after the formation of the impression. Similar micrographs of the same impression, (c) and (d) respectively, some weeks later.

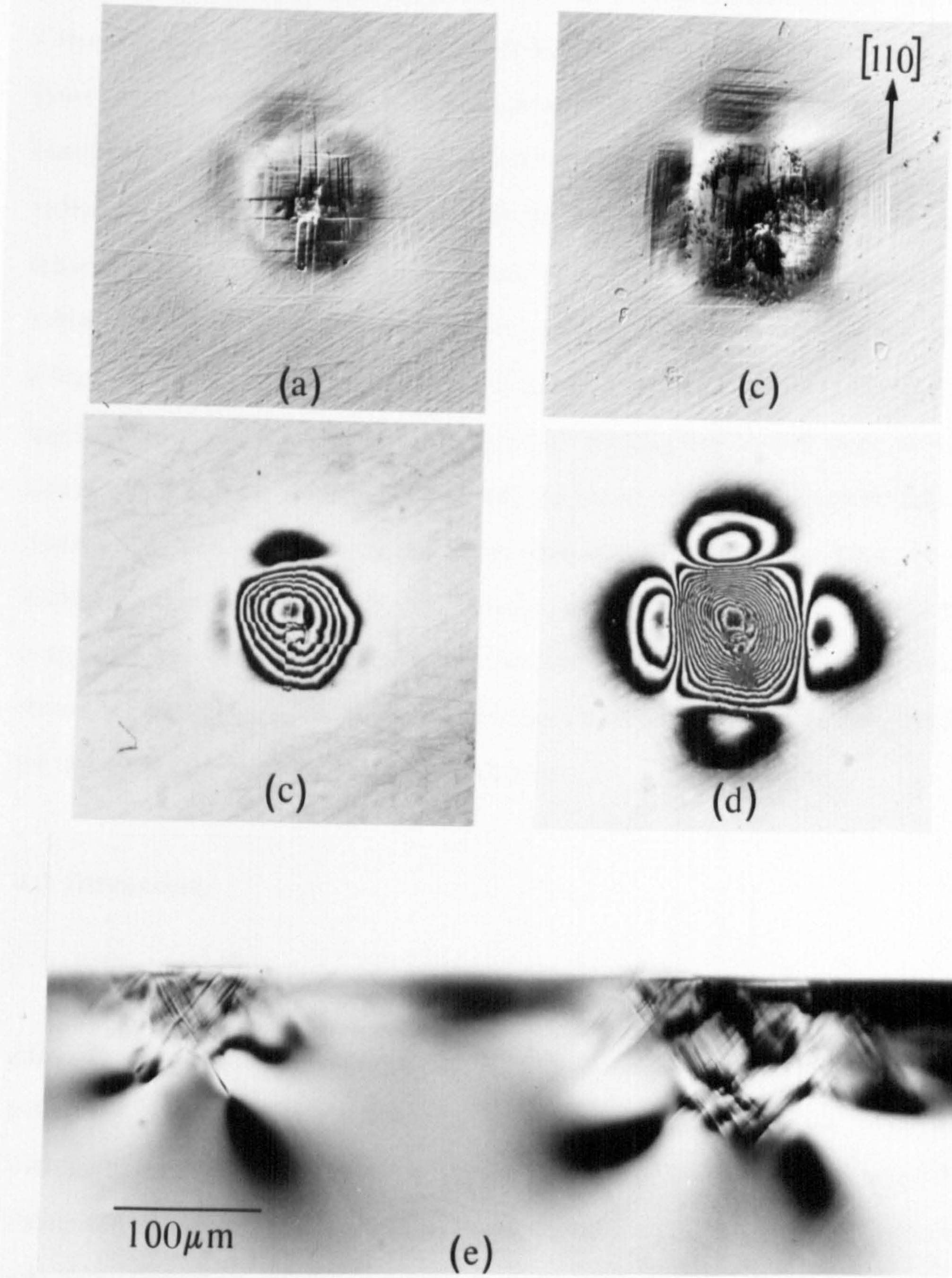

Figure 4.9 Impressions formed on (001) plane of type Ia diamond at 1250° C using a Si_3N_4 cone, (a) with a dwell time of 300 seconds, P_m = 3.7 GPa, (b) with a dwell time of 3000 seconds, P_m = 2.8 GPa. (c) and (d) show interferograms of (a) and (b) respectively. (e) side view of the impressions shown in (a) and (b) through a (110) section, using transmitted polarised light, indicating the geometric similarity of the dislocated volume with change in dwell time.

For a given set of experimental conditions, a mean pressure of between 8 to 10 GPa develops a significant amount of strain in the diamond lattice. With a given load, a lower mean pressure means a larger contact area but reduced lattice strain. The likelihood of cracking during the indentation process, and stress relief by crack nucleation and propagation, increases with the degree of strain. The extent of uplift is related to the impression depth and this uplift, as measured using interferometry techniques described in the next chapter, reflects plastic deformation and cracking around the impression. The extensive slip in type I diamond, shown in Figure 4.10(a), appears inhomogeneous, producing slip steps of differing heights with irregular spacing between them and the interferometry reveals the extent of the pile-up outside the area of contact. The fine homogeneous slip observed in type IIa diamond and shown in Figure 4.10(b), produces less easily observed rosettes, but the uplift associated with the rosette is apparent, and can be seen to increase with the depth of the impression. However, as shown in Chapter 3, the conditions for plasticity for type IIa diamond are different in that the threshold experimental temperature is higher.

4.3 Discussion.

At room temperature, elastic deformation and, at sufficiently high mean contact pressures, crack initiation and propagation in the diamond may be developed by softer indenters. The cracks are mainly classical Hertzian cone cracks and lie on {111} cleavage planes inclined at 54°44' to the (001) surface. At experimental temperatures above 450°C, dependent on the type of diamond, cracks are no longer formed. A schematic illustration of the sequence of dislocation initiation through to complete rosette formation is given in Figure 4.11. At approximately 500°C the contact area is apparent, often 'dimpled', and the grain structure of the indenter material is replicated on the surface of the diamond. In the temperature range 500 - 1000°C, it is not possible with this technique to be sure of the extent of dislocation generation and movement. However, at the upper end of this temperature range, slip steps are observed after quite prolonged dwell times and it is suggested that some new and enlarged dislocation loops

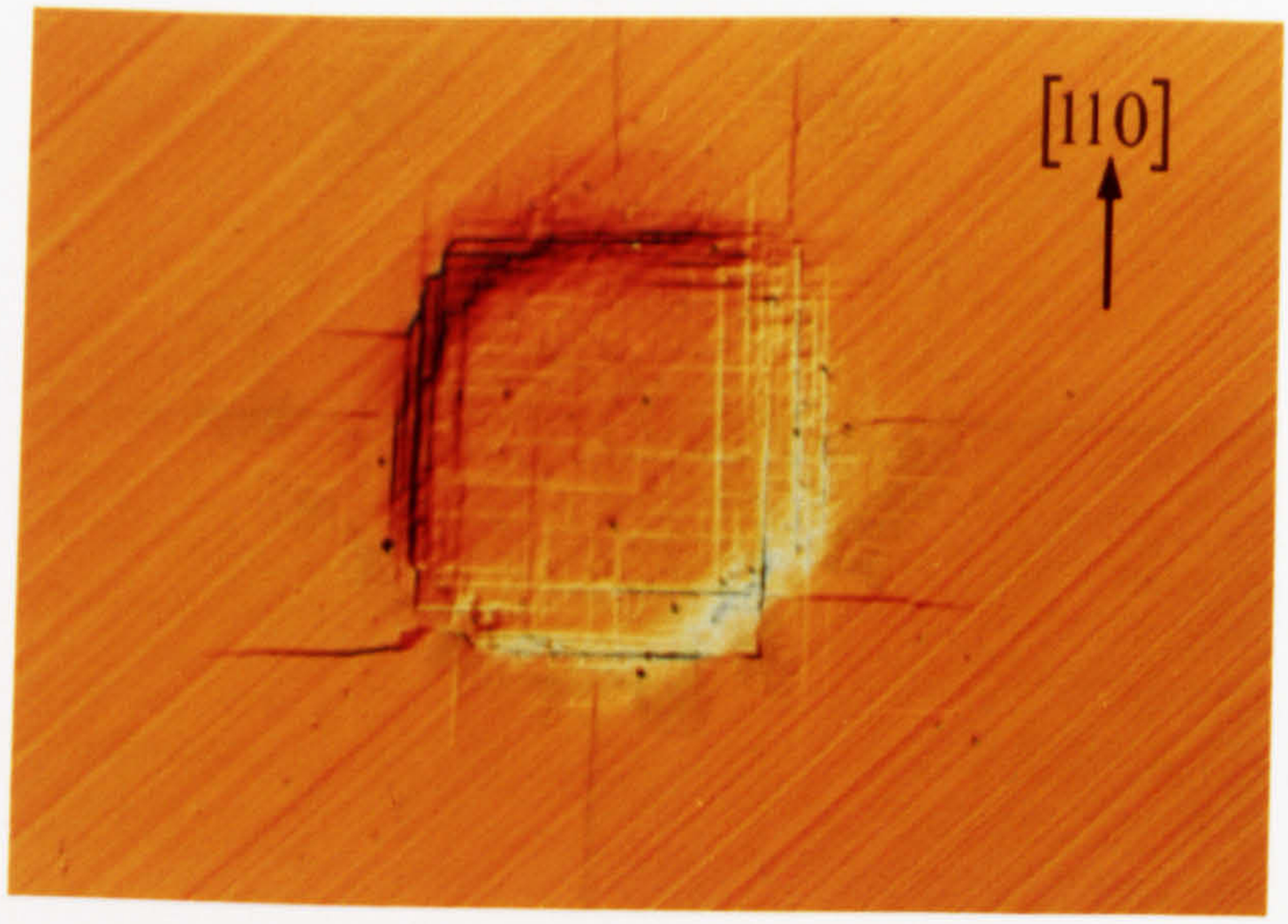

(a)

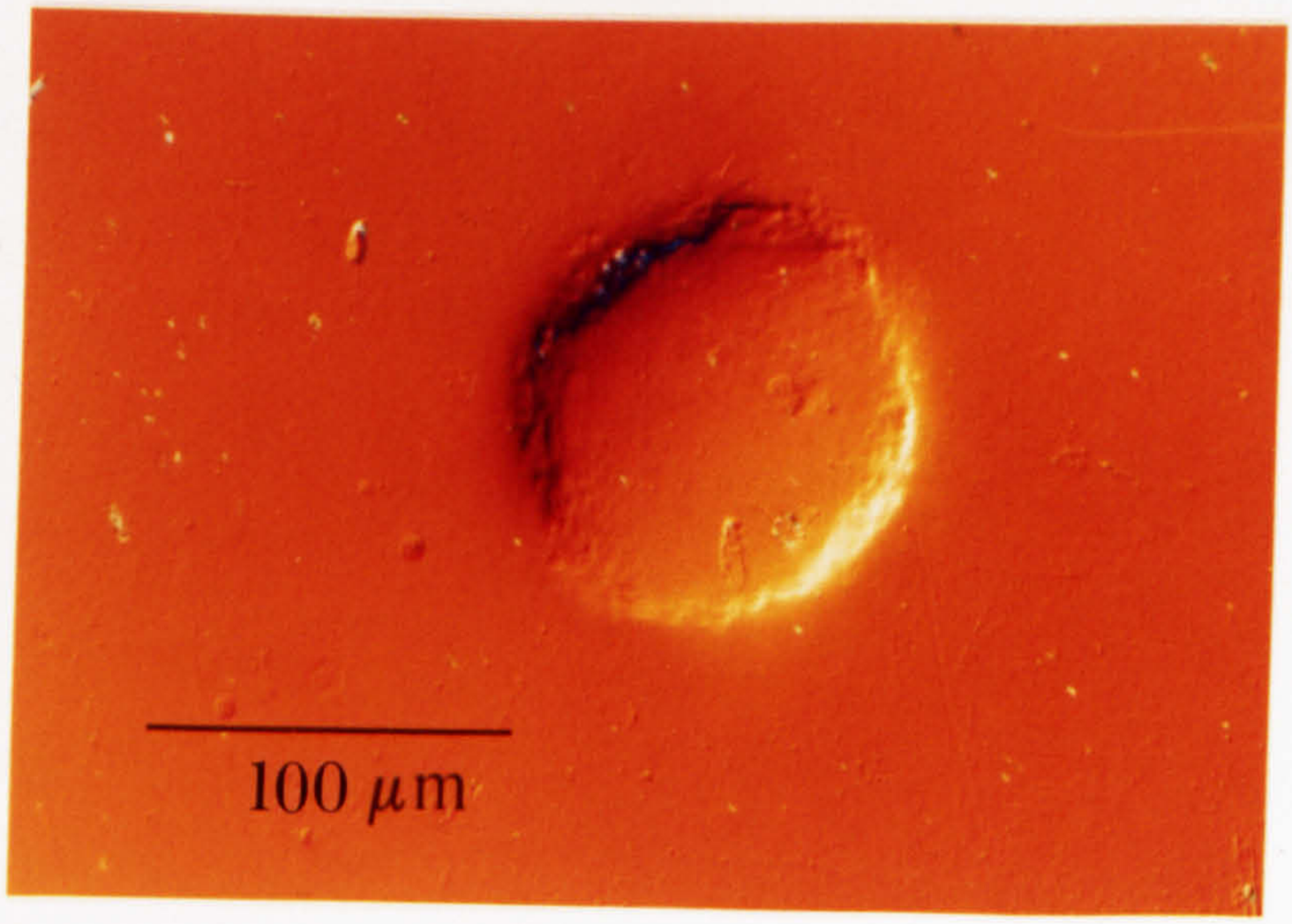

(b)

Figure 4.10 Impressions produced in (a) type Ia diamond, (b) type IIa diamond by the same experimental conditions.

are present, Figure 4.11(a). At 1000°C coarse intersecting slip lines are formed within the impression in type I diamonds, indicative of inhomogeneous slip, Figure 4.11(b). At still higher temperatures, the slip extends outside the actual contact area giving rise to picture frame slip, Figure 4.11(c). Rosette slip, along ⟨110⟩ directions radiating away from the impression, is developed at the highest temperatures and cracking is not observed. These features are a function of increased strain and therefore may be induced by increasing the normal load; or the temperature; or the dwell time.

Examination of the plastic zone beneath the impression, Figure 4.9, reveals two distinct regions. (A) An area of slip on converging planes in the highly stressed region beneath the indenter; the depth of which is limited by dislocation interaction, i.e. presumably work-hardening, and is geometrically related to the width of the impression. (B) A deformed area outside the work-hardened zone where slip is on diverging planes and penetration into the crystal is determined by the Peierls stress. This type of slip is particularly sensitive to temperature and impurity content, eg nitrogen concentration (see Chapter 7), probably through the dependence of the lattice friction stress on such parameters. Divergent slip and rosette formation varies more rapidly with temperature than the convergent dislocated zone beneath the indenter, reflecting the unimpeded increase in dislocation velocity with increasing temperature.

It is the behaviour of dislocations which intersect on the convergent slip planes beneath the contact region which will have the greatest effect on the size and growth of an impression. Consider then dislocations, on those planes, which dissociate into two partial dislocations separated by a stacking fault. If such dislocations meet at the line of intersection of the two planes, the leading partials will attract or repel each other depending on their Burgers vectors, b. Dissociated dislocations may interact:

$$a/6\,[\bar{1}21] + a/6\,[112] \rightarrow a/2\,[011]$$

Undissociated dislocations may also react:

$$a/2\,[101] + a/2\,[\bar{1}01] \rightarrow a\,[001]$$

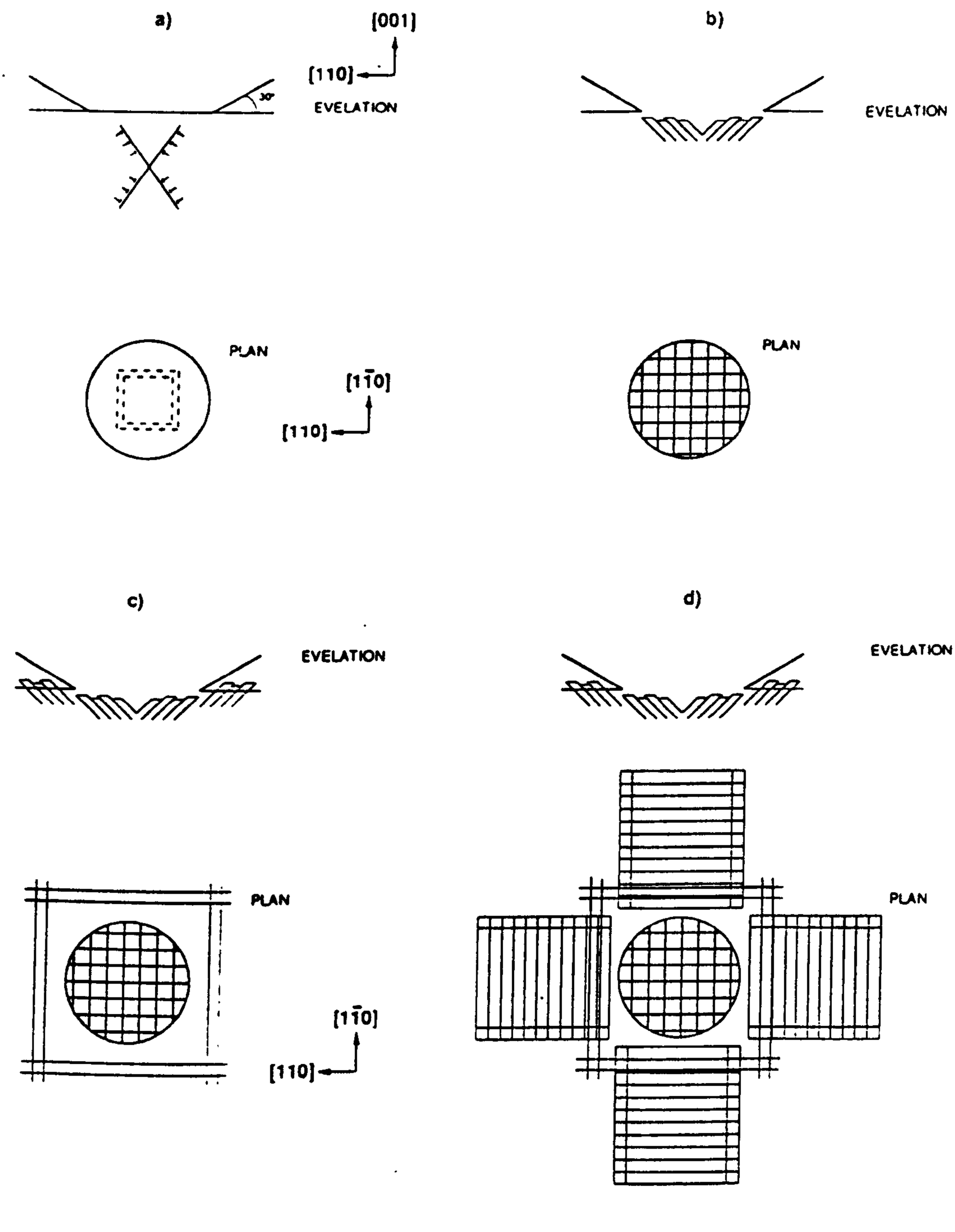

Figure 4.11 A schematic of increasing dislocation mobility on a (001) surface of a crystal with {111} <110> slip systems showing:
(a) initial slip within the contact area, (b) coarse slip (c) picture frame slip
(d) full rosette formation.

Either of these reactions will be favoured because they both result in a reduction of strain energy associated with the dislocations as that energy is directly proportional to b^2. The resultant partial dislocation forms along one of the six ⟨110⟩ directions at the intersection of the stacking faults on the {111} planes but lies in a {100} plane, which is not a slip plane. Therefore, the dislocation is sessile and exerts a repulsive force on the two remaining Shockley partials. These three dislocations form a stable sessile barrier to the glide of further dislocations and are known as *Lomer-Cottrell* locks.

There is a marked and consistent difference between type Ia / Ib and type IIa diamonds in response to a soft indentation . The features typical of type Ia / Ib include the coarseness of the slip, the formation of laths within the deformed volume and the formation of strain induced cracking. As most of the slip under the indenter occurs on converging inclined planes, this will lead to the formation of Lomer-Cottrell locks along the lines of intersection of the slip planes, i.e. the same geometry as the laths, as shown in Figure 4.3. The clarity with which the spacing of the laths, and the associated shear bands, can be observed beneath impressions in diamond encourages comparison with the model used by Bull *et al* (1989) to explain the indentation size effect, ISE, for pyramidal indenters.

For such rigid indenters, a critical load is necessary to induce plastic deformation in well annealed, defect-free single crystals (Page *et al,* 1989). Up to this load the response is elastic and reversible. This implies that a permanent impression involves mixed contributions of both elastic and plastic deformation and that the elastic contribution would be particularly significant in ceramic materials at low loads, i.e. the indentation size effect. Applying the principle of geometric similarity to rigid indenters, the effective strain will be the same whatever the size of the indentation and the measured hardness independent of the magnitude of the applied load. This is generally true in diamond at loads above 20 N where the relationship:

$$P = A\,d^n$$

holds and the exponent 'n' has a value of 2. However, at low loads, n = 1.49 for ⟨110⟩ Knoop indentations on a (001) surface, and the ISE is particularily marked in diamond at

room temperature. Bull *et al* (1989) suggest that, as the contact area supporting the applied load is increased, yielding occurs at the outer edges of the deformation zone, where the tensile stresses are prominent, but on yielding, the contact area is supported elastically for some time. The pile-up of sessile dislocations, such as Lomer-Cottrell locks, would provide significant obstacles to continued slip and an increased stress would be required to overcome such a barrier and permit the continuation of plastic deformation. This incremental slip is resolved as the spacing between discrete slip bands and the critical stress necessary to nucleate each band must vary with changes in the contact-affected volume.

In this work, discrete bands of slip, of an average spacing of 5 - 10 μm, are observed in type Ia / Ib diamond, both in the impression and in the surrounding rosette. Bands are also observed in the deformed region beneath the impression, i.e. laths, with an average spacing of 10 μm. The spacing is of the same order of magnitude as the spacing measured between discrete deformation bands in the work of Bull *et al* (1989) on the ISE in ceramics. The implication is that the plastic deformation occurs in discrete bursts and that in diamond this takes the form of a cascade of tetrahedral cages beneath the contact area. These features are not apparent in type II diamond. Here the slip is much finer, and bands of slip are not observed either on the surface or within the dislocated zone. We might therefore anticipate that the ISE would be more pronounced in type Ia than in type IIa but this is an aspect of indentation in diamond which is yet to be explored.

Also, similar crack formation in type Ia and Ib diamond can be explained by dislocation reactions. Consider the symmetrical median cracks which are initiated beneath the plastically deformed zone and lie on {110} planes at 90° to the surface. Sessile [011] dislocations, formed as a result of the interaction of either undissociated or dissociated dislocations and which lie on (100) planes, form vertical arrays in the (110) plane with the extra half plane of atoms inside the dislocated zone, and therefore, under compression, serve as a wedge to produce tensile stresses in the crystal immediately below the zone. Once the crack has nucleated, it continues to propagate on the {110} plane as the energy for {110} cleavage is only ≈25% greater than for the more common

{111} cleavage mode (13.0 Jm^{-2} for {110} compared with 10.6 Jm^{-2} for {111} cleavage). As Figures 4.3 and 4.8(b) show, these cracks are initiated beneath the heavily plastically deformed zone and are often contained within the bulk of the crystal. They propagate around the periphery of the deformed zone and only reach the free surface when considerable strain has accumulated in the crystal. An illustration of these observations is presented in Figure 4.12.

Similarly, Novikov *et al* (1992) have shown that half-penny median cracks on {110} planes form at temperatures up to 1225°C beneath indentations made in type Ia diamond using a Vickers indenter. At 1225°C, Palmqvist cracks develop whilst above 1350°C fracture did not occur. In general, impressions made in type Ia diamond using a soft indenter showed a marked reduction in cracking, however median cracks were observed in the temperature range 1300 to 1450°C when considerable strain had accumulated in the lattice as a result of plastic deformation.

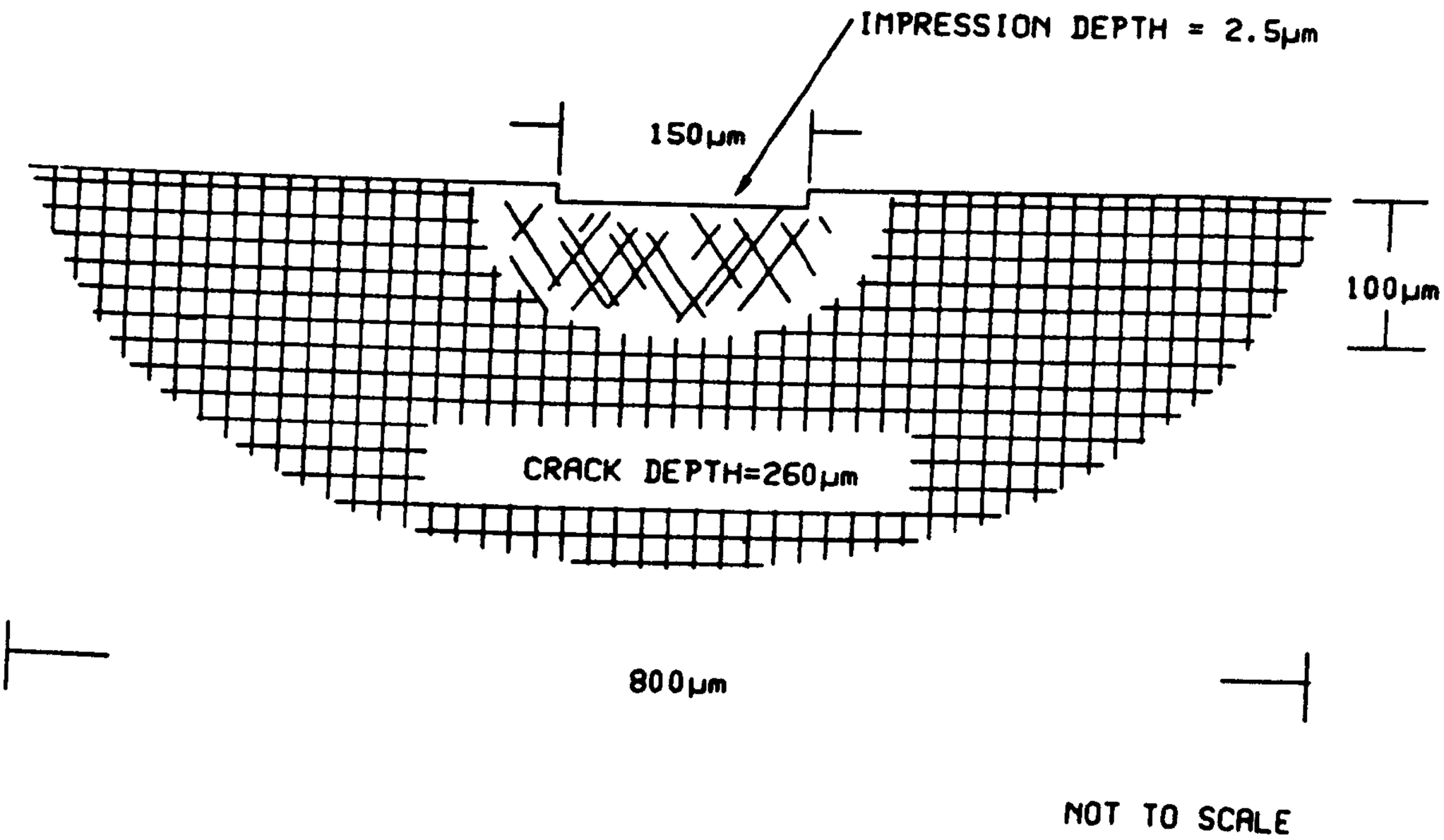

Figure 4.12 Schematic to show cracking beneath the dislocated zone.

4.4 Summary

Certain aspects of the plasticity and fracture of diamond, deformed by softer indenters, are common to all types. Firstly, at homologous temperatures up to about 0.16 Tm and at sufficiently high mean pressures i.e. 20 GPa, there is elastic deformation accompanied by the classical Hertzian cone cracking on {111} planes. Secondly, there is an intermediate temperature range in which such cracking is not observed and there is some evidence, i.e. dimpling, of a degree of dislocation movement, but not sufficient to form visible slip steps. Finally, there is a higher temperature regime where there is no evidence of cracking and the deformation is entirely ductile.

There are other aspects of deformation which are very clearly associated with different types of diamond.

(i) Multiple intersecting slip was initiated in all three types of diamond at experimental temperatures below half the melting point. However, the slip steps within the area of contact, and comprising the picture frame and rosette, were relatively coarse in type I diamonds, but finer slip was found to prevail in type IIa diamond. Deep impressions, several micrometers in depth, were formed in all the diamonds either at temperatures approaching half the melting point or as a result of increasing the contact time.

(ii) Crystallographically aligned features, laths, were always formed within the heavily dislocated zone of type Ia and type Ib diamond, but not in type IIa diamond.

(iii) Several forms of cracking were consistently observed in type Ia and type Ib diamond. Strain induced cracks were often formed in type Ia diamond, usually in type Ib diamond but never in type IIa diamond. These cracks lie predominantly on the {110} planes, although {111} cracks were observed in type Ib diamond, and form around the periphery of the dislocated zone beneath the impression. Other cracks, which appear to emanate from the intersection of slip steps at the edges of the contact area, formed on the {110} planes which intersect the (001) surface at 45°.

Chapter 5. Time dependent plastic flow - Impression creep.

5.1 Introduction.

Creep is defined as the time-dependent and permanent deformation of materials when subjected to a constant load or stress. Typically, a creep test consists of applying a load to a specimen and measuring the deformation or strain as a function of time for a given experimental temperature. Most tests are performed with a constant load which provide useful data for the engineer. Constant stress tests provide information towards a greater understanding of the mechanisms of creep. Creep is normally undesirable in service and may often be the limiting factor in the lifetime of a component.

Creep properties have proved difficult to measure and data has been accumulated using a variety of techniques. Creep tests by bending, compression and tension, some with a constant strain rate, some with a constant load, have been conducted over a wide range of experimental temperature. The criterion for creep in the literature tends to be based on a test temperature which is generally greater than half the melting point. Similarly, mechanical property data for single crystals is limited and experimental work tends to concentrate either on the determination of the critical resolved shear stress as a function of temperature for a selected slip system, or involve a detailed investigation of dislocation configurations and interactions. Results obtained by measuring deformation with time, stress and/or temperature are even more limited. It is often difficult to interpret creep data for single crystals in terms of the mechanisms developed for polycrystals as much of the single crystal deformation occurs by unrestricted slip on a primary slip system.

Most mechanisms of high-temperature creep predict a steady state creep rate, $\dot{E}$, as a function of the applied stress and can be described by the empirical equation:

$$\dot{E} = C \sigma^n e^{-Q/RT}$$

where n and C are material constants, Q is an activation energy and R is the gas constant. Routbort (1991) points out that assumptions frequently made include those that many materials exhibit the same behaviour both in tension and in compression and that a

standard creep equation can be applied. This is not so, therefore the physical interpretation of power-law creep is only valid for steady state conditions and activation energy calculations are of little value when calculated from a region where the stress exponent, n, changes. It is difficult to compare values of Q or n taken from different experiments unless the steady state is verified and a constant deformation mechanism is operative. These observations should be borne in mind when analysing the process of indentation or impression creep with rigid indenters and soft indenters respectively.

Nevertheless, the hardness test provides a simple and fairly non-destructive method of measuring the mechanical properties of solids and the creep properties of many difficult to handle materials may be inferred in this way. The standard hardness test utilises a rigid indenter, conventionally at least three times as hard as the specimen and the load is maintained constant over the duration of the experiment. Such investigations have revealed that all materials continue to deform under a constant load and that this effect is observed at all temperatures. However, below half the melting point this may not be a creep process in the accepted sense as the extent of the deformation depends on many variables, such as the Peierl's potential, diffusion, normal load, resolved shear stresses and the dwell time.

Moreover, conventional uniaxial creep experiments invoke an increase in the strain in a constant volume of the specimen, whereas in the case of the indentation test the strained volume is localised, but the volume immediately below the indenter enlarges with time. In indentations, initial stresses are high and the magnitude of strain is such that cracking frequently occurs to relieve the strain in the lattice, constraining further plastic flow. The soft indenter technique permits the application of a wider range of applied mean pressure and the creep resistance can be studied in a time/temperature regime where the deformation is predominantly plastic.

Perhaps the first researcher to systematically investigate the dependence of hardness on the dwell or hold time, was Hargreaves (1928). Investigating a number of soft metals and eutectics he observed a power law relationship between the indentation diameter, d, and the time, t, under load of the form:

$$\log p = H - h \log t$$

at constant temperature and constant load, where p is the time varying hardness, and H and h are materials constants.

A number of investigators have subsequently found that the dependence of both ball indentation and diamond pyramid hardness on the load time and test temperature can, in part, be predicted. However, our understanding and modelling of indentation creep is far from complete and it is convenient here to identify and separate several distinct modes of behaviour.

'Anomalous' indentation creep.

Westbrook and Jorgensen (1964, 1968) reported that, for indentations made at room temperature using low applied loads, 'anomalous' indentation creep occurs in non-metallic crystals due to the presence of adsorbed water. This adsorbed water was thought to be present within the crystal in two states: strongly bound water affecting response of the crystal to the hardness test and weakly bound water permitting indentation creep. The phenomenon was not observed at heavier loads or, more particularly, at depths of indenter penetration > 2μm. They suggested that 'drying' the crystal or indenting at slightly elevated temperatures removed the effect, hence the term 'anomalous' indentation creep.

Morgan (1976) subsequently confirmed the observation of Westbrook and Jorgensen (1964, 1968) that indentation creep occurs in both magnesium oxide and lithium fluoride single crystals when using loads < 20 gf. However, he demonstrated that indentation creep occurs over the entire load range used and that for magnesium oxide there is an increase in the creep rate with decreasing applied loads. He suggested that this increase in creep rate is associated with increased elastic strain produced beneath a small indentation. He further suggested that applied loads > 100 gf frequently result in surface and subsurface fracture which inhibits the indentation creep process. For a constant applied load, similar creep rates were observed for 'wet' or 'dry' surfaces and that increasing the experimental temperature caused an increase in the indentation creep rate. Morgan also noted that the creep rates measured in rocksalt single crystals were anisotropic.

Conventional indentation creep.

Atkins, Silverio and Tabor (1966) analysed the kinematics of the creep process during indentation, using a transient-creep equation derived by Mott (1953) for constant-stress conditions. Hardness measurements on a wide range of materials, using either a rigid indenter or the mutual indentation of crossed cylinders or wedges, were used to investigate the creep properties at elevated temperatures, particularly above half the melting point. Based on log hardness vs log indentation time they showed that for each of the experimental temperatures considered, straight lines of constant slope are obtained. From the separation of the lines Atkins *et al* (1966) calculated the activation energy for the temperature range considered and found a good correlation with activation energies for self-diffusion.

However, the hardness data is better correlated if a primary creep equation is assumed (Atkins *et al* 1966) rather than a steady state equation. They suggested that the use of a transient creep equation is more reasonable than a steady-state one, since the plastic zone is constantly enlarging with time. The relationship between hardness and creep is implicit, but Atkins *et al* (1966) demonstrated that hardness data could be used to rank the relative creep resistance of a variety of materials over a range of temperatures, and to determine the activation energies and stress exponent, particularily in metals above 0.5 T_m. They also established that the variation in hardness with loading time is independent of indenter shape for small and large spheres and for cones of apical angles 105° through 150°, indicating that the strain rate is not associated with the geometry of the indenter.

A fundamental difficulty in relating time dependent hardness to a creep equation is that the creep equation for uniaxial stress is based on data obtained under constant stress conditions and hardness values are generated under continuously decreasing stress/pressure conditions. To overcome this problem Chu and Li (1977) proposed a test using a flat, rigid, cylindrical indenter impressed into a material under constant load, and therefore constant pressure conditions. The indenter reaches a constant velocity at a relatively shallow penetration, and in theory, the velocity should vary with the indenter diameter in a

manner characteristic of the creep processes taking place in the indented material. In other words, the indentation velocity and pressure can be related to the creep data at a given applied stress in a fundamental way and then the creep stress exponent and the activation energy can be obtained as a function of the punching stress.

Chu and Li (1977) also analysed their data from finite element analysis of the indentation creep test and concluded that, by using the end of a cylindrical indenter, two steady state velocities are observed under a constant load; one near the surface, impression creep, and the other deep in the material, penetration creep. The latter may involve friction between the penetrating rod and the specimen, and for this reason they restricted their investigations to impression creep. Three controlling mechanisms were considered for the impression creep of single crystals; bulk diffusion, surface diffusion and dislocation creep. In the diffusion regime, the impressing velocity is proportional to the punching stress while in the dislocation regime, a power law is observed. This power law has the same exponent as that found in conventional creep. For the same punching stress, the impressing velocity varies inversely with the punch diameter in the bulk diffusion regime, inversely with the punch area in the surface diffusion regime and proportionally with the punch diameter in the dislocation regime. The latter was confirmed experimentally by these authors.

In an investigation of the impression creep of LiF, Yu and Li (1977) confirmed that the time/depth creep curves resemble standard creep curves derived from uniaxial tests, with both primary and secondary regions. The activation energies and the power law stress exponents obtained were found to compare well with the results derived from uniaxial tests. Furthermore, dislocation etch pit studies showed that the depth of the plastic zone beneath the punch was the same as the punch diameter and that the diameter of the dislocated zone was about 2.5 times larger than the punch diameter. In general, the dislocation density was higher for larger stresses and lower temperatures.

Sargent and Ashby (1990) recently derived the creep exponent and activation energy from hot-hardness data for metals and ceramics using the following constitutive law of creep:

$$\dot{E} = \dot{E}_0 \left(\frac{\sigma}{\sigma_0} \right)^n$$

where $\dot{E}$ is the strain rate, $\dot{E}_0 = k e^{-Q/RT}$ k a kinetic constant, σ the shear stress and σ_0 a reference stress at which the strain rate is $\dot{E}_0$. The indentation pressure is equal to the load divided by the projected indentation area and creates a stress field below the indenter which changes in scale but not in shape as a result of the creep process. The activation energy of the creep process is found by plotting either $\ln (H/\mu)$ against T/T_m at a constant time giving a gradient of Q/nRT_m, or a plot of ln time against T/T_m at constant H/μ, which has a gradient of $+Q/RT_m$.

Sargent and Ashby (1990) drew their data from a number of sources. They normalised the hardness by the shear modulus to overcome any slight temperature dependence in σ_0. They express activation energies in kJ / mol, and also in RT_m. The use of RT_m offers two advantages: the number is dimensionless and the activation energy cannot be confused with homologous temperatures. The fit of the data used and the inferred creep parameters n and Q are most accurate when the indentation temperature is above half the melting point (0.5 T_m) and the dwell time is long. Low homologous temperatures and high indentation pressures result in a power-law breakdown, not surprising in a region dominated by dislocation movement on activated slip planes rather than diffusion controlled creep, and how best to analyse this data is still unclear.

Creep in diamond.

The first investigation of time-dependent plastic deformation in diamond was carried out by Evans and Sykes in 1973. Type I and type II diamond octahedra were mutually indented in the temperature range 1500 - 1850°C and the rate of indentation measured. They showed that the deformation for the type II diamonds was fully plastic at 1700°C and above, but for type I diamond the plastic region was 1750° and above. The relationship:

$$\dot{\varepsilon} = \sigma e^{-Q/kT}$$

was derived giving values for Q = 10.7 eV (31 RT_m) for type II diamond and Q = 14 eV (40 RT_m) for type I diamond and where σ is the imposed tensile stress and $\dot{\varepsilon}$ is the strain rate. At temperatures lower than the quoted temperatures plastic deformation was accompanied by cracking in the indentations produced under an applied load of 16.4 Kgf. The experimental temperatures in this work are in the region of half the melting point of diamond, as are those in the work of Atkins *et al* (1966). At temperatures above 1800°C diamond graphitizes, reducing the reliability of the results. Evans and Sykes (1973) conclude that the indentation hardness is determined at 'high' temperatures by the creep relation and the hardness should continue to fall indefinitely at a slower rate as the time of indentation progresses.

Harrison (1973) measured the Knoop hardness and indentation creep of diamond and silicon over a range of experimental temperatures. No indentation creep was observed at room temperature in either material, but significant indentation creep was observed in silicon at 300°C (0.34 T_m) and in diamond at 1100°C (0.32 T_m).

Low temperature indentation creep.

When a test bar is subjected to a constant stress it undergoes an instantaneous deformation - both elastic and plastic. Its dimensions then vary with time i.e. creep under constant stress. The mechanisms of deformation depend on the temperature and stress and can be portrayed on a deformation mechanism map. Four creep mechanisms can be identified:

(i) logarithmic creep $T < 0.3\ T_m$,

(ii) dislocation creep $T > 0.3\ T_m$,

(iii) dislocation glide and

(iv) diffusional creep $T > 0.9\ T_m$.

Dislocations move, multiply and interact on intersecting slip planes and the resultant increase in dislocation formed obstacles will limit further mobility and probably result in cross slip and work hardening at temperatures $< 0.3\ T_m$. Obstacles may be overcome by thermal activation enabling a limited amount of edge dislocation climb. As dislocation mobility becomes more restricted, reflecting the logarithmic strain-rate relationship, the activation energy for creep increases with strain. When $T > 0.3\ T_m$ the mobility of vacancies is sufficient to allow dislocations to climb readily, therefore obstacles will be bypassed and this is the rate controlling process and steady state glide will prevail.

Li *et al* (1991) have derived seven rate-equations for the different possible mechanisms of indentation creep, some or all of which contribute to the indentation creep process. The possible mechanisms include:

plasticity - dislocation glide, described by two rate equations, H_1 and H_2.

power law creep - climb plus glide, H_3,

power law breakdown - glide plus climb, H_4,

recovery - dislocation climb, H_5,

diffusion - volume, grain boundary or dislocation pipe diffusion, - H_6 and H_7.

The processes H_1 - H_5 involve similar defects, basically describing the movement of dislocations under different conditions. The diffusion mechanisms H_6 and H_7 and the dislocation mechanisms H_1 to H_5 are independent and involve different defects. All of the rate equations can be expressed in the form:

$$\dot{H} = f(H)\, H^{m+1}$$

where $\dot{H}$ is the rate of change of hardness and H is the initial hardness. Assuming a constant microstructure $f(H)$ can be treated as a constant.

The activation energy in H_1 reflects the energy for the indentation - creep mechanism of dislocation glide limited by the resistance of the lattice, whereas that in H_2 reflects the glide mechanism limited by obstacles such as other dislocations, precipitates or grain boundaries. At elevated temperature dislocations overcome obstacles by climb, and H_3 describes power-law creep, where dislocations move mainly be climb. At high stresses, power-law creep changes to control by glide, H_4, and the mechanism is known as power-law breakdown. Rate equation H_5 describes the climb controlled dynamic recovery - creep process. Diffusion creep occurs in polycrystalline materials by grain boundary sliding with diffusional accommodation, H_6, and in single crystals by dislocation pipe diffusion or volume diffusion H_7.

Whereas the overall creep rate is determined by a combination of all the mechanisms, Li *et al* (1991) found that the contribution from power - law creep (H_3) is much smaller than that of dislocation glide (H_1) and concluded that dislocation glide dominated creep in all of the materials studied, over the temperature range 0.15 - 0.58 T_m. Earlier attempts to explain indentation creep based on a power-law mechanism predicted constant log H vs log t slopes independent of temperature. However, the plasticity mechanism (H_1 or H_2) is more realistic, predicting an increase in the slopes of the creep curves with temperature, as the experimental results confirm.

Experimental work on MgO (Brookes *et al*, 1991) and diamond (Brookes *et al*, 1990) using the soft indenter technique have provided some insight into the dislocation mechanisms involved in creep at low homologous temperatures. It has been established that dislocations are initiated in the harder crystal when the mean pressure due to point

contact developed by softer materials exceeds a certain level and that the dislocated volume continues to expand whilst the mean contact pressure causes the critical resolved shear stress to be exceeded (Chapter 3). The dimensions of the dislocated zone, under similar experimental conditions, are the same for soft and for conventional diamond pyramidal indenters, but the density of dislocations within that volume increases with the hardness of the indenter. Therefore the effective strain within the dislocated volume increases with indenter hardness. A similar effect can be achieved by repeated loading of the soft indenter on the same contact area. However, increasing the dwell time increases the dislocated volume such that geometrical similarity is preserved. A recent publication (Brookes *et al*, 1990), and this work, have shown that the dimensions of impressions in diamond made by a soft indenter increase with dwell time. Both the contact diameter and the depth of the impression increase with time to maintain geometric similarity. Whereas the increased diameter of the impression may be due to creep of the indenter material, the increased depth of the impression must be assumed to be due to creep of the diamond. This is particularly significant as an increased indenter diameter leads to a reduced contact pressure, but, despite a reducing pressure, there is measurable creep in all types of diamond over a wide temperature range below half the melting point ($< 0.5\ T_m$).

5.2 Experimental details.

The indenter material selected for the initial experiments was cubic boron nitride (Amborite) and a normal load of 100N was used. The indenter was ground to an included angle of 120° prior to each set of experiments. A conditioning impression was made for a duration of 300s to both flatten the indenter tip and to establish the working temperature. Any rearrangments of the position of the diamond or adjustment of the applied current could be made at this time. Impressions were then made for dwell times of 300s, 1000s, 2000s and 3000s, in that order, for a constant temperature. Thus the dwell time for each impression measured was as stated but the time under load for the indenter was cumulative.

Contact areas were measured using a calibrated filar eyepiece on the Nikon Optiphot light microscope. Square counting of the contact area from a photographic print of known magnification provided a check on the accuracy of this method.

A more sophisticated method of obtaining data from the impressions involved the use of a direct phase detecting interferometer, DPDI, developed in this department. The DPDI utilises a Mirau lens mounted on a standard objective turret on a Nikon Optiphot microscope. The specimen was mounted on a tilting stage which can be adjusted until the surface of the specimen is normal to the optical path through the Mirau lens. Light and dark bands are produced by constructive and destructive interference of two beams of light. A single source emits a beam of monochromatic light which is separated into two. One portion of the beam is reflected to a mirror. The second portion of the beam is reflected by the specimen and back through the lens parallel with the first 'half' where both beams merge to a single light beam variable in intensity. The distance between the beam splitter and the mirror is such that the path the light travels is approximately the same distance whether it has been reflected by the specimen or the mirror. A dark fringe indicates destructive interference and represents a merging of the two beams when one has travelled either half a wavelength or (2n + 1)/2 wavelenths farther than the other. A light fringe indicates constructive interference. The difference in height of the specimen between a light fringe and a dark fringe is one quarter of the wavelength of the light, in this case 136.5 nm. A circular impression in the surface, providing it is 136.5 nm or deeper, is visible by concentric bands of dark and light.

Once an interferogram has been produced, a frame grabber records the information from a video camera mounted on the microscope. Three different images of a selected area are used. Background adjustments are made to the image and a point on that image is selected as a reference point. The equipment is further adjusted to obtain the largest intensity range possible and the information at that point recorded. The specimen is then moved the equivalent of 1/8 the wavelength of the light and the second of the pictures recorded. This is repeated once more, with the result that three pictures with the reference point at maximum, average and minimum intensity are recorded. The software is then enabled to produce a three dimensional profile plot of the impression. If, however the

fringes overlap due to irregularities on the surface or the spacing between them is insufficient to enable discrimination between them, then a computer analysis is not possible.

Direct phase detecting interferometry using computerised methods produces data in the form of the depth against position and from this can be found the area and the volume of the impression. The lowest part of the impression is detected and the pixels are "filled in", ie the area of the base of the impression. The levels are filled up until an "overflow" is achieved indicating the top of the impression or the surrounding original surface. Counting the pixels gives a direct reading of the parameters required.

Impressions which were either too contaminated with indenter material or too steep-sided to be measured using the computerised technique had to be evaluated by an alternative method. Photographic enlargments of the interferograms of the impressions were made and the fringes traced onto transparent paper. Co-ordinates of numerous points on a given fringe were taken and using suitable software the area of individual fringes were calculated. The depths were then computed using the number of fringes and partial fringes per impression. Volumes were calculated using a simple mathematical formula valid for a truncated cone or pyramid

$$V = \frac{d\,(A_1^2 + A_2^2 + A_1 A_2)}{3}$$

where V = volume of a truncated cone

d = depth between the two fringes

A_1 = area of the first fringe

A_2 = area of the second fringe

The volumes of the truncated cones are then summed to give the total volume of the impression.

5.3 Results.

The applied mean pressures, resulting impression volumes for a given dwell time and the experimental temperature are summarised in Table 5.1. The results are shown in Figures 5.1, 5.2 and 5.3 as plots of volume against time.

The rate of change of volume for a given experimental temperature was evaluated and the results are summarised in Table 5.2, and plotted as the volume rate change against the reciprocal of temperature in Figure 5.4. The slopes of the lines shown in Figure 5.4 give activation energies Q, of 2.89 eV (8.38 RT_m) for type Ia diamond, 1.2 eV (3.5 RT_m) for type Ib diamond and 2.92 eV (8.48 RT_m) for type IIa diamond.

5.4 Discussion.

According to Bernholc *et al* (1988) the dominant mechanism for self diffusion in diamond is vacancy diffusion and for a neutral vacancy, the activation energy was calculated as 9.1 eV (26.4 RT_m). By comparison, the activation energy for N diffusion in diamond is given as 2.6 eV (7.5 RT_m), (Chrenko *et al* 1977). Maugis (1979) in his review of creep, surface diffusion and segregation, indicates RT_m values for some of the mechanisms of creep. The activation energy Q_L for the self diffusion mechanism is given as 17.5 RT_m, but at lower temperatures the activation energy Q_D for the dislocation pipe mechanism is given as 12 RT_m. Values of Q are given as 19 RT_m for temperatures greater than 0.78 T_m, and as 13 - 14 RT_m for $0.54 < T/T_m < 0.78$. Examination of hardness data for tin (Atkins *et al,* 1966) produces two master curves with activation energies of 19 RT_m for temperatures greater than 0.78 T_m, and 13 - 14 RT_m for $0.54 < T/T_m < 0.78$. Maugis concludes that creep by dislocation pipe diffusion occurs at about 0.5 T_m, and that creep by lattice diffusion occurs at temperatures above 0.78 T_m.

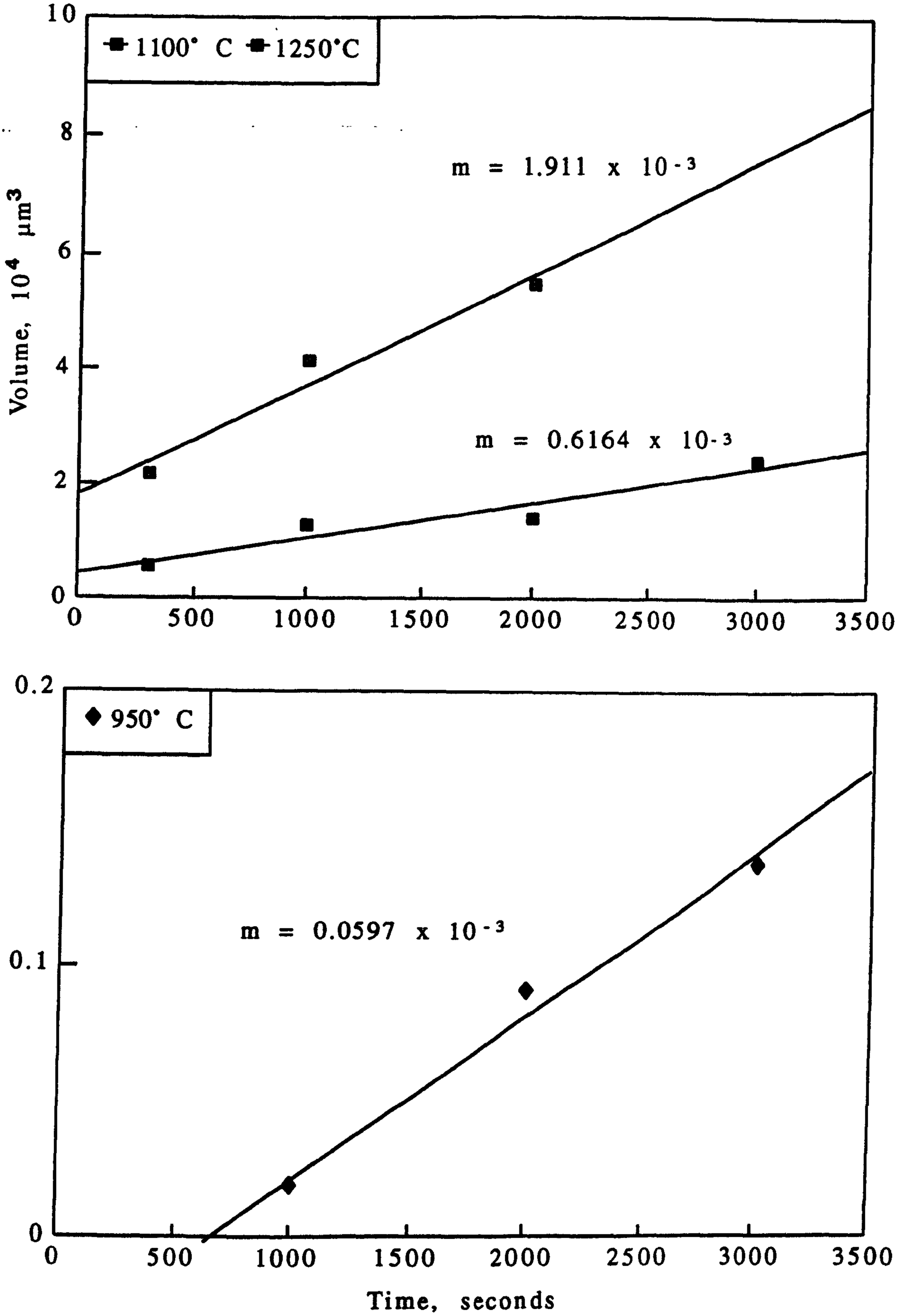

Figure 5.1 Impression volume vs dwell time for type Ia diamond

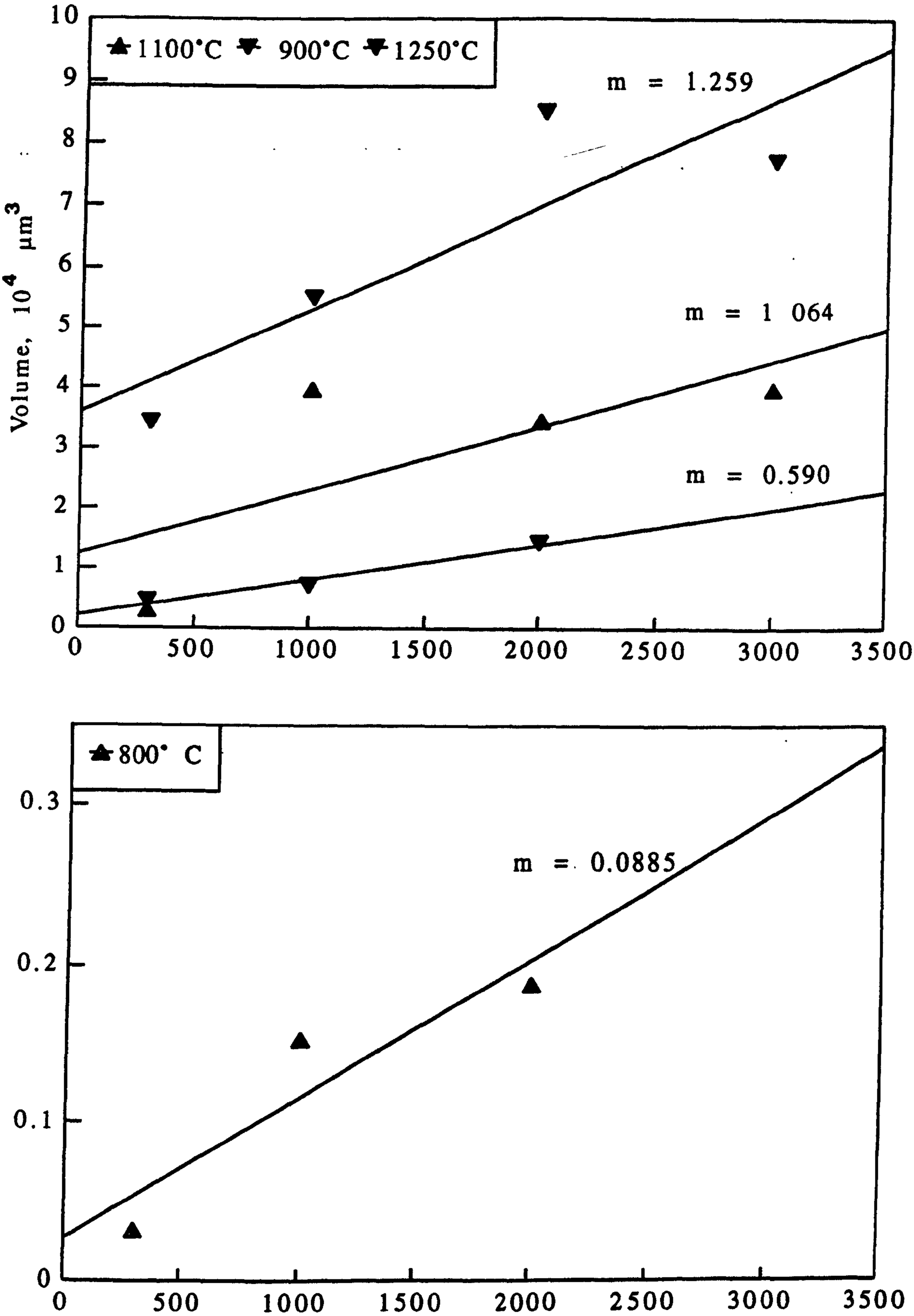

Figure 5.2 Impression volume vs dwell time for type Ib diamond

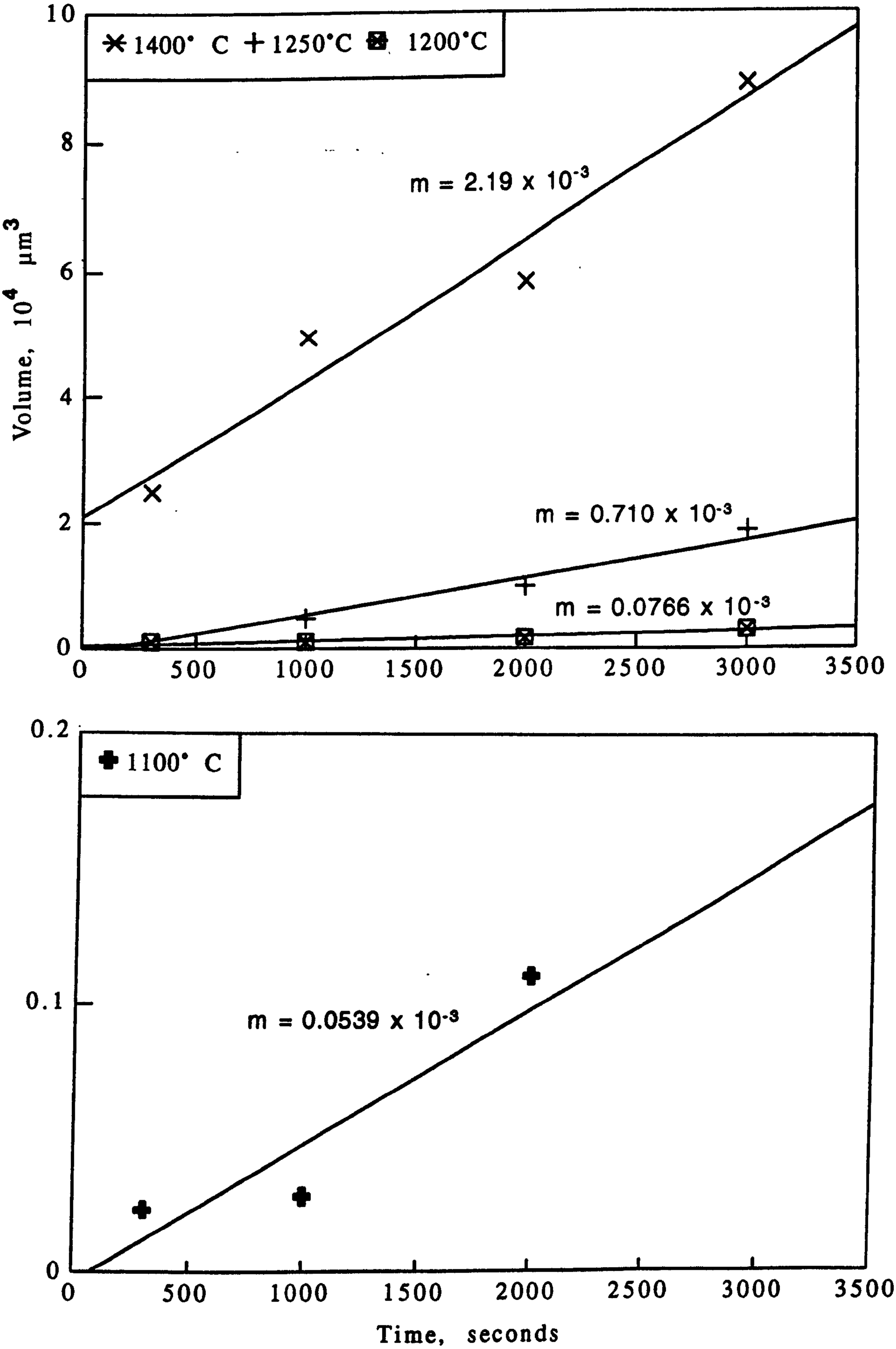

Figure 5.3 Impression volume vs dwell time for type IIa diamond

Table 5.1. Impression volumes, μm^3, different dwell times, for type Ia, Ib and IIa diamond.

		300s	1000s	2000s	3000s
type Ia:					
	950°C	-	186 (9.3)	912 (10.2)	1,380 (9.9) (10.6)
	1100°C	5,740 (6.0)	12,860 (5.3)	14,010 (5.1)	24,110 (4.8)
	1250°C	21,600 (5.0)	41,400 (4.3)	54,800 (4.1)	33,500 (4.6)
type Ib:					
	800°C	-	320 (10.2)	1,530 (9.9)	1,890 (9.4)
	900°C	4,540 (9.9)	7,180 (8.9)	14,400 (8.2)	- (8.1)
	1100°C	3,100 -	3,970 -	3,460 -	3,950 -
	1250°C	3,420 (6.3)	5,500 (6.0)	8,510 (5.3)	7,700 (5.6)
type IIa:					
	1100°C	230 -	280 (10.7)	1,110 (11.0)	- (10.0)
	1200°C	1,030 (6.5)	1,000 (8.3)	1,750 (7.80)	3.050 (7.5)
	1250°C	- -	4,700 (6.4)	10,000 (5.4)	18,900 (4.6)
	1400°C	24,900 (5.8)	49.500 (4.8)	58,400 (4.3)	88,800 (4.5)

The mean contact pressures, in GPa, are given in brackets.

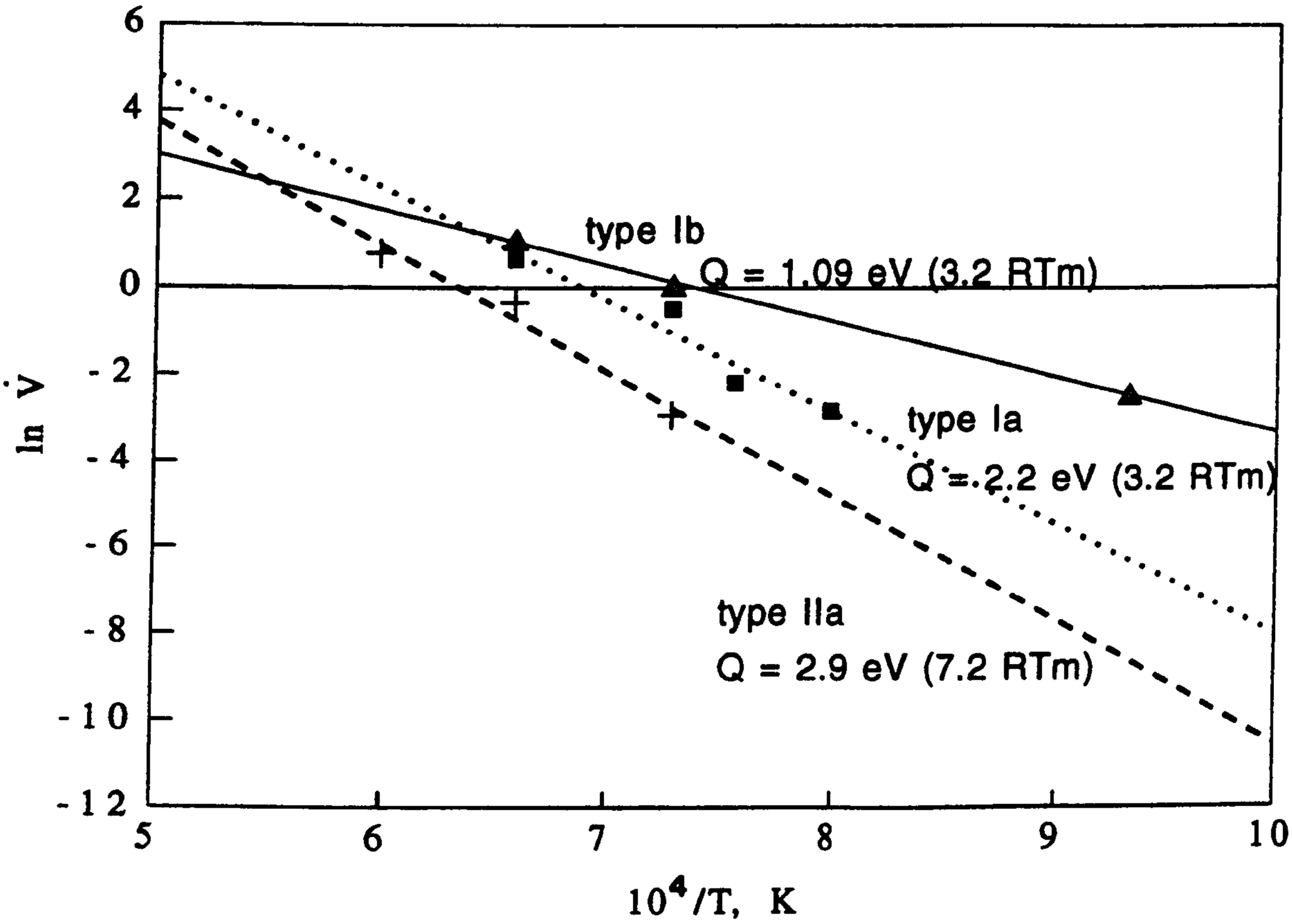

Figure 5.4 Arrhenius plot of volume rate change vs the reciprocal of temperature for type Ia, type Ib and type IIa diamond

Table 5.2 The rate of change of volume for a given experimental temperature,°C.

	$10^4/T$	V	ln V
type Ia:			
980°C	7.981	0.0060	-2.818
1100°C	7.280	0.0616	-0.484
1250°C	6.565	0.1911	0.647
type Ib:			
800°C	9.32	0.0885	-2.4248
900°C	8.525	0.5900	-0.527
1100°C	7.283	1.0643	0.062
1250°C	6.565	3.000	1.0986
type IIa:			
1100°C	7.283	0.054	-2.921
1200°C	6.788	0.077	-2.569
1250°C	6.566	0.710	-0.342
1400°C	5.977	2.187	0.782

Measurement of the creep indentation of type I and type II diamond in the temperature range 0.44 to 0.53 T_m (Evans and Sykes, 1974) give values of Q of 10.7 eV (24 RT_m) for type II diamond and 14 eV (66 RT_m) for type I diamond. These values seem high even when compared with those typical of creep controlled by self diffusion at homologous temperatue above $0.78T_m$.

Li *et al* (1991) have concluded that for the range of temperature 0.25 - 0.5 T_m, dislocation glide dominated creep in all of the materials they studied. The activation energies measured in this work were obtained in the temperature range 0.27 - 0.4 T_m. The values of activation energy fall below the 13 - 14 RT_m at 0.54 T_m set by Maugis and they are also significantly lower than those obtained by Evans and Sykes.

The values obtained show little difference between type Ia diamond (2.89 eV) and type IIa diamond (2.92 eV) and compare well with the activation energy for N diffusion in diamond (2.6 eV). The value for type Ib diamond (1.2 eV) is somewhat lower and this is difficult to understand.

Calculating the activation energy from the data presented in this Chapter does not appear to assist in a greater understanding of the mechanism which controls the time dependent increase in the depth of impressions, and the associate dislocation volumes, which is observed beneath rigid and soft indenters. The fact that the calculated activation energy is close to that for diffusion of nitrogen in the diamond lattice would appear to be coincidental, since the same value is obtained for type IIa, with low levels of nitrogen impurity and for type Ia with about 500 ppm nitrogen, most of which is in aggregated form. In addition, quite different activation energies are observed for type Ib diamonds where significant nitrogen does substitute for carbon. A clearer understanding must therefore await further experimental data for diamond and other covalent solids at homologous temperatures up to 0.5 T_m.

5.4. Summary.

As a result of this investigation into the low homologous temperature 'creep' properties of diamond, some important new observations can be made concerning indentation / impression creep.

(i) Recent work by Brookes *et al* (1991) on MgO, established that geometric similarity prevails in the deformed zone. A similar phenomenon has now been observed in diamond.

(ii) The applied strain rate decreases with time due to creep of the indenter material, with a corresponding decrease in the mean pressure and an increase in the dislocated volume.

(iii) Creep in the diamond continues as the mean contact pressure is decreasing, resulting in an expansion of the dislocated volume, but not an increase in the effective strain. The effective strain increases only with the hardness of the indenter. In other words, the dimensions of the dislocated zone beneath an indentation and / or impression are essentially the same for a given load and dwell time but higher mean pressures induce greater dislocation activity within the same volume. This dislocated volume continues to expand, even though the applied mean pressure may be decreasing, and the effective strain decreases with time. This process continues whilst the mean pressure is sufficient to exceed the critical resolved shear stress.

(iv) Strain induced cracking occurs, outside the elastic plastic boundary, to relieve the volumetric strain in the lattice.

Chapter 6. The application of the soft indentation technique to isotopically enriched synthetic diamonds.

6.1 Introduction.

Natural diamond contains two stable isotopes; the more common form ^{12}C, with a nucleus composed of six protons and six neutrons, and the minority form ^{13}C, with *six* protons and *seven* neutrons. Properties dependent on the charge, such as the strength of the covalent bond, are unlikely to be affected by the difference in isotopic content. However, the heavier ^{13}C atoms tend to vibrate at lower frequencies than the ^{12}C and this difference is sufficient to affect the scattering of phonons. From the theory of thermal conductivity, predictions of a possible 5% increase in thermal conductivity at room temperature were made for isotopically enriched diamond (Slack, 1957). In fact, Anthony *et al* (1990) found an increase of 50% in the thermal conductivity of an isotopically enriched diamond, compared with diamond with a natural abundance of carbon isotopes grown under the same conditions as the isotopically enriched diamond, and with a natural type IIa diamond supplied to him by Drukker.

Two samples of synthetically produced diamond were provided by Dr. William F. Banholzer of the G.E. Corporation, Schenectady. The samples weighed just under one carat each and had been polished by Kaplan of New York as rectangular bars with at least two parallel (001) faces. The isotopic composition of one bar was 99·9% ^{12}C, henceforth referred to as the IE bar. The other sample contained a natural abundance of carbon isotopes and was measured at 98·9% ^{12}C, referred to as the NA bar. Both samples were almost colourless.

Isotopic enrichment was achieved by a two stage process. Firstly, films of polycrystalline diamond, PCD, were grown by chemical vapour deposition (CVD) using ^{12}C enriched methane as the source gas and a reaction chamber constructed from materials that do not dissolve carbon, namely quartz and copper. The PCD was then crushed and used as a source material for high-pressure/high-temperature growth on seed crystals,

using the temperature-gradient technique (Anthony *et al*, 1990). The outcome of this work was good quality, type IIa diamonds.

The 'soft' indentation technique has established favourable conditions for plastic deformation in diamond, and in this respect distinguishes between type Ia and type IIa diamond, where the basic difference is the presence or absence of nitrogen coupled with the absence or presence of significant numbers of existing dislocations. The GE diamonds are virtually nitrogen free and contain a lower dislocation density than natural type IIa diamond. Therefore it was of some interest to include the GE isotopically enriched ^{12}C diamond in this study.

6.2 Experimental procedure.

Optical micrographs of the two diamonds were taken. The (001) surfaces had been polished flat and parallel but a certain amount of chipping was evident. The quality of the samples was good, but they were not inclusion free. The NA sample contained a large number of small inclusions, apparently located on or close to growth-sector boundaries, forming a cross pattern which was visible under the microscope. The IE sample contained a larger cigar-shaped inclusion which was visible to the naked eye.

Birefringence studies showed that the NA sample was quite severely strained with the strain nucleus located at the centre of the inclusion cross pattern. The IE sample was less severely strained, but a pattern of birefringence emanated from the presumed position of the seed crystal.

As the basis of the distinction between the type I and type II diamond lies in the amount and distribution of nitrogen impurity atoms, a measurement of the impurity content was made. Isolated substitutional nitrogen was present at the very low concentrations of 0.6 ppm and traces of uncompensated boron were also found to be present. Raman measurements confirmed the stated isotopic abundances. These measurements were carried out at the DTC Research Centre in Maidenhead.

There is a limited amount of data available to show that, at room temperature, type IIa diamond is harder than type I diamond (Brookes, 1979), and that anisotropy in Knoop

hardness is not observed in synthetic diamonds containing less than 60 ppm nitrogen (Doi *et al*, 1984). Knoop indentation hardness measurements were made on the (001) surface of the IE diamond, at room temperature, with a normal load of 1kgf. Six indentations were placed, three in the <100> direction and three in the <110> direction.

The experimental temperature for the 'soft' indenter study was 1100°C,the normal load was 100 N, the indenter material was cBN, and the dwell times were the same as those used in the investigation of the 'creep' of diamond, i.e. 300, 1000, 2000 and 3000 seconds successively. These conditions were selected to enable a direct comparison with the results and observations on natural type I and type II diamonds which had been reported in a previous publication, (Brookes *et al*, 1990).

6.3 Results.

(A) Isotopically enhanced diamond.

The Knoop hardness indentations in the IE diamond were well formed, of the order of 40 μm in length, and quite shallow. The <110> direction was determined to be the harder direction, with very shallow indentations which had undergone significant elastic recovery of the short diagonal. The <100> direction was found to be the softer direction, with less elastic recovery of the short diagonal, and some cracking associated with the indentation. These results, together with the Knoop hardness of different types of diamond are summarised in Table 6.1.

The set of micrographs in Figure 6.1 illustrates the nature of plastic deformation of the 99.9% ^{12}C deformed at 1100°C by a cBN cone with a normal load of 100N. The intersecting slip steps produced within the area of contact are relatively coarse and resemble those formed in type Ia and synthetic type Ib diamonds under similar experimental conditions. The slip steps outside the area of contact i.e. the picture frame, are fine and are similar to the slip observed in type IIa diamond. The mean contact pressure decreased with increasing dwell time from 8.5 to 6.7 GPa.

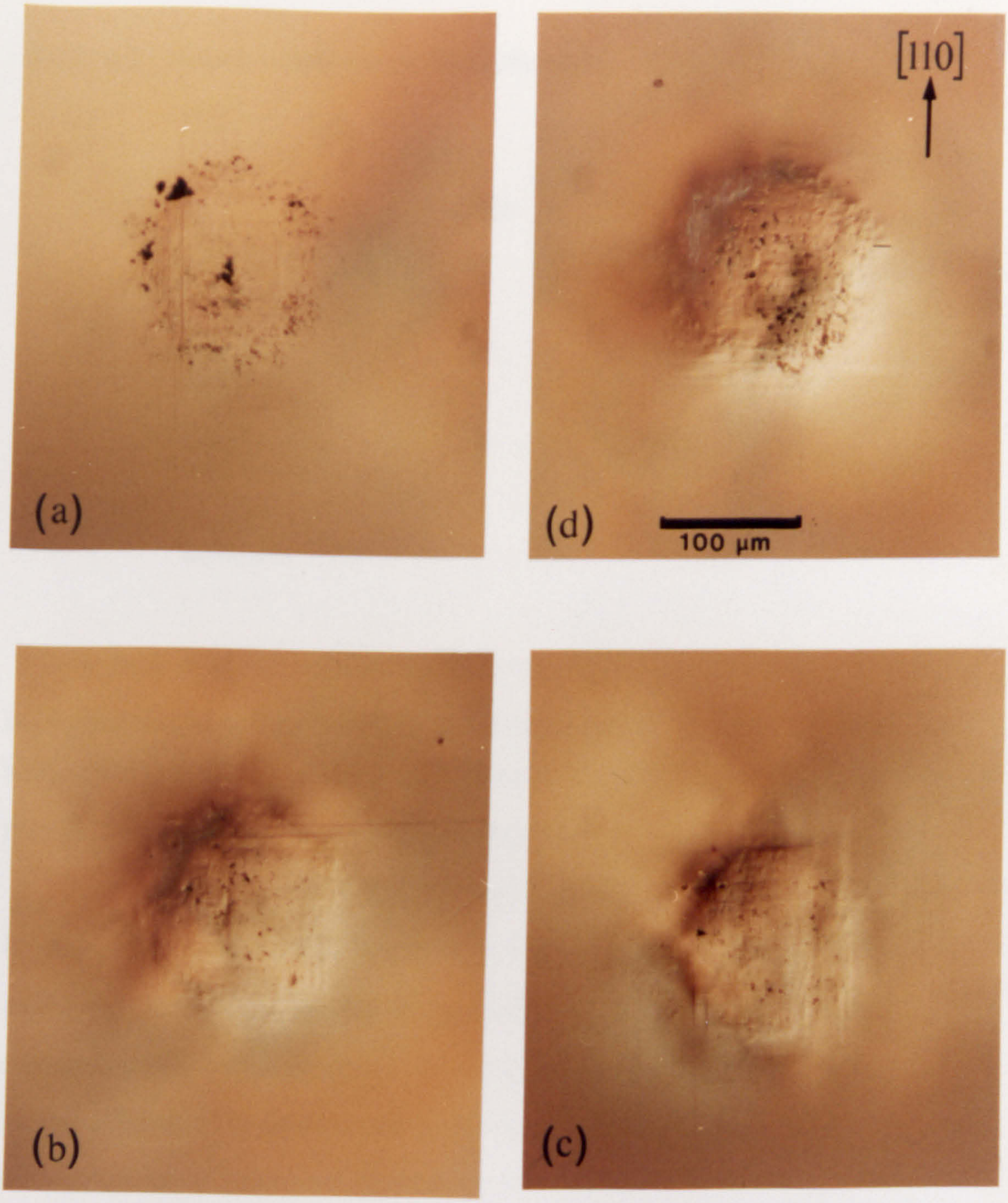

Figure 6.1 Differential interference contrast micrographs of individual impressions in the isotopically enriched (IE) diamond:

(a) 300 seconds, (b) 1000 seconds, (c) 2000 seconds, (d) 3000 seconds.

Table 6.1. Knoop hardness of (001) diamond, (GPa).

	(001)	
	<100>	<110>
type Ia (natural)	98	83
type IIa (natural)	103	91
type Ib (synthetic)	74	68
type II (synthetic ^{12}C)	90	83

A high level of residual strain, which increases in intensity and extent with increasing time of contact, is observed. The micrographs in Figure 6.2 establish that the surface and sub-surface cracking and the tetrahedral laths, always observed in type Ia and type Ib diamond, are not formed in these diamonds.

Mirau interferograms of the four impressions, Figure 6.3, show that the volume of the impression increases significantly with time. The nature of the 'pile-up' changes with increasing dwell time as a result of the impression creep process. With longer times, the pile-up is prominent along the <110> directions consistent with impressions which have formed a rosette. The interferograms also indicate that the shape of the boron nitride cone was maintained as subsequent impressions were made during periods of creep by both the cone and the diamond specimen.

It was also observed that the heating of the IE diamond during the experiments resulted in a strain pattern developing about the visible cigar-shaped inclusion. The inclusion appeared to be larger and a crack interface was observed in the vicinity of the inclusion, presumably due to the need to accommodate the increased volume of the inclusion.

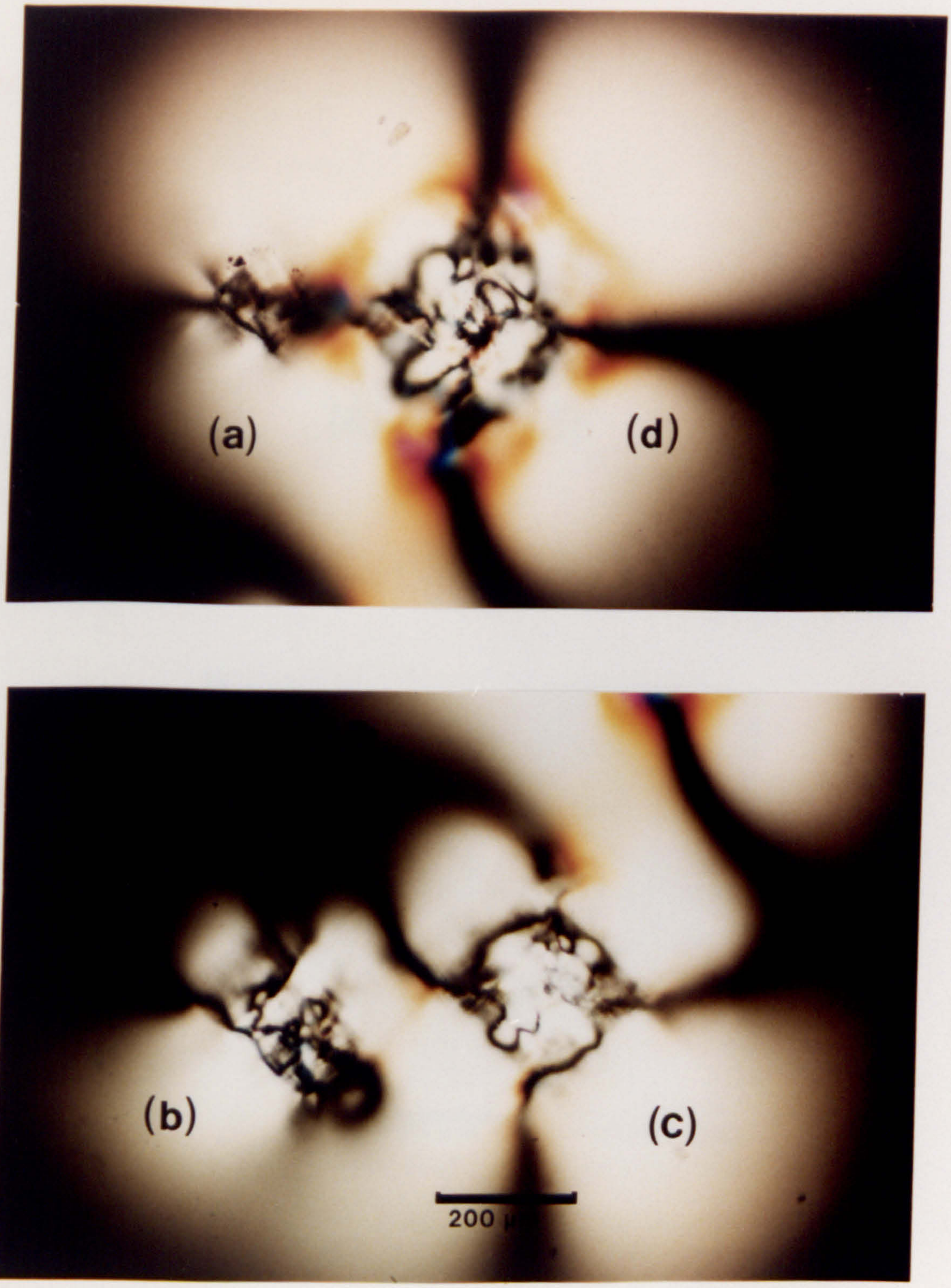

Figure 6.2 Transmitted light micrographs of the impressions shown in Figure 6.1.

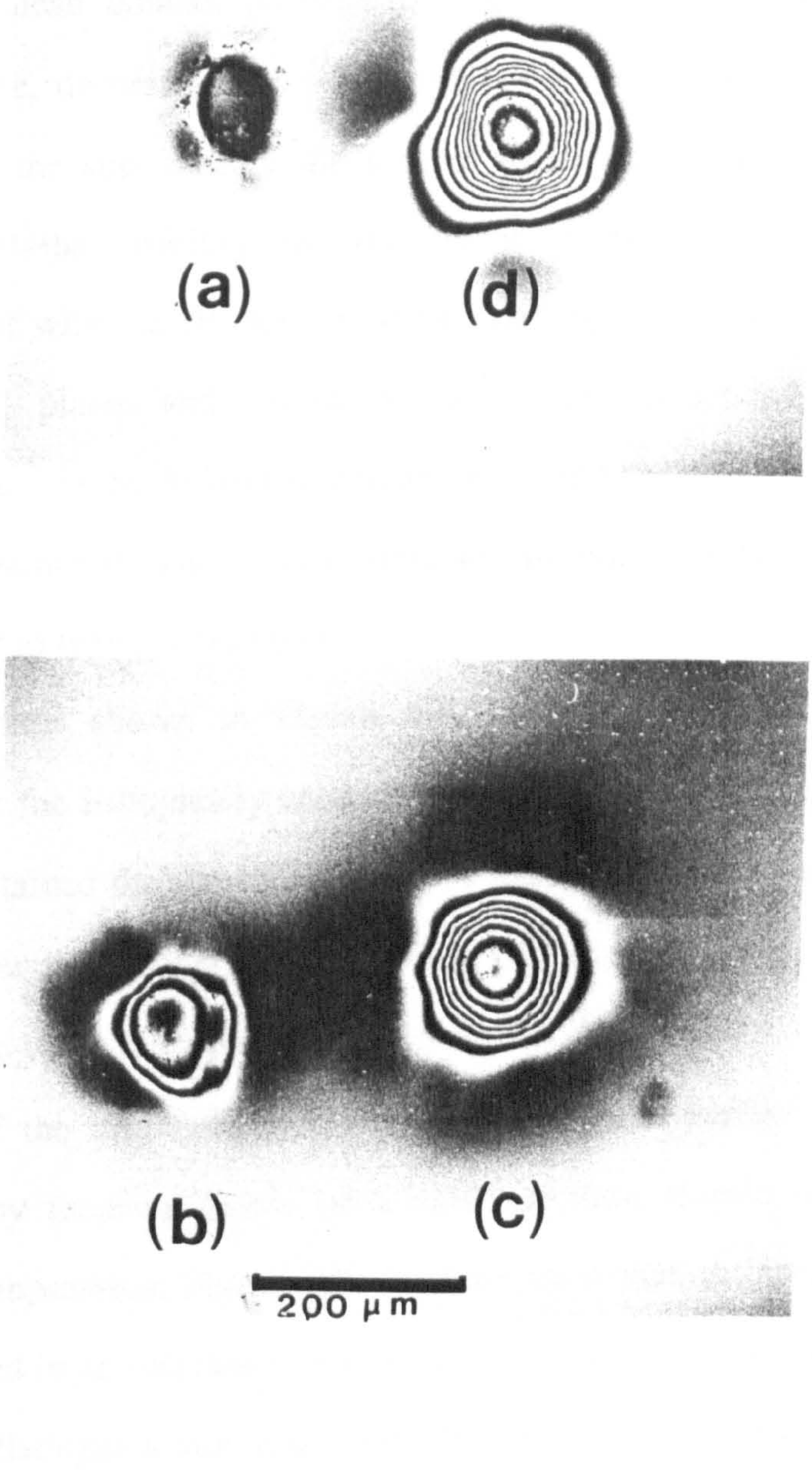

Figure 6.3 Interferograms of the impressions shown in Figure 6.1.

(B) Natural abundance diamond.

The equivalent set of micrographs for the 98.9% ^{12}C sample are shown in Figure 6.4 and 6.5. Here the mean contact pressure is slightly lower and does not change as significantly with time, decreasing from 6.5 to 5.9 GPa with the increased impression times. The scale of the slip beneath the area of contact is similar to the isotopically enhanced sample, but the visibility and the extent of the fine picture frame slip is increased. In contrast with the IE sample, some cracking has developed with increased dwell time on {111} planes and within the region of contact. Subsurface fracture emanating from the base of the deformed area and bisecting the edges of the picture frame, so typical of type I diamonds, has not been observed in either sample, In this respect the deformation is similar to type IIa diamond.

The interferograms shown in Figure 6.6, reveal impression depths of similar magnitude to those in the isotopically enhanced sample. Again, the shape of the blunted cone appears to be retained through the successive loadings. The 300s impression in the NA diamond is deeper than in the IE diamond, whilst the reverse is true for the 3000s impressions. The 'pile-up' is most pronounced in the NA diamond.

Examination of the impressions at 90° to the original surface using transmitted polarised light, i.e. by focusing below on a (110) section, reveals the strained region directly beneath the impression, Figure 6.7. It is apparent that an increase in impression dwell time has resulted in an increase in the volume of plastically deformed diamond, but it is not possible to distinguish any significant difference between the two samples with respect to the level of strain produced by the soft indentation process.

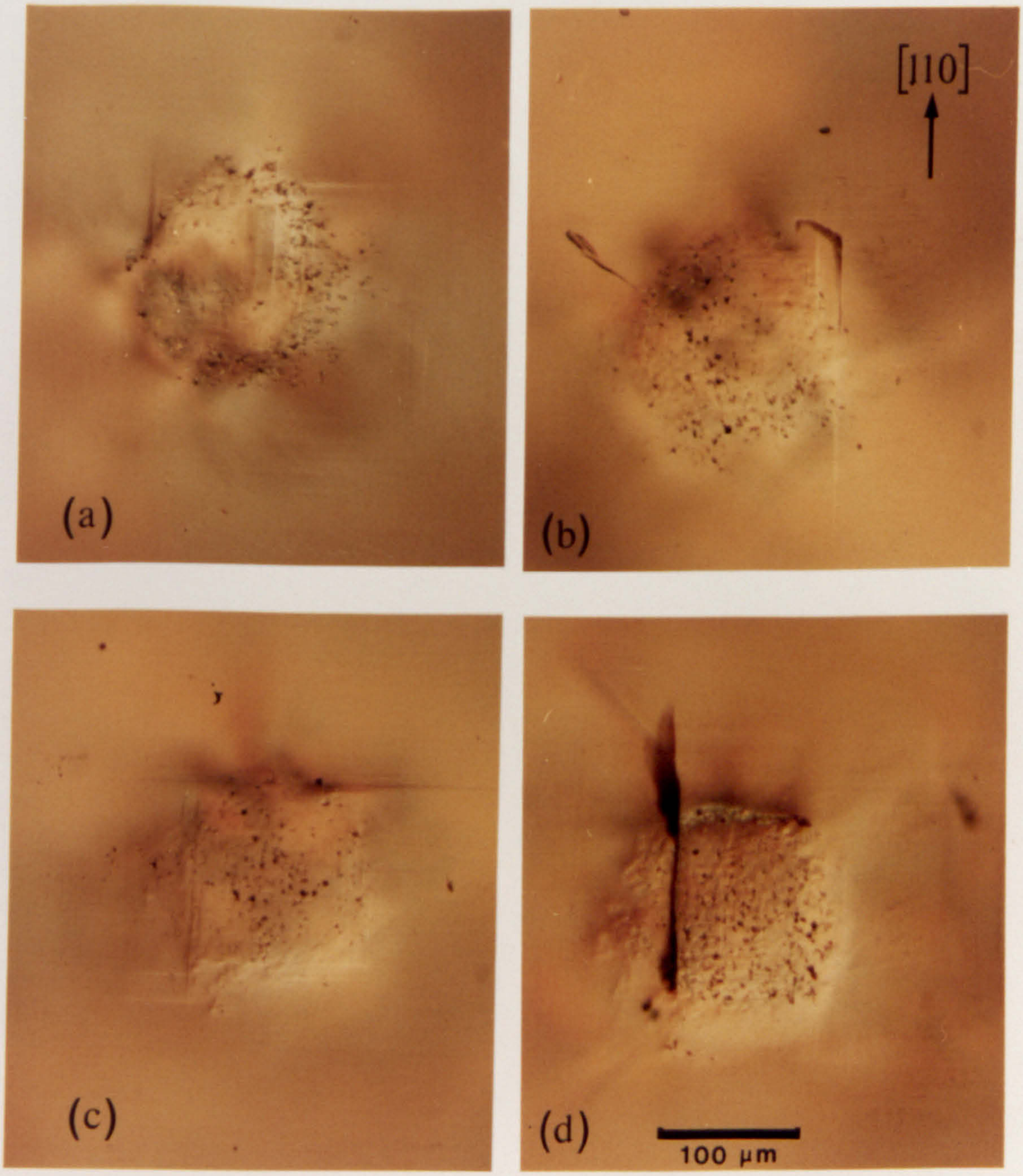

Figure 6.4 Differential interference contrast micrographs of the individual impressions made in the natural abundance (NA) diamonds:

(a) 300 seconds, (b) 1000 seconds, (c) 2000 seconds, (d) 3000 seconds.

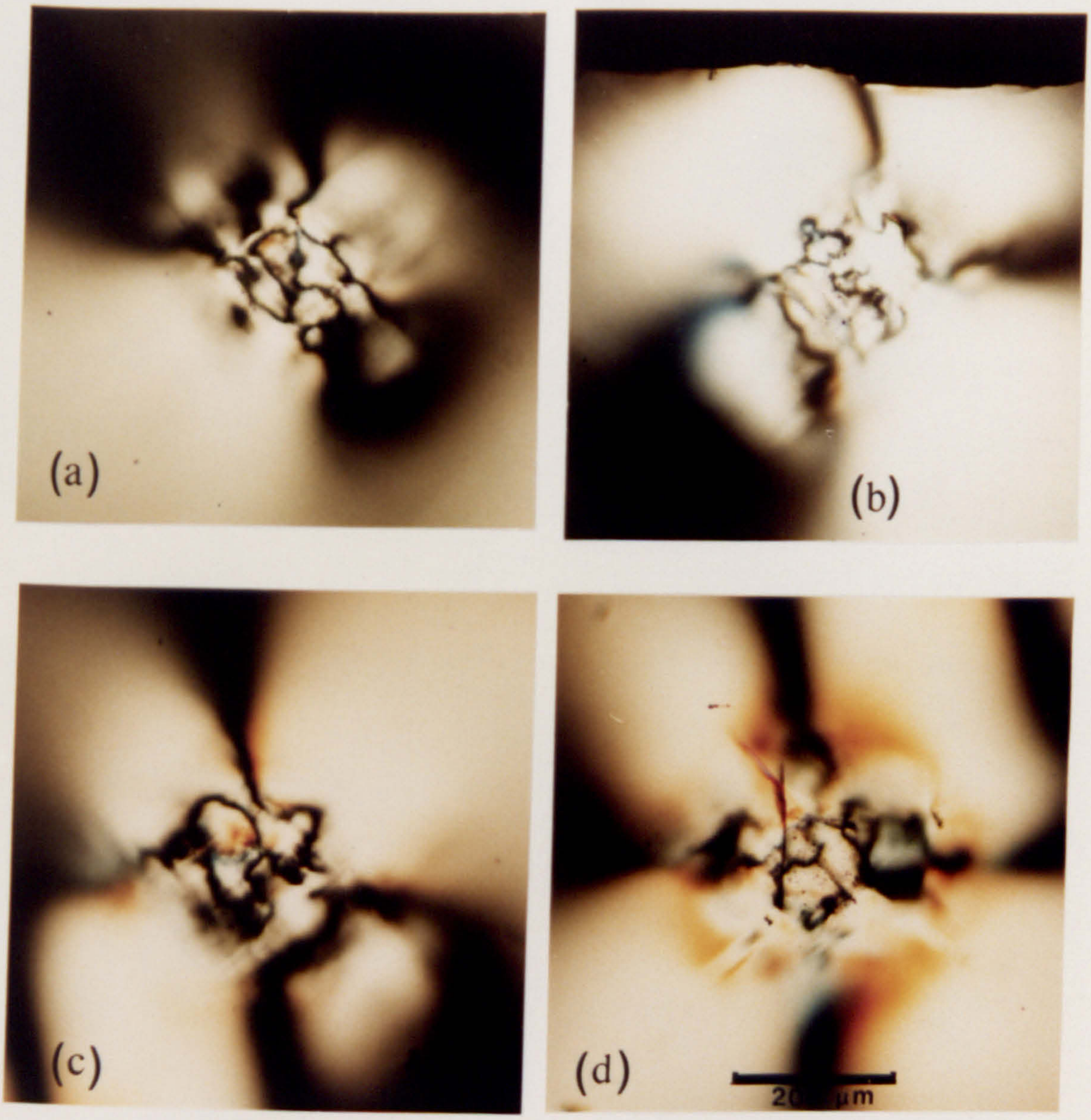

Figure 6.5 Transmitted light micrographs of the impressions shown in Figure 6.4.

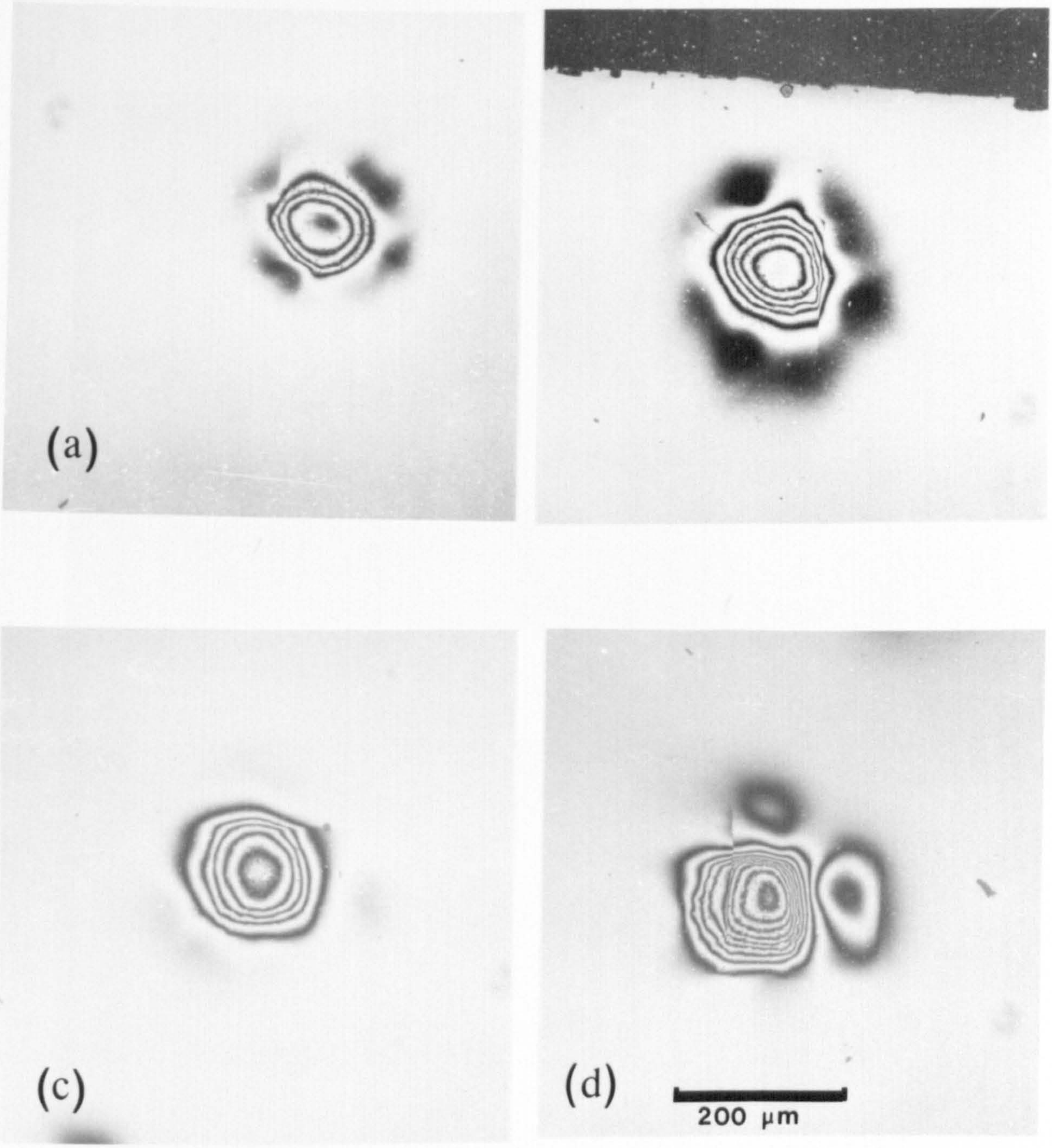

Figure 6.6 Interferograms of the impressions shown in Figure 6.4.

Figure 6.7 Side view, giving a (110) section of the impressions shown in Figure 6.1.

6.3 Discussion.

The Knoop hardness and the anisotropy at room temperature is consistent with natural diamond. The difference between the hardness of the IE diamond and natural type IIa appears to be significant, but further results are required both on the IE and the NA diamond.

Multiple intersecting slip was produced in the IE and the NA diamonds as a result of a mean contact pressure of 6.5 GPa at 1100°C (0.35 T_m). Relatively coarse slip prevails beneath the area of contact of the indenter but the slip lines outside the area of contact are significantly finer than observed in type I diamonds. Thus, the amount of plastic flow in these diamonds bears greater similarity to type I diamond than to type IIa diamond. As a result, it is likely that the critical resolved shear stress for both the IE and NA diamonds, in comparison with the types of diamond studied in this thesis, decreases in the order:

type IIa → IE and NA → type Ia → type Ib

for these experimental conditions. A lower value of the critical resolved shear stress for the synthetic type IIa diamond, compared with the natural type IIa diamond, is likely to be due to the difference in initial dislocation distribution.

In Chapter 4 it was established that laths and {110} cracking characterise the behaviour of both type Ia and Ib diamond under these experimental conditions. Neither of these features are observed in type II diamond and in those respects both the IE and NA diamond behave more like type II than type I diamond.

In these experiments there is no significant difference in the plastic deformation of the isotopically enriched and the natural abundance diamonds. The evidence of a tendency to {111} cracking in the NA diamond might be related to the degree of adhesion between the cBN indenter and the surface, or to the intrinsic strain in the diamond before the impressions were made, rather than to a genuine effect of isotopic concentration. More work is needed to establish those possibilities.

Time dependent plastic flow of both the IE and NA diamond is observed as the depth of the impression increases with dwell time despite a continuously decreasing applied

pressure. However, the rate of increase of the contact area of the indenter is slower than that for impressions made by a cBN cone on natural type Ia diamond. In other words, the time dependent flow of the indenter appears to be more constrained by the deforming diamond.

6.4 Summary.

In the previous chapters it has been established that laths and {110} cracking characterise the behaviour of both natural type Ia and synthetic type Ib diamonds under these experimental conditions, Neither of these features were observed in natural type IIa diamond, In this respect, both the IE and the NA diamond behave more like type II than type I diamond.

In contrast the extent of plastic flow in these diamonds is more akin to type I than natural type II diamond. However, these experiments have not demonstrated a significant difference in the plastic deformation of the isotopically enriched and the natural abundance synthetic diamond grown by CVD followed by high pressure-high temperature growth.

Chapter 7 The effect of nitrogen on the plastic deformation of diamond.

7.1 Introduction.

In general, point defects in metallic materials, whether vacancies or interstitials, will tend to increase the resistance to dislocation movement. Thus, the well known yield drop in impure, annealed body centred cubic metals is known to be due to the segregation of small interstitial atoms i.e. carbon, which diffuse to enlarged sites at dislocation cores forming Cottrell atmospheres. As a result dislocations are pinned and there is an increase in the initial yield stress. A yield drop is also observed in covalent diamond cubic crystals, such as silicon and germanium. In addition, the presence of certain dopants in semi-conducting materials can be shown to increase the dislocation mobility, eg n-type silicon, or to decrease the dislocation mobility, eg p-type silicon (Hirsch, 1985). Accompanying these effects, the critical resolved shear stress is either decreased or increased respectively. For example, Rabier *et al*, (1983) have measured the lower yield stress as a function of temperature for heavily doped n-type silicon and for intrinsic silicon. At about 500°C, $\sigma_{ly\ doped}$ / $\sigma_{ly\ intrinsic}$ is about 0.3, i.e. under their experimental conditions, the softening due to the electronic effect was found to be considerable. Roberts *et al* (1985) have shown that doping semi-conductor materials with small concentrations of electrically active solutes causes significant changes in dislocation velocity, yield stress, hardness and fracture behaviour in the temperature range in which plastic flow becomes important.

The soft impression technique has provided a sensitive means of discriminating between the plastic behaviour of type I and type II diamond. The basis of the distinction between type I and type II diamond depends on the presence or absence of nitrogen in the lattice and the sites occupied and the presence or absence of significant numbers of dislocations. The work presented in this thesis has indicated that nitrogen-containing diamond deforms plastically and fractures more easily, for a given set of experimental conditions, than diamonds with very low levels of nitrogen but high dislocation densities. However, each diamond is unique and a rigid distinction between the various type of diamond is not always possible. Some diamonds are

mixed type I and type II. Type I diamond may vary in nitrogen content, which may be in the form of A, B, A and B aggregates and in some diamonds, platelets. The amount of nitrogen in synthetic diamond can vary between wide limits according to the growth conditions but is always in substitutional sites. Indeed the distribution can vary within a diamond, as nitrogen substitution in the growing diamond occurs along specific crystallographic directions. In order to further our understanding of plastic deformation and creep, the mechanical processes involved in the formation of an impression by a softer indenter, and to make meaningful comparisons between diamond types, the classification of each individual diamond is very important.

The aim of the work presented in this chapter was to isolate the effect of varying the nitrogen concentration from the effect of grown-in dislocations by studying well characterised type Ia diamonds.

7.2 Experimental procedure.

Three natural diamonds, with varying nitrogen concentration, were provided by Dr. G S Woods. Two parallel (001) planes had been polished and the infra-red absorption spectra of the diamonds measured. The spectra showed predominantly A features although one diamond, containing the intermediate level of concentration, had a very small platelet peak. The spectra correspond to A nitrogen concentrations of 14 ppm, 345 ppm, and 779 ppm. The (001) surfaces and the bulk birefringence were photographed prior to annealing and indenting.

The experimental conditions were selected to produce essentially plastic impressions, with no cracking, in all the diamonds. The indenter material was TiB_2, to produce a relatively low mean contact pressure. The experimental temperatures used were 1100°C, in order to just exceed the brittle-ductile transition temperature for type IIa diamond, and 1400°C, where significant plastic deformation was found to occur in all types of diamond.

In order to ensure that the indenter had been ground to specification, an impression was made in a synthetic diamond at 1000°C, prior to making an impression in the specimen, This produced a flat on the indenter of approximately 120 μm diameter. A blunt indenter, produced under controlled conditions by plastic deformation, has been found to be less liable to form a

junction with the diamond, and therefore adhesion between the indenter and the specimen was reduced. The indenter was then used to make one impression, with a dwell time of 3000 seconds. After the measurements had been made, the indenter was reground and the procedure repeated, making an impression in another diamond.

7.3 Results.

The experimental temperature of 1100°C produced a mean contact pressure of 3.6 GPa for all the diamonds indented in this study. Figure 7.1 shows the DIC micrographs of the type IaA diamonds, (a) containing 14 ppm, (b) containing 345 ppm, and (c) containing 779 ppm. Coarse intersecting slip is visible within the contact area in all three diamonds. Slip is limited in the diamond with 14 ppm nitrogen, and confined within the contact area of the indenter. More extensive slip can be seen in the diamonds of higher nitrogen content, with many more slip lines visible within the contact area and some coarse slip lines extending beyond the area of contact. In Figure 7.2, the interferograms of the impressions are shown. The impression in the diamond with 14 ppm nitrogen is approximately 400 nm deep, whereas the impressions in the diamonds with increased nitrogen levels are both approximately 800 nm deep. Laths are present beneath the impression in the 345 ppm and 779 ppm diamonds but not in the 14 ppm diamond. There is no evidence for rosette slip under these experimental conditions and cracks were not formed.

Figures 7.3, 7.4 and 7.5 show the impressions made at 1400°C, where the applied mean contact pressure was 2.8 GPa. In Figure 7.3 it can be seen that in all three diamonds, coarse intersecting slip has occurred beneath the impression and that a rosette has developed. In the diamond containing 14 ppm nitrogen, the rosette is large by comparison with the impression diameter, but the slip lines are finely spaced and not very high. In the diamond containing 779 ppm nitrogen however, the rosette slip is much coarser, with some predominant slip lines which appear higher and evenly spaced. The size of the rosette is reduced with increasing nitrogen content and the interferograms in Figure 7.4 confirm these observations. The impression in the 14 ppm nitrogen diamond is approximately 4.6 μm deep, and the 'pile-up' outside the impression is approximately 0.5 μm above the original surface, Figure 7.4(a). This

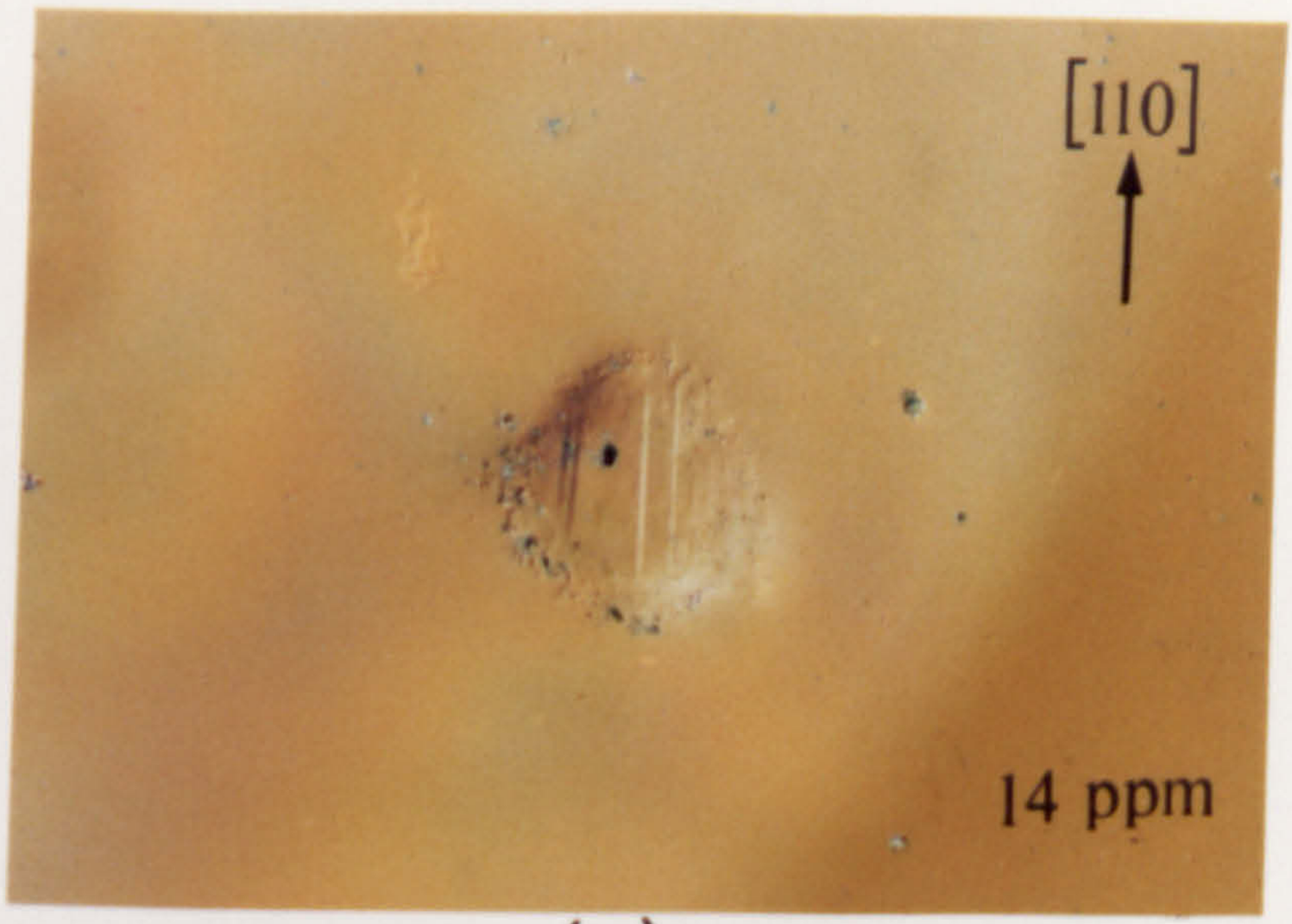

(a)

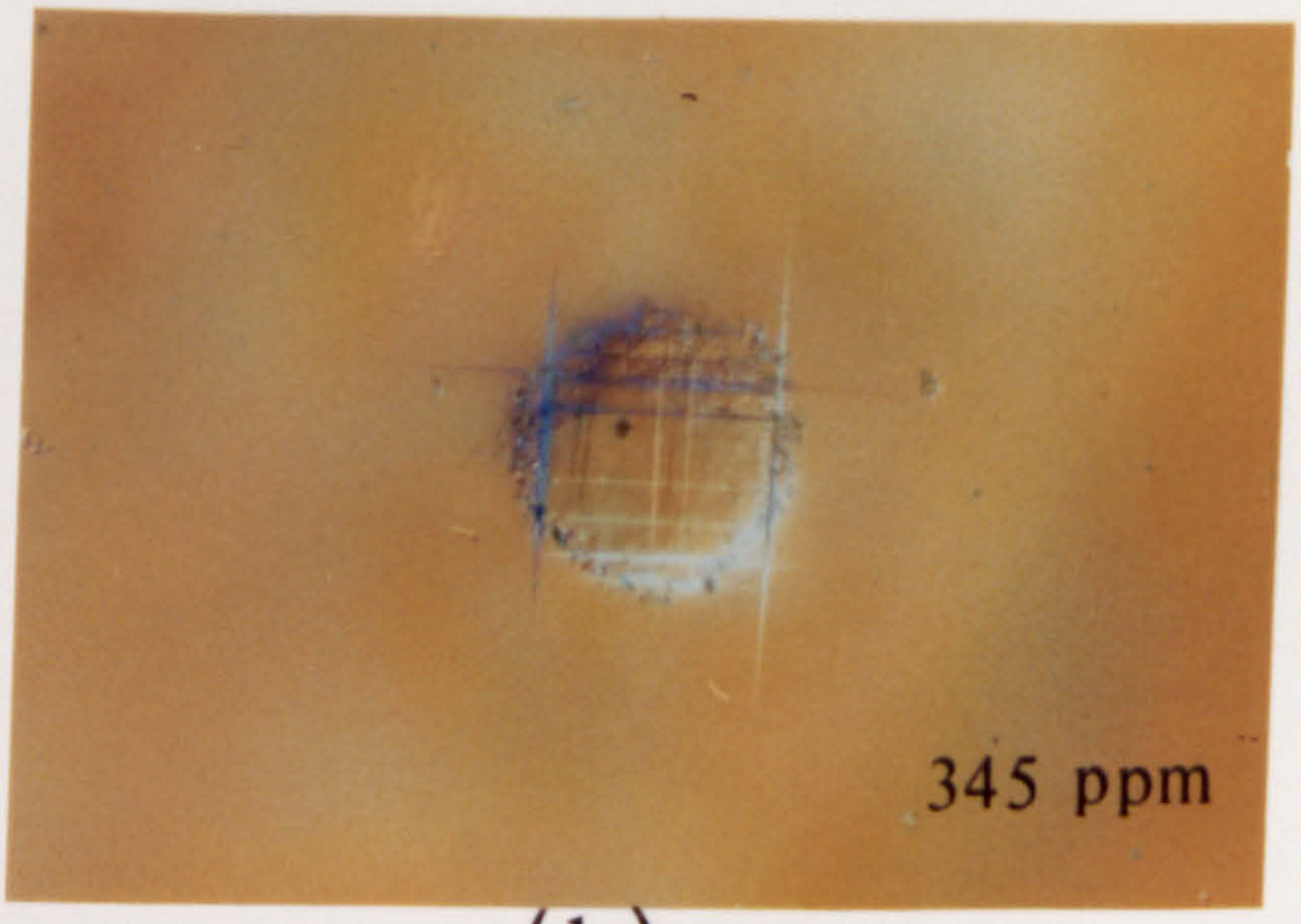

(b)

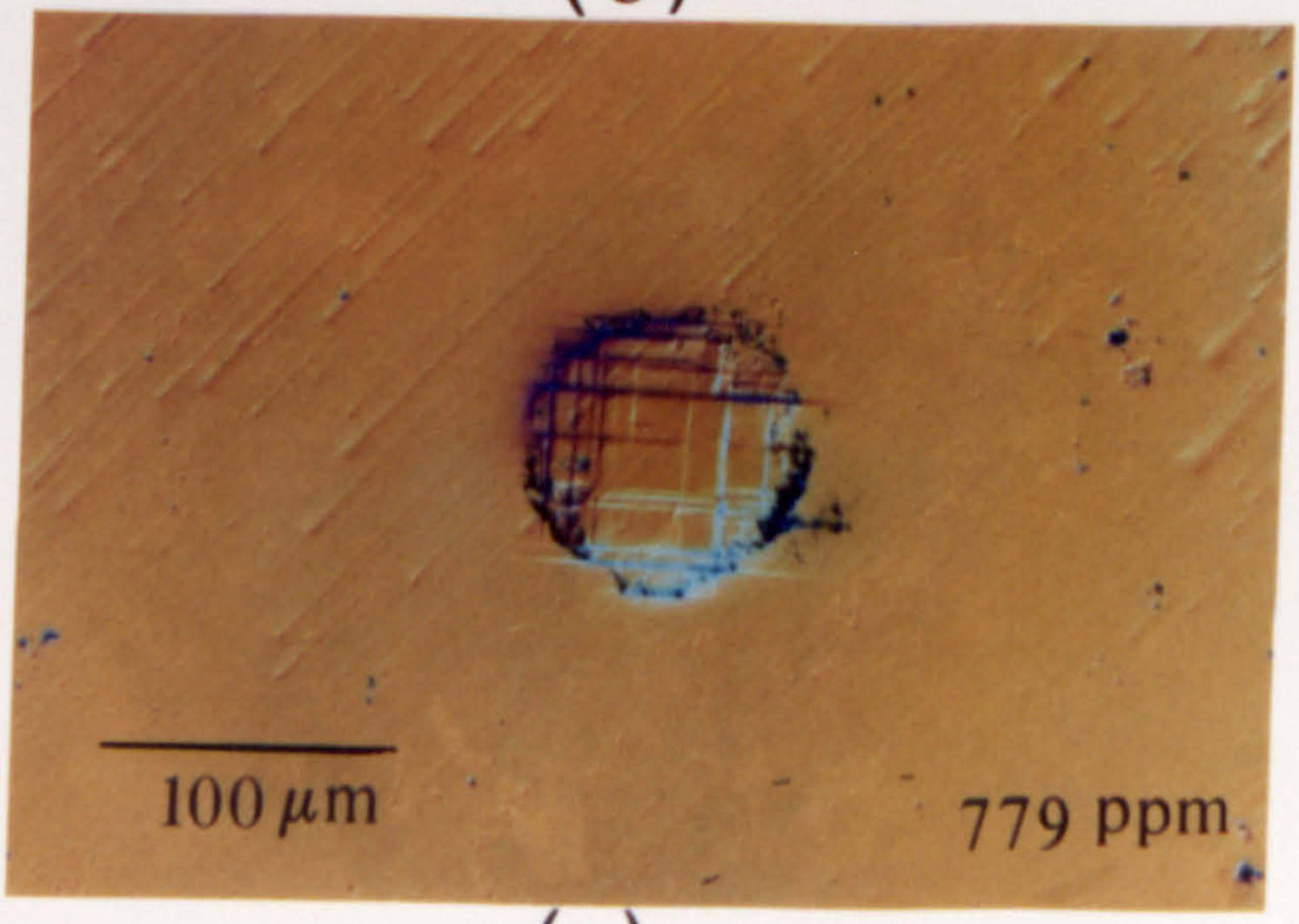

(c)

Figure 7.1 Demonstrating the effect of nitrogen on the plasticity of type IaA diamond, {001} plane, deformed by a TiB_2 cone, at 1100° C, for 3000 seconds.

P_m 3.6 - 3.8 GPa.

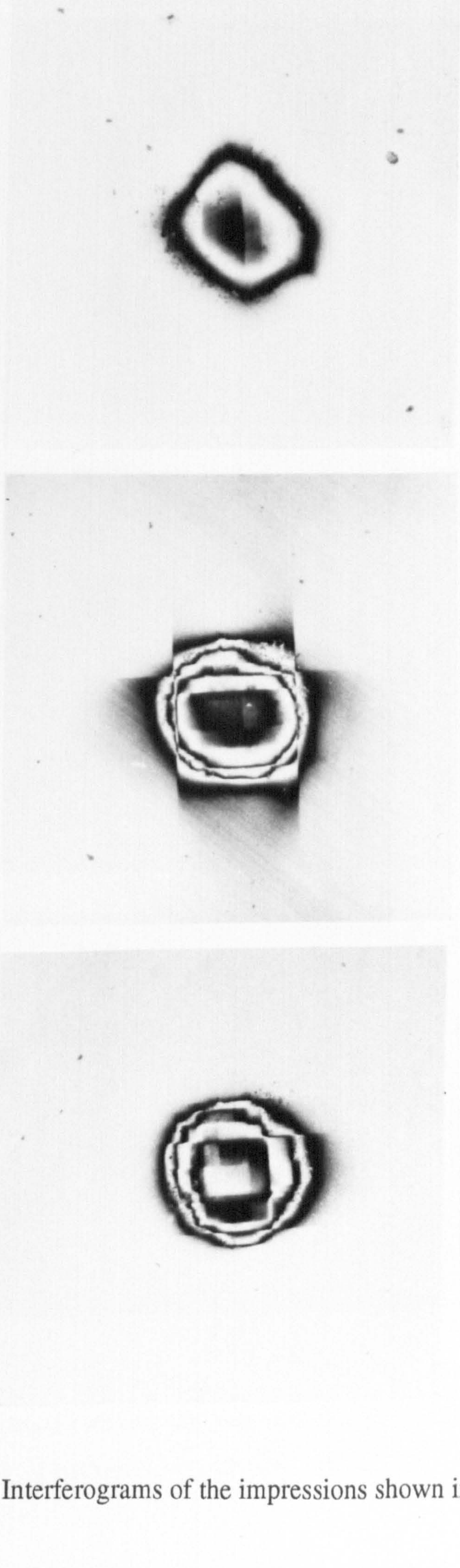

Figure 7.2 Interferograms of the impressions shown in Figure 7.1.

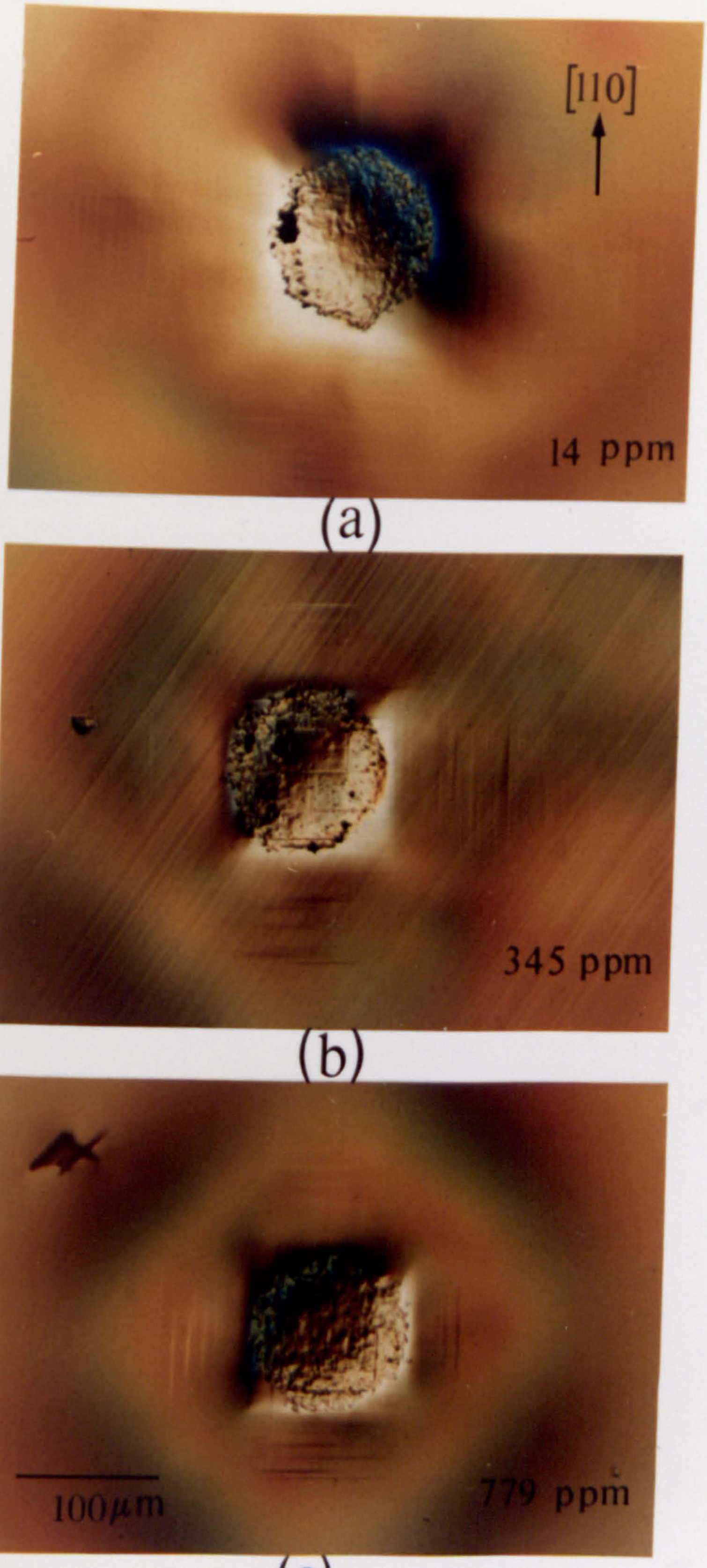

Figure 7.3 Demonstrating the effect of nitrogen on the plasticity of type IaA diamond, (001) plane, deformed by a TiB2 cone, at 1400°C, for 3000 seconds. Pm = 2.8 GPa.

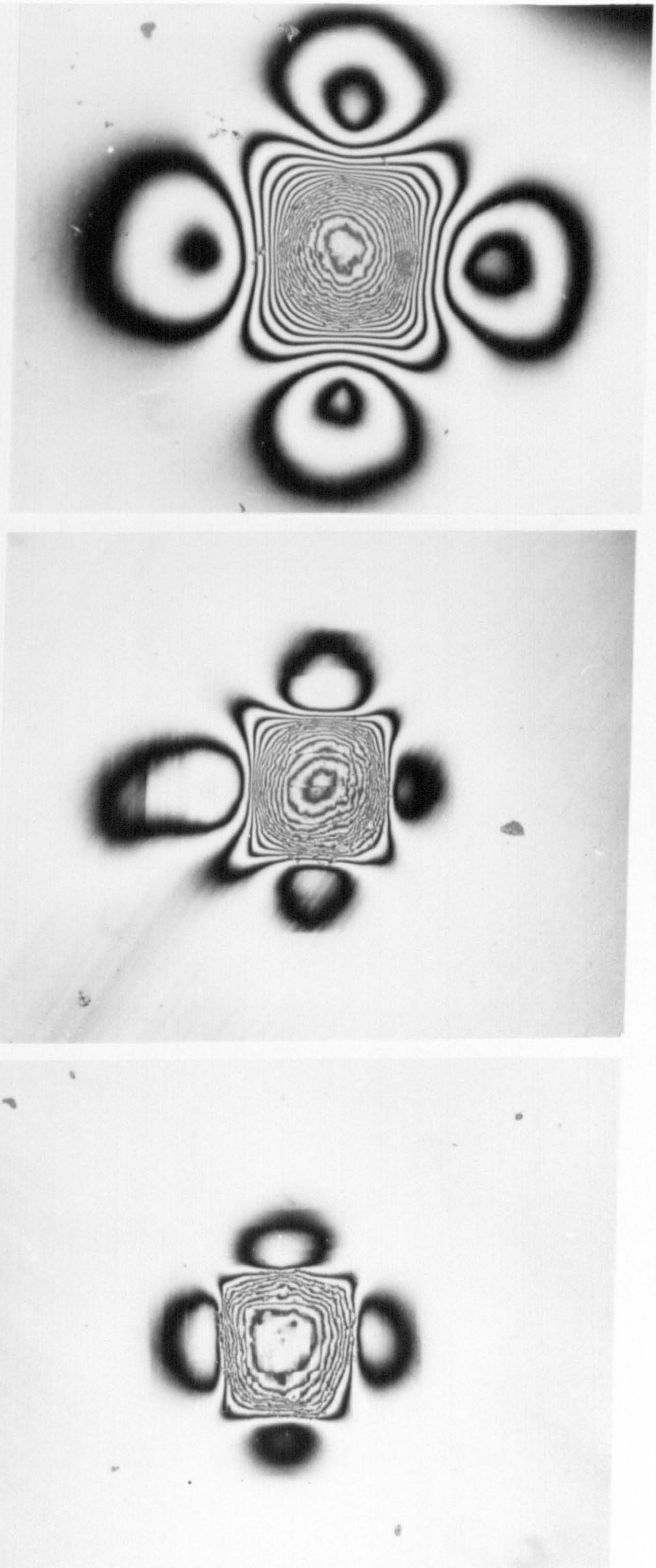

Figure 7.4 Interferograms of the impressions shown in Figure 7.3.

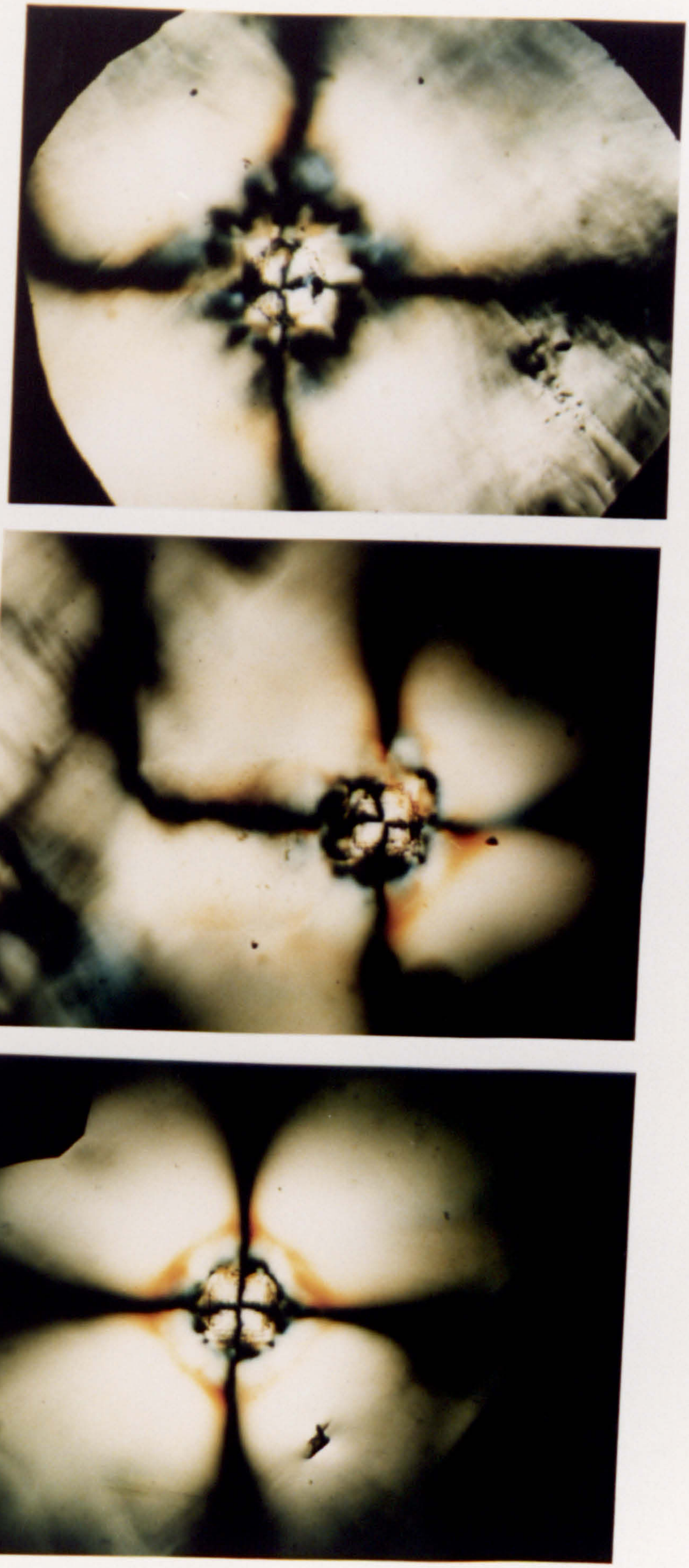

Figure 7.5 Transmitted light micrographs to show the birefringence associated with the impressions shown in Figure 7.3.

compares with a depth of approximately 3.5 μm for the 345 ppm nitrogen diamond, Figure 7.4(b) and 2.2 μm for the 779 ppm nitrogen diamond, Figure 7.4(c). Clearly the surface area and the volume of plastic deformation has decreased with increased nitrogen concentration. It can be seen from the interferogram in Figure 7.4 (a) that the contact area of the indenter is not the same as the impression area, and that there has been 'sinking in' of the impression of the order of 1.2 μm. This is not nearly as marked in the 345 ppm nitrogen diamond and in the 779 ppm nitrogen diamond the contact area and the impression area are virtually the same. Laths are not observed in the 14 ppm nitrogen diamond but are present in the diamonds with higher nitrogen concentration. Cracking has not occurred in any of the diamonds.

The micrographs obtained from transmitted polarised light, Figure 7.5, show that with increased nitrogen content the residual strain developed in the diamond increases as the volume of strained diamond appears to decrease. The measurements of the impressions made in the three type IaA and the type IIa diamond are summarised in Table 7.1.

Table 7.1 Dimensions of the impression in type IaA diamonds of differing nitrogen concentration.

	P_m (GPa)	Depth (μm)	Volume (μm^3)
1100° C			
14 ppm	3.9	0.4	5,900
345 ppm	3.7	0.9	11,900
779 ppm	3.6	0.85	13,300
1400° C			
14 ppm	2.8	4.62	117,700
345 ppm	2.8	3.54	51,000
779 ppm	2.8	2.18	33,100

7.4 Discussion.

Clearly this work demonstrates that the level of nitrogen concentration in the diamond lattice markedly affects the plastic deformation at temperatures above 0.3 T_m and there are three main observations which can be made. Firstly, increased levels of nitrogen reduce the critical resolved shear stress of diamond, secondly, visible laths are formed when the nitrogen concentration is substantial and thirdly, a significant difference in the surface topography in the neighbourhood of the impression is observed in diamonds with different concentrations of nitrogen.

More work is required for a detailed explanation of these observations, however, there are a number of points for discussion which are worth enumerating:

1. The reduction in the critical resolved shear stress with increased nitrogen can be envisaged as a direct consequence of the reduction in the strength of the covalent bond with a corresponding decrease in the Peierl's force. In this respect, it may simply be the presence of impurity atoms rather than the nature of the structural defects which cause the change in bond strength. To develop this hypothesis, future studies should include doping of synthetic diamond with boron and other light elements.

2. A direct result of the lowering of the critical resolved shear stress is the effect on the extent of dislocation movement within the dislocated zone. The contour maps in Figure 2.6 indicate that, for a contact pressure for a given experimental temperature, dislocations will move at a deeper point beneath the area of contact than for a higher critical resolved shear stress. Therefore, the higher the nitrogen content, the greater the extent of plastic deformation and the higher the total strain energy. This is likely, particularly in the presence of sessile dislocations and other stress concentrators, to result in a greater tendency to crack initiation and propagation.

3. The dislocation velocity may be affected by the presence of nitrogen in a similar way to the dopants in semiconductors (Hirsch, 1984). However, the levels of impurity atoms in semiconductors is substantially smaller than the concentration of nitrogen in these diamonds and the development of a suitable dislocation etchant is vital to our understanding of this effect.

4. Laths are visible in the two diamonds containing larger levels of nitrogen, and in fact the work presented in this thesis indicates that laths are always observed in the presence of all forms of nitrogen defect. Possible explanations *include:*

(a) direct decoration of defects by impurity atoms,
i.e. nitrogen atoms,

(b) dislocation pinning by nitrogen aggregates,

(c) crack nucleation as a result of the formation of
Lomer - Cottrell locks and / or impurity
atmospheres

(d) discrete localised phase transfromations as
observed in silicon by Pirouz *et al*, 1990.

(e) twin formation within the dislocated volume,

(f) intense and discrete shear bands.

The use of other techniques, i.e. cathodoluminescence, x-ray topography, and TEM, will resolve many of the uncertainties in the above observations but are beyond the scope of this work. Neverthless, the soft indenter technique has unambigously demonstrated that nitrogen plays a major role in the plastic deformation of diamond.

7. 5 Summary.

This part of the project has been a preliminary investigation, with a limited number of specimens, into the influence of nitrogen on the plastic deformation of diamond. Nevertheless, the results are entirely consistent with the work presented in the previous chapters and support the following tentative conclusions:

- the critical resolved shear stress is reduced by nitrogen,
- the formation of laths is dependent on a certain level of nitrogen in the lattice,
- nitrogen directly influences the surface topography of the deformed diamond adjacent to the contact area.

Since the level of nitrogen in synthetic diamond is relatively easy to control, the above observations have particular significance for technological applications.

Chapter 8. Conclusions and proposals for future work.

8.1 Conclusions.

Plastic deformation, under conditions of a uniform uniaxial stress, may be inhibited in ceramic materials which normally have a marked tendency to brittle behaviour, simply due to catastrophic crack initiation produced at the most severe stress concentrator anywhere within the volume of the specimen. In contrast, the nature of the stresses produced beneath an indenter tends to increase the plastic contribution to deformation, whilst inhibiting the formation of cracks. However, the use of a rigid pyramidal indenter, with the relatively high level of strain it induces in an indentation, may produce radial and/or median cracks. Also, the rigid spherical indenter tends to induce ring cracks due to tensile stresses around the circumference of the contact area. Additionally, both shapes of indenter may cause subsurface lateral cracks on the removal of the normal load. Replacing the hard indenter with a cone of a softer material further encourages plasticity in hard crystals. This is because the softer cone blunts as the load is applied and the mean contact pressure, limited by the flow stress of the indenter material, can be controlled so as to be insufficient to cause fracture. In addition, the predominantly compressive stresses beneath the contact prevents stress concentrators from developing into propagating cracks.

Careful selection of the indenter material, enables a mean pressure to be applied which initiates plastic deformation - i.e. just exceeding the critical resolved shear stress. Above that threshold contact pressure, dislocations move in the harder crystal without necessarily producing cracks. In this work it has been demonstrated, for the first time, that this method can be used at elevated temperatures in the range of 0.3 to 0.5 T_m. Furthermore, it is shown to be remarkably effective in demonstrating the differences not only between the various types of diamond but also the effect of temperature, dwell time and nitrogen content on the nature of plasticity and cracking associated with the deformation process. The following conclusions may be drawn on the basis of the results and observations made in earlier chapters:

- onset of plastic flow, under these experimental conditions, occurs at different threshold temperatures for various types of diamond; i.e. 750°C, 900°C and 1100°C for type Ib, type Ia and type IIa respectively.

- at a given temperature above the threshold temperature, the critical resolved shear stress increases in the order type Ib - type Ia - type IIa.

- above the critical threshold temperature, the critical resolved shear stress decreases very rapidly with a further 200°C increase in temperature by almost an order of magnitude, and then tends to a constant value for all types of diamond. The value of the critical resolved shear stress for type Ia diamond obtained at these higher temperatures in this work is shown to be entirely consistent with earlier measurements based on a three point bending technique - i.e. about 0.3 GPa (Trevilov, 1988).

- the ratio of the critical resolved shear stress / shear modulus for diamond, and the effect of temperature on this property, is directly comparable with other covalent crystals and is thought to reflect the characteristics of the relatively high Peierls forces which resist dislocation movement.

- it has been shown that 'impression creep' occurs under these experimental conditions, even whilst the mean contact pressure is decreasing, by the expansion of the dislocated volume such that it maintains geometrical similarity with the impression size. Therefore, it is considered probable that the controlling mechanism is one of dislocation glide although the calculated activation energy, about 2.9eV for natural diamond and 1.2eV for synthetic diamond, cannot be used to substantiate that hypothesis at this stage.

- strain induced cracking on {110} planes is observed in type Ia and Ib diamonds but not in type IIa. The criterion for this effect appears to be the total volumetric strain and thus may be produced by using cones of harder materials and/or by increasing the dwell time enabling impression creep.

- <110> crystallographically aligned defects, laths, are observed in both type I diamonds but not in type II, and are apparently formed along the edges of tetrahedral cages formed by intersecting {111} slip planes. It is considered likely that these laths are associated with nitrogen defects but further evidence is required both to substantiate that possibility and to identify their precise structure.

- the further potential of the soft indenter technique, for sensitively monitoring the effect of impurities on both the structure and properties of diamond, is demonstrated by remarkable differences in plasticity associated with impressions formed in type Ia diamond containing nitrogen in the range of 14 to 750 ppm. In general, the critical resolved shear stress is influenced by the levels and nature of nitrogen in the lattice where higher levels of nitrogen not only lower this value, but tend to increase cracking on the {110} planes.

8.2 Future research.

Future research, based on extending and verifying the use of the soft indentation technique, might include the following:

1. To increase our understanding of the mechanical and, in particular, the plastic deformation of diamond, it will be necessary to study a wider range of carefully characterised single crystals of diamond. Research on other ceramic materials, eg silicon carbide, aluminium oxide and cubic boron nitride, could serve to complement the work already done on diamond and contribute to a general understanding of the mechanisms of deformation of such materials.

2. The creep process observed in diamond as a result of impressions made by softer cones appears to result in an increase in the volume of the plastically deformed diamond but not the density of dislocations within that volume. The possibility of the modification of the shape and texture of ceramic materials, including diamond, to optimize their behaviour is worthy of investigation.

3. Further evidence is required to determine whether the effect of nitrogen in diamond is due to the original nature of the defect, i.e. whether it is an individual substitutional point defect or aggregated, and/or to its interaction with mobile dislocations. It is known that the level and nature of doping in semiconductor materials can significantly influence the mobility of dislocations. Therefore, the controlled implantation of nitrogen and / or boron in natural and synthetic diamond, and the subsequent assessment of the threshold temperature and pressure for plastic deformation would be very useful. This, together with the use of other physical examination techniques, eg TEM,

cathodoluminescence, photoluminescence and x-ray topography, plus the development of a dislocation etchant, would permit a further assessment of the role of impurity defects on the mechanical properties of diamond.

4. The technological advantages of controlling the levels of nitrogen in diamond may be found to be extremely significant. Therfore a greater understanding of both the ductile and the brittle response to the application of a stress through a point contact, at experimental temperatures below half the melting point, and the correlation of these results with the studies of the form of nitrogen impurity in the diamond lattice should yield very useful information.

5. Whilst conventional fatigue is considered unlikely in diamond and other covalent materials, there is evidence to support the contention that, when subjected to repeated traversals by softer sliders and where the contact pressure is sufficient to exceed the critical resolved shear stress, they are susceptible to localised plastic deformation, work-hardening and fragmentation. The soft indentation technique is well suited to the evaluation of this possibility, and the assessment of this mechanism of fatigue wear in diamond and related materials.

References.

Ablova, M. S., 1962, Sov. Phys. Sol. State 3 (10), 2278 - 2280.

Anthony, T. R., Banholzer, W. F., Fleischer, J. F., Lanhua, Wei, Kuo, P. K., Thomas, R. L. and Pryor, R. W., 1991, Phys. Rev. B, 42 (2), 1104 - 1111.

Atkins, A. G., Silverio, A. and Tabor, D., 1966, J. Inst. Metals, 94, 369 - 378.

Barry, J. C., Bursill, L. A., Hutchinson, J. L., Lang, A. R., Rackham, G. M. and Sumida, N., 1987, Phil. Trans. Roy. Soc. Lond., A321, 361 - 401.

Berkovich, E., 1951, Ind. Dia. Rev., 11 (11), 129

Berman, R., ed. 1965, *Physical Properties of Diamond*. Clarendon Press, Oxford.

Bernholc, J., Antonelli, A., Del Sole, T. M., Bar-Yam, Y. and Pantelides, S. T., 1988, Phys, Rev. Lett. 61, 2689 - 2692.

Bowden, F. P. and Brookes, C. A., 1966, Proc. Roy. Soc. Lond., A295, 244 - 258.

Bowden, F. P. and Hanwell, A. E., 1966, Proc. Roy. Soc. Lond. A295, 233 -243.

Brookes, C. A., 1971, Ind. Dia. Rev., Jan. 21 - 24.

Brookes, C. A., 1979, in *The Properties of Diamond*, ed. Field, J.E., Academic Press, London.

Brookes, C. A., Brookes, E. J., Howes, V. R., Roberts S. G. and Waddington, C. P., 1990, J. Hard Mater., 1 (1), 3 - 24.

Brookes, C. A., Brookes, E. J. and Xing, G., 1991, Proc. Mechanics of Creep-Brittle Materials, Leicester,

Brookes, C. A. and Green, P., 1973, Nature, 246 (115), 119-221.

Brookes, C. A., O'Neil J. B. and Redfern, B. A. W., 1971, Proc. Roy. Soc. Lond., A322, 73 - 88.

Brookes, C. A., Howes, V. R. and Parry, A. R., 1988, Nature, 332, 139 - 141.

Brookes, C. A., Shaw, M. P. and Tanner, P. E., 1987, Proc. Roy. Soc. Lond., A409, 141 - 159.

Bull, S. J., Page, T. F. and Yoffe, E. H., 1989, Phil. Mag. Letters, 59 (6), 281 - 288.

Burnand, R. P., 1974, Ph.D. Dissertation, University of Exeter.

Chrenko, R. M., Tuft, R. E. and Strong, H. M., 1977, Nature, 270, 141 - 144.

Chu, S. N. G. and Li, J. C.M., 1977, J Mat Sci., 12, 2200

Churchman, A. T., Geach, G. A. and Winton, J., 1956, Proc. Roy. Soc. Lond., A238, 194 -203.

Clark, C. D., Ditchburn, R. W. and Dyer, H. H., 1956, Proc. Roy. Soc. Lond., A234, 363 - 381.

Collins, A. T., 1980, J. Phys. C: Solid State Physics, 13, 2641 - 2650.

Custers, J. F. H., 1952, Physica, 18, 489 - 496.

Custers, J. F. H., 1954, Physica,20, 183 - 184.

Daniels, F. and Dunn, C., 1949, Trans. Am. Soc. Metals, 41, 419 -442

Davies, G. and Lawson, S., private communication.

Davies, G., Welbourn, C. M. and Loubser, J. H. N., 1978, Diamond Research, 23 - 30.

DeVries, R. C., 1975, Mat. Res. Bull., 10, 1193 -1200.

Doi, Y., Sato, S., Sumiya, H. and Yazu, S., *Proc. Second Int. Conf. Science of Hard Materials*, Rhodes, eds. Almond, C.A., Brookes, C.A. and Warren, R., *Inst. Phys. Ser.* 75, 233 - 237.

Enomoto, Y. and Tabor, D., 1980, Proc. Roy. Soc. Lond., A 373, 405 - 417.

Evans, T., 1978, Diamond Research, 17 - 22.

Evans, T. and Phaal, C., 1962, Proc. Roy. Soc. Lond. A 270, 538 - 552.

Evans, T. Sykes, J, 1974, Phil. Mag., 29, 135 - 147.

Evans, T. and Wild, R. K., 1965, Phil. Mag. 12, 479 - 489.

Evans, T. and Zengdu, Qi, 1982, Proc. Roy. Soc. Lond. A381, 159 -178.

Field, J.E., 1979, ed. *The Properties of Diamond*. Academic Press, London.

Field, J. E., 1984 *Proc. Second Int. Conf. Science of Hard Materials*, Rhodes, eds. Almond, C.A., Brookes, C.A. and Warren, R., *Inst. Phys. Ser.*, 75, 181 - 205.

Field, J. E. and Freeman, C. J., 1981, Phil. Mag., 43, 595 - 618.

Frank, F. C., 1956, Proc. Roy. Soc. Lond., A237, 168 -174.

Fujita, S., Maeda, K. and Hoyodo, S., 1987, Phil. Mag., A55 (2), 203 - 215.

Gerk, A. P., 1977, J. Mat. Sci., 12, 735 - 738.

Groves, C. W. and Kelly, A., 1963, Proc. Roy. Soc. Lond., A275, 233 - 244.

Hargreaves, F., 1928, J. Inst. of Metals, 39, 301

Harrison, P., 1973, Ph.D. Dissertation, University of Exeter.

Hirsch, P. B., Hutchinson, J. L. and Titchmarsh, J., 1986, Phil. Mag., 54, L49 - 54.

Hirsch, P. B., Pirouz, P., Roberts, S. G. and Warren, P. D., 1985, Phil. Mag. B, 52, 761 - 786.

Hirsch, P. B., Roberts, G. G. and Samuels, J., 1987, Scripta metall., 21, 1523 -

Hirsch, P. B., Roberts, S. G.and Samuels, J., 1989, Phys. Rev. Appl., 23, 409 -

Howes, V. R. and Tolansky, S., 1955, Proc. Roy. Soc. Lond., **A 230**, 287 - 293, ibid. 294 - 300.

Humble P. and Hannink, R. H. J., 1978, Nature, **273**, 37 - 39.

Hutchings, I., 1980, unpublished work.

Kaiser, W. and Bond, W., 1959, Phys. Rev., **115**, L857 -863.

Kelly, A., 1966, *Strong Solids*, Oxford Universty Press, London.

Knoop, F., Peters, C. G. and Emerson, W. B., 1939, J. Res. Nat. Bur. Stand., **23**, 33 - 61.

Lee, M., DeVries, R. C. and Koch, E. F., 1984, *Proc. Second Int. Conf. Science of Hard Materials*, Rhodes, eds. Almond, C.A., Brookes, C.A. and Warren, R., *Inst. Phys. Ser.* **75**, 181 - 205.

Li, H. and Bradt, R. C., Proc. ICSHM4, to be published.

Li, W. B., Henshall, J. L., Hooper R. M. and Easterling, K. E., 1991, Acta Metall. Mater., **39** (12), 3099 - 3110.

Loubser, J. H. N. and Wright, A. C. J., 1973, in Diamond Research, 16 -20.

Madiba, C. C. P., Sellschop, J. P. F., Derry, T. E. and Fearick, R. W., 1984, Abstracts, Diamond Conference, Bristol.

Mao, H. K. and Bell, P. M., 1978, Science **2000**, 1145 -1147.

Maugis, D., 1980, Wear, **62**, 349 - 386.

Meyer, H. O., in *Mantle Xenoliths*, 1987, ed. Nixon, P.H., Wiley, New York 501 -525.

Morgan, J. E., 1976, PhD Dissertation, University of Exeter.

Mott, N., 1953, Phil. Mag. **44**, 742

Novikov, N. V. and Dub, S. N., 1991, J. Hard Mater., **2**, 1, 3 - 11.

Novikov, N. V. and Dub, S.N., J. Hard Mater., in press.

Palmqvist, S., 1962, Arch. Eisenhutenw., 33, 29

Pirouz, P., Chaim, R., Dahamen, V. and Westmacott, K. H., 1990, Acta Met., **38** (2), 313 - 337.

Pirouz, P., Cockayne. D. J. H., Sumida, N., Hirsch. P. B. and Lang, A. R., 1983, Proc. Roy. Soc. Lond., A386, 241 - 249.

Raman, C. V. and Nilakantan, P., 1940, Proc. Ind. Akad. Sci., **A11**, 389 - 397.

Rabier, J., Veyssière, P. and Dement, J. L., 1983, J. de Physique, Colloque C4, Suppl. 9, **44**, C4 - 243 - 253.

Roberts, S. G., Pirouz, P. and Hirsch, P. B., 1985, J. Mat. Sci., **20**, 1739 - 1747.

Roberts, S. G. Warren, P. D. and Hirsch, P. B., 1986, J. Mats. Res., 1, 162 - 178.

Robertson, R., Fox, J. J. and Martin, A. E., 1934, Phil. Trans. Roy. Soc. A232, 463 - 535.

Ross, J. D., 1984, PhD Dissertation, University of Exeter.

Routbort, J. L., Goretta, K. C., Dominiguez-Rodriguez and de Arellano-Lopez, A. R., 1991 J. Hard Mater., 1 (4), 219-221.

Sargent, P. M. and Ashby, M. F., 1989, CUED / C Mats. / TR. 145.

Seal, M., 1958, Proc. Roy. Soc. Lond., A248, 379 - 393.

Shaw, M. P. and Brookes, C. A., 1989, J. Mater. Sci., 24, 2727 - 2734.

Slack, G. A., 1957, Phys Rev., 105, 829

Slawson, C. B., 1950, Am. Min., 35,

Sobolev, E. V. and Lisoivan, V. I., 1972, Sov. Phys. Dokl., 17, 425 - 427.

Stephenson, R.F., 1978, Ph.D. Dissertation, University of Reading.

Sutherland, G. B. B. M., Blackwell, D.E. and Simeral, W.G., 1954, Nature, 174, 901 - 904.

Swalin, R. A., 1961, J. Phys. Chem. Solids, 18, 290 - 296.

Tabor, D., 1951, *The Hardness of Metals*. Oxford University Press.

Tolkowski, M., 1920, Ph.D. Dissertion, University of London.

Trefilov, V. I., Borisenko, V. I., Grigor'ev, O. N. and Mil'man, Yu V., 1975, Sov. Phys. Dokl., 19 (7), 464 - 466.

Trefilov, V. I., Mil'man, Yu V. and Grigor'ev, O. N., 1988, J. Cryst. Growth and Charact., 16, 225 - 277.

Yu, E. C. and Li, J. C. M., 1977, Phil Mag., 36 (4), 811-825.

Westbrook, J. H., 1958, General Electric Research Laboratory Report No. 58 - RL - 2033, cited in Gilman, J.J., in The Science of Hardness Testing and its Research Applications, 1973, edited by Westbrook J. H. and Conrad, C., American Society for Metals, 51-74.

Westbrook, J. and Jorgensen, P., 1964, General Electric Research Laboratory Report No. 64 - RL - (3688 M).

Westbrook, J. and Jorgensen, P., 1968, General Electric Research Laboratory Report No. 68 - C - 041.

Wilks, E. M. and Wilks, J., 1965, *The Physical Properties of Diamond*, ed. Berman, R. Clarendon Press, Oxford.

Wilks, E. M. and Wilks, J., 1972, J. Phys. D: Appl. Phys., 6, 1772 - 1281.

Wilks, J. and Wilks, E. M., 1991, *Properties and Applications of Diamond.* Butterworth - Heinemann Ltd., Oxford.

Williams, W. S., 1964, J. Appl. Phys., 35, 1329 - 1338.

Woods, G. S., 1976, Phil. Mag., 34, 993 - 1012.